CHAPTER 1

Introduction

Photovoltaic devices (PVs) convert sunlight directly into electricity. PV technology clearly offers tremendous environmental benefits, requiring no fuel and producing no emissions or other waste beyond that inherent in the manufacturing process. Moreover, photovoltaics have proven to be economical for a wide range of applications that have traditionally relied on diesel generators. Water pumping and rural village electrification are prime examples. Other applications profitably employing PV generation include vaccine refrigeration, remote radio and satellite link stations, railroad signaling, and rural vacation homes. In each of these cases, PV proves to be the most economical energy choice because the cost of purchasing and installing a photovoltaic system is less than that of extending utility service to an off-grid area. Developing countries without the electrical infrastructure of the North America and Europe provide a major market for PVs. Of the 31051 peak kW (kWp) of US PV shipments in 1995, 19871 kWp were exported [Holihan, 1997]. The photovoltaic industry has been growing exponentially at a rate of about 20% over the last ten years, supported primarily by applications where utility service is unavailable. It is essential that PV also penetrate the grid-tied market if it is to compete with such large-scale utility power technologies such as nuclear and fossil plants.

Grid-tied PV plants may be installed at a central generating station just as large fossil and nuclear plants. The Corporation for Solar Technology and Renewable Resources is planning to install up to 270 MWp of centralized PV generating capacity in the Nevada desert north of Las Vegas [SMUD, 1998]. Another option is to employ building-integrated photovoltaic (BIPV) systems in which PV power is generated at the point of consumption. BIPV provides several advantages over central generation. Since power is generated and consumed at the same location, there are no energy losses in the utility's transmission and distribution (T&D) system. A central plant requires a large area of dedicated land, but building-integrated

systems may be incorporated into a roof or façade without consuming additional ground area. Utilities have successfully sponsored programs in which electric customers pay for the "privilege" of mounting a utility-owned BIPV system on their roofs. The Sacramento Municipal Utility District (SMUD) has the most ambitious such program. Residential and commercial SMUD customers currently provide roof space for over 1.5 MWp of installed BIPV capacity, paying an additional four dollars per month to do so [SMUD, 1998].

The long-term aggregate performance of any grid-tied photovoltaic system is dependent on the parameters of the system itself and on the weather. These factors are no different for a central PV generating plant and an identical BIPV system in the same geographic location. An additional issue comes into play when evaluating the profitability of privately owned BIPV systems, however. This question is how PV performance varies from hour to hour and from season to season. Utility rates are often subject to hourly and seasonal variations, so the value of a solar kWh is not necessarily constant over time. Since commercial customers are usually subject to demand charges, it is also important to understand how closely PV generation coincides with a building's electrical load. The software developed in this work determines the monetary saving from BIPV based on hourly system performance, building load, and the utility rate schedule.

The progress of grid-tied BIPV depends on the potential benefits for the electric utility as well as for the customer. The cost of generation varies from one plant to another, so the value of a photovoltaic kWh to the utility depends on the operating cost of the most expensive plant running in the generating mix at that time. If PV is to replace traditional gas turbine plants for meeting a utility's peak loads, it is necessary to understand how PVs perform during the times when loads are greatest.

On a purely monetary basis without considering environmental externalities, photovoltaic electricity is not yet competitive with traditional generating technologies in the grid-tied market. The PV market is booming, however, and economies of scale may force prices down to the point where PV becomes a viable alternative to fossil, nuclear, and hydroelectric

technologies for utility-scale generation. In the meantime it is important for architects, building owners, and utilities to understand the economic ramifications of installing BIPV systems.

1.1 Motivation for Research

At the present time, the choice for electric customers and utilities to invest in grid-tied BIPV systems is not driven primarily by economic considerations. Photovoltaics are economical for many applications, but only when utility grid service is unavailable. Assuming a realistic lifetime of 30 years for a PV system, the cost per kWh is on the order of $0.15 in a favorable climate. This does not in any way imply that the BIPV market cannot grow; in fact it has experienced spectacular growth in the last 10 years. From 1994 to 1995, grid-interactive PV shipments more than doubled from 2296 to 4585 kWp [Holihan, 1997]. It is encouraging that growth of this magnitude can be maintained in the face of adverse economics.

There are several reasons why a building owner may choose to invest in PV at a loss. Perhaps the most clear-cut example is government subsidies that make PV appear more enticing. Of course, a subsidy does not eliminate the loss but merely shifts some of its burden from the shoulders of the investor. Homeowners usually elect to install BIPV for environmental reasons. Businesses may realize that an expensive and visible PV installation on a commercial building makes a bold public statement about environmental commitment. A growing number of architects are taking interest in solar design, incorporating PV as well as daylighting, passive construction, and solar thermal systems into their building plans. PV arrays provide striking building facades and may also be incorporated into window glass and roof tiling. In recent years thin-film architectural PVs have become available in a wide range of colors. Architect Steven Strong of Solar Design Associates has pointed out that many new technologies "take off" despite existing alternatives which fulfil the same need at lower cost [1998]. A notable example is the automobile; the first cars were slower, dirtier, less reliable, and far more expensive than horses. However, people bought these cars for status, curiosity,

or some other reason despite certain monetary loss. These initial purchases paved the way for continued innovation and economies of scale in the auto industry, eventually giving rise to vehicles which were competitive in their own right.

The PV industry is likewise growing at an impressive pace. However, photovoltaics must become competitive with conventional energy sources if they are to extend beyond their present small niche markets. In 1995 the US photovoltaic generating capacity was 333 MW, less than a single large coal plant, while the total generating capacity was 769530 MW [Carlin et al., 1997]. Further innovation and economies of scale may eventually allow PV to compete with fossil and nuclear power on a purely economic basis. The need for accurate predictions of solar savings will become more pressing as economics becomes an increasingly important driving force in the decision to invest in BIPV.

Much of this project is focused on developing software to calculate the solar savings from grid-tied BIPV systems. A number of solar simulation packages are commercially available. These programs are useful for estimating long-term photovoltaic energy generation, but they do not combine these results with time-dependent building loads and utility rate schedules on an hourly basis. This type of analysis is essential to evaluating the economics of a privately owned BIPV system.

1.2 Objective of Research

There are two primary goals motivating this project. The first objective is to develop a program for evaluating the performance of BIPV systems. This program should be intuitive enough that an engineer or architect with only a general knowledge of PV can use it to quickly estimate the performance of a proposed BIPV project. The modular energy simulation program TRNSYS [Klein et. al, 1997] was used to develop this program. TRNSYS provides a framework to link the components of an energy system, each of which is represented by an open-source Fortran subroutine. TRNSED, a menu-based graphical user

interface for TRNSYS, was employed to develop the front end for the BIPV simulation package. A new "five-parameter" photovoltaic model was developed for this program. Unlike the standard four-parameter TRNSYS PV component, the new five-parameter model is applicable to amorphous as well as crystalline PV modules. Chapter 3 explains the mathematical basis of the five-parameter model along with its implementation into a TRNSYS subroutine. The BIPV program has been named PHANTASM, for PHotovoltaic ANalysis and TrAnsient Simulation Method. The structure and use of this program is discussed in Chapter 4 and in the PHANTASM User's Manual [Fry, 1999].

The second project goal is to examine the economic feasibility of large-scale BIPV implementation in Wisconsin. Several utility-organized BIPV projects are presently underway.. Of the major Wisconsin utilities, Wisconsin Public Service Corporation (WPSC) has the most aggressive photovoltaic program. 6 high schools in WPSC's service area have rooftop-integrated arrays with a total capacity of 72 kWp [WPSC, 1998]. PHANTASM was used to determine the solar savings and optimal array orientation for 20 kWp rooftop arrays for three commercial buildings in Milwaukee. These simulations employed 1990 weather data for Milwaukee and historical electrical loads for the three buildings along with rate schedules from Wisconsin Electric, the Milwaukee utility. Chapter 5 discusses the data sets used for these simulations and Chapter 6 presents the results.

The economics of BIPV are also examined from the utility's point of view. EUSESIA, a TRNSYS package developed by Trzesniewski [1995], was used to investigate the utility impact of an ensemble of 20 kWp rooftop BIPV arrays. EUSESIA evaluates the average value of PV-generated kWh as well as PV's peak shaving potential relative to standard combustion turbine technology. Chapter 7 explains the methods and results of the utility study.

1.3 Literature Review

Several software packages for PV simulation are currently available. TRNSYS has been employed for a number of PV research projects at the UW Solar Lab and elsewhere. A mathematical method for deriving PV electrical characteristics from readily available manufacturers' data was developed by Townsend [1989]. Eckstein later incorporated this model into the standard TRNSYS PV component [1990]. The mathematical basis of this "four-parameter" model is addressed in Chapter 3. The PV F-chart program [Klein and Beckman, 1992] extrapolates long-term PV performance from the results of multiple TRNSYS simulations employing Typical Meteorological Year weather data. PV F-chart provides a quick and straightforward method for evaluating annual PV energy generation. However, it does not calculate hourly generation results and thus cannot be used to compare PV performance to electrical load profiles. Another PV simulator, Sandia National Lab's PVFORM [1994] does produce hourly output. These programs may be used to simulate performance for a wide range of PV systems and locations.

PHANTASM, developed for this work, differs from other PV simulators in two main respects. The first is that PHANTASM employs numerical iteration along an IV curve to determine PV output at the maximum power point. The new five-parameter PV model facilitates the simulation of amorphous modules. PVFORM and PV Design Pro, on the other hand, assume a baseline PV efficiency that varies with temperature. The second unique feature of PHANTASM is the capability to factor in the utility rate schedule and building load when calculating savings for grid-tied buildings. Demand charges may play an important role in solar savings, as shown in the case studies in Chapter 6.

Krom [1997] has carried out a simulation project similar to this one involving rooftop BIPV arrays for several buildings in the Madison area. Krom's study focuses on solar savings for buildings, accounting for both usage and demand savings. PV Forum was employed to generate hourly solar output. A spreadsheet analysis was then used to find annual solar

savings based on building loads and the rate schedules of Wisconsin Gas and Electric (MGE). The rate schedule analyses were essentially similar to those employed by PHANTASM, although the economic analysis was not automated. Krom also accounts for such economic factors as inflation, market discount for investment, and renewable energy subsidies specific to Wisconsin.

CHAPTER 2
Background

Photovoltaics are semiconductor devices that convert radiant energy directly into electricity. PV technology is simple, elegant, and reliable. It requires no fuel, produces no emissions, and involves no moving parts. The physics of photovoltaic energy conversion is outlined briefly in Chapter 3 in the context of developing mathematical models for PV modules.

As discussed in Chapter 1, photovoltaics are most economical in remote applications where utility service is unavailable. These remote applications may be divided into two broad categories. One type of remote application is the **direct-coupled** system. In a direct-coupled application the PV is connected directly to a DC load; the most common example is a water pump. A direct-coupled system does not include batteries for energy storage, so electricity is available only during daylight hours. Both a PV array and a load such as a pump motor have distinct current-voltage (IV) characteristics. The electrical characteristics of each device may be represented by curves on an IV graph (current as a function of voltage), and the system operates at the two curves' point of intersection. Since the electrical characteristics of PV are dependent on solar radiation and ambient temperature, the system operating point varies over the course of the day.

The second main type of remote PV application includes one or more batteries for electrical storage. Energy storage is essential if the system is to provide power after dusk. Examples include lighting in remote villages and parking lots, railroad signals, and vaccine refrigeration. Off-grid cabins and houses also usually include a battery bank for energy storage. Batteries are bulky and expensive and some energy loss is always inherent in storage. In addition, all batteries require periodic maintenance and charge control systems to prevent excessive charge or discharge. Despite these issues, PV storage systems have proven to be economical for a wide range of applications.

2.1 Components of a Grid-Tied BIPV System

This work focuses on a third type of PV application, the **utility interactive system**. A utility interactive system is employed in applications where utility service is already available. There is no need for battery storage because grid power may be used to supplement photovoltaic generation when the load exceeds available PV energy. BIPV systems in urban and suburban areas comprise the majority of utility-interactive photovoltaics. In a BIPV system, the load is simply the total energy consumption in the building. Most electrical appliances in grid-connected buildings employ AC, while PV arrays produce DC. For this reason a BIPV system must include an **inverter**, a device to convert photovoltaic DC to grid-voltage AC. The efficiency of most inverters is on the order of 90% to 95%.

A BIPV system also requires a **maximum power-point tracker**, or MPPT. The MPPT is an electronic device that monitors PV output and provides a constantly varying impedance such that the PV always operates near its point of maximum power along the IV curve. This issue is addressed in more detail in Chapter 3. The MPPT is usually purchased along with the inverter as a single unit. Trace Engineering and Omnion Power Engineering Corporation are the largest manufactures of inverter/MPPT units [1998]. A utility-interactive inverter has the capability to feed PV electricity back into the grid when PV generation exceeds the total building load. This energy is purchased by the utility, so in essence the whole grid is used as a storage medium for excess energy generation. The grid provides more efficient storage than a battery; transmission and distribution losses may be around 5% while battery cycle inefficiencies are on the order of 20%. Figure 2.1-1 illustrates the major components of a BIPV system.

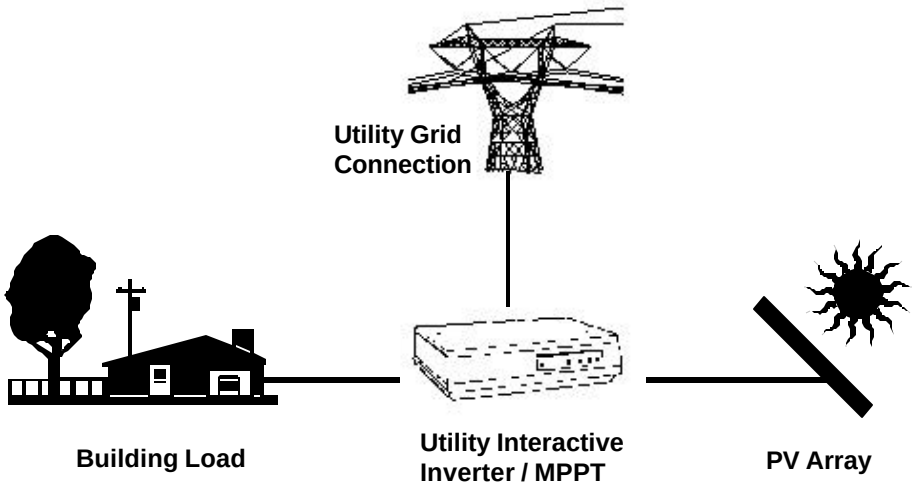

Figure 2.1-1: Schematic of a grid-tied BIPV System

2.2 Net Metering

An important issue is the economics of privately owned grid-tied PV systems is the price the utility pays for excess PV generation. During times when the utility experiences extreme loads and its generating capacity is pushed to the limit to avoid brown-outs, private generation may prove quite valuable. Under most circumstances, however, the value of parallel generation is equal to the wholesale operating cost of the most expensive plant in the generation mix at that time. For fossil and hydro plants in Wisconsin this cost is usually between $0.01 and $0.02 per kWh, and for nuclear plants it is even less [Trznesnieski, 1995].

Under a **net metering** policy a customer employing parallel generation may "turn back" the electric meter when excess energy is fed back into the grid. In this case the utility is essentially buying power at the retail rather than wholesale price. Under a net metering policy the utility subsidizes private on-site generation. Wind and diesel parallel generation as well as PV may also be subject to net metering policies. 22 states, including Wisconsin, currently regulate net metering practice [Wan and Green, 1998]. Wisconsin

utilities are required to provide net metering services to all BIPV customers. The software and analysis in this work assume that net metering is provided.

2.3 Electric Rates and BIPV

Both the operating cost for conventional plants and local climatic conditions are important in evaluating the feasibility of PVs. Retail utility rates vary greatly from one region to another, and these variations generally reflect the costs of generation. Strong and Scheller [1993] have summarized the standard residential rates for several municipal utilities, as shown in Table 2.3-1

Table 2.3-1: Residential electric rates in several US cities

City	***Residential Energy Usage Rate [$/kWh]***
Atlanta, GA	0.065
Denver, CO	0.074
Albuquerque, NM	0.100
San Diego, CA	0.130
Hilo, HI	0.143
New York, NY	0.157

Denver, for instance, has a sunny climate with abundant solar energy. However, low electric rates offset the advantages of climate when considering the economics of PV. On the other hand, high electric rates in New York compensate for a marginal solar climate. Of the cities shown in this table, Hilo and San Diego probably offer the most promise for PV, combining relatively high electric rates with favorable solar climates. This work focuses on PV in Wisconsin. The Midwestern climate is fairly sunny during the summer months, but solar energy is scarce for much of the year. Moreover, Wisconsin's electric

rates are among the lowest in the nation. It is important to take these issues into consideration when evaluating the results of this study.

2.4 Utility Interest in BIPV

The electric utility stands to benefit from distributed PV generation for several reasons. Power consumed at the point of generation requires no transmission or distribution, potentially reducing infrastructure costs. PV systems without batteries are simple and reliable, requiring little maintenance. Photovoltaic modules themselves very rarely fail or malfunction, although inverters do require occasional repair or replacement.

An important factor for utilities considering investing in PV is when photovoltaic performance is at its best. Ideally, PVs should perform well during those hours when the total draw on the utility is large. PV can more easily serve as a substitute for gas-fired peaking plants if photovoltaic output coincides well with extreme loads. This is always true to some extent since PV generation occurs during the daylight hours, and on average loads are greater during the day than at night. Utility loads are driven largely by weather, as is PV performance. For most utilities, the greatest loads occur during hot summer days. These days are often sunny, particularly in dry Western climates. Utilities in northern areas such as Wisconsin may also experience large loads during cold winter days because of electric heating usage. Exceptionally cold days may coincide with clear skies, although this correlation is weaker than for peak summer loads.

Cragan [1994] and Trzesniwski [1995] have shown that retrofitting electric domestic hot water systems with solar collectors can provide a significant benefit to the utility by reducing peak loads. Unlike thermal solar collectors, PVs perform better at low ambient temperatures than during hot periods. However, solar insolation is a more important consideration than ambient temperature in the performance of both thermal and PV systems. Thus, PV and thermal systems usually generate the large quantities of useful energy at the same times. Yet there is one major difference between the impact of PV

and solar domestic hot water (SDHW) systems on peak utility loads. SDHW systems include energy storage in the hot water tank, so an ensemble of SDHW systems may continue to impact the total utility load even after the sun has set. This energy storage can also help to level the load during cloudy periods in the daytime hours. Grid-tied PV systems do not generally include batteries for energy storage. This means that PV can help the utility only during sunny periods. Utility benefit will be greatly reduced if the sun is obscured by clouds during part of the day.

Commercial and industrial building owners also must consider issues of coincidental loads when evaluating the feasibility of a BIPV system. Commercial rate schedules often include demand charges, penalizing the customer for large instantaneous power consumption. PV has the potential to reduce demand charges, but only if it performs well when building loads are high. The hourly load patterns of some buildings prohibit PV demand reduction; a nightclub might be an example of such a building. Rate schedules for residential customers do not generally include demand charges. In this case the coincidence of load and generation does not affect solar savings.

2.5 Environmental Impact of PV

In the long term, environmental benefits may be the most important reason for the implementation of grid-tied PV. The environmental impact of PV is small when compared with all nonrenewable energy sources. Coal plants produce huge quantities of CO_2 as well particulates and oxides of sulfur and nitrogen. Of course, CO_2 is inherent in the combustion process and cannot be avoided. Scrubbers can reduce but not eliminate sulfur and particulate emissions. Gas-fired plants are cleaner than coal plants but still produce greenhouse gases. Atmospheric emissions from nuclear plants are negligible but radioactive waste is an incessant problem with no clear-cut solution. One can also make a strong argument that PV provides "greener" electricity than other renewable sources. This is certainly true when PV is compared to hydropower, which can drastically alter the flow of major rivers. Biomass combustion makes no net contribution to atmospheric CO^2

levels, but it does produce other emissions. Even wind power may produce a greater environmental impact than PV when its land requirements and impact on bird populations are taken into account.

Central PV plants do require a considerable investment in land area, but this is not an issue with distributed BIPV systems since they are mounted on building surfaces which would otherwise go unused. The only other environmental consideration in assessing the environmental impact of PV systems is the energy consumed in their manufacture. The manufacture of single crystal PV modules is quite energy intensive, relying on electric furnaces to melt and purify large quantities of silicon. The same is true, to a lesser extent, of polycrystalline modules. Amorphous silicon modules, manufactured using semiconductor chemical deposition processes, require less energy per unit module area. However, amorphous modules are less efficient and require a larger system to generate power output comparable with polycrystalline or single crystal modules. Module glass and metal mounting structures also contribute the energy requirements for PV system manufacture.

Kato et al. [1998] have compiled information on the energy consumed in the manufacture of single crystal, polycrystalline, and amorphous PV cells in Japan. This information was then combined with energy requirements for producing glass covers, inverters, and steel array support structures. The results of this study are presented in terms of the energy payback periods for 3 kWp rooftop arrays employing each of the three major PV technologies. Table 2.5-1 summarizes these results. Given present technology, the efficiency estimate for the amorphous case may be a bit optimistic. However, this study assumes a system lifetime of 20 years, while many current estimates place PV system lifetime at 25 or 30 years. The energy payback times presented here for polycrystalline and amorphous photovoltaics are encouraging.

White [1998] has compared the cradle-to-grave CO^2 emissions for four types of electrical power plants: coal, nuclear fission, wind turbine, and hypothetical nuclear fusion. This is

Table 2.5-1: Estimates of energy payback time for 3 kWp rooftop BIPV arrays manufactured and deployed in Japan

PV Technology	*Module Efficiency*	*Energy Payback Time*
Single Crystal	12.2%	8.9 years*
Polycrystalline	11.6%	2.2 years
Amorphous	8%	1.7 years

a very detailed study accounting for the energy content of a number of specialized materials required for building the plants as well as energy expended in procuring fuel. Not surprisingly, White's work shows the lifecycle CO^2 emissions from fossil plants to be much greater than those from the other three types. Table 2.5-2 compares White's emission calculations for coal, fission, wind and fusion to those of Kato et. al. [1998] for rooftop arrays employing the three main PV technologies.

Table 2.5-2: Life-cycle CO^2 emissions from coal, LWR fission, wind, fusion (hypothetical) and PV. From White [22] and Kato et al. [37].

Plant Type	*Capacity*	*Lifetime*	*Lifecycle CO^2 Emissions [g C / kWh]*	*Notes*
Coal	1000 MW	40 years	**336**	Conventional steam
Nuclear Fission	1000 MW	40 years	**4**	Liquid water cooled
Wind	25 MW	25 years	**4**	3 blade turbine, single speed
Nuclear Fusion	1494 MW	40 years	**1**	Deuterium-tritium fusion
Single Crystal PV	3 kWp	20 years	**61**	Rooftop array
Polycrystalline PV	3 kWp	20 years	**20**	Rooftop array
Amorphous PV	3 kWp	20 years	**17**	Rooftop array

* The single crystal energy payback time quoted in Table 2.5-1 assumes that $SiCl_4$, a biproduct of the manufacturing process with high energy content, is put to productive use in other industries. The energy content of $SiCl_4$ is subtracted from the total energy required to manufacture the module. Without this assumption, the energy payback time increases to 11.8 years.

Photovoltaics, particularly those employing polycrystalline and amorphous technology, produce much less CO^2 than coal. Gas turbine plants produce a bit less CO^2 per energy output than coal. Nevertheless, Table 2.5-2 shows that photovoltaics offer a vast improvement in CO^2 emissions over any fossil fuel combustion. Furthermore, this analysis does not consider the other emissions (CO, NO_x, SO_2, CH_4, particulates) which are virtually eliminated by using PV. The work of Kato et al. assumes that the electricity employed in PV manufacture is generated from Japan's mix of fossil, nuclear, and hydroelectric power. In an ideal "renewable energy economy" where this energy was supplied by installed PV capacity or another renewable technology, the lifetime CO^2 emissions from all three photovoltaic technologies would become negligible.

Wind, fission, and fusion all offer lower CO^2 emissions than PV. Each of these technologies presents its own difficulties, however. Nuclear fission, of course, generates radioactive waste. Commercially applicable fusion power has not yet been developed, and this situation that will not change in the foreseeable future. Wind turbines provide clean, renewable, and often economical power for both remote and utility-scale applications. Like hydropower, however, wind energy may only be effectively harvested in specific regions. The solar resource is also unevenly distributed, but not to the same extent as wind. If new renewable energy sources eventually comprise a major portion of utility generation, wind and PV may prove to be important complimentary power sources. Most US locations are significantly windier in winter than in summer [Elliot, 1986], while PV is generally most productive during the summer months.

2.6 Progress of PV in the Grid-Tied Market

Chapter 1 discusses the fact that adverse economics have not stopped the explosive growth of PV development and shipment, even in the grid-tied market. However, it is unlikely that environmental concerns and architectural design considerations will be able

to propel the BIPV industry indefinitely. Photovoltaic shipments will eventually "top out" unless large-scale grid-tied PV generation can compete in the energy marketplace.

The Sacramento Municipal Utility District (SMUD) has an ambitious solar energy program including both PV and solar thermal systems. In the SMUD's PV Pioneers program, residential and commercial customers pay the utility to mount PV arrays on their buildings. The building owner sees no economic benefit from this program as the PV generation is fed directly into the grid without going to satisfy the building owner's loads. Nevertheless, SMUD cannot install enough systems to keep up with customer enrollment demand.

In addition to rooftop distributed generation, SMUD has installed grid-connected PV capacity at Hedge, a substation. SMUD has experimented with both fixed PV arrays and single-axis tracking systems. Table 2.6-1 summarizes the costs of SMUD's residential and substation systems installed from 1993 to 1995 [Osborn and Collier, 1996].

Table 2.6-1: Cost improvements in SMUD's PV installations from 1993 to 1995

PV Installation	***Tracking System***	***Capacity Cost [$/kWp]***	***30-Year Lifetime Energy Cost [$/kWh]***
1993 Substation	Fixed Array	$10.15	$0.32
1993 Residential	1-Axis Tracking	$8.78	$0.23
1994 Substation	Fixed Array	$7.75	$0.21
1994 Residential	Fixed Array	$7.13	$0.20
1994 Substation	1-Axis Tracking	$6.97	$0.19
1995 Residential	1-Axis Tracking	$6.87	$0.18
1995 Substation	1-Axis Tracking	$6.62	$0.18

SMUD believes (perhaps a bit optimistically) that the price for installed PV may drop below $3 per kWp by 2000. However, the trends shown in Table 2.5-1 are quite

encouraging. At $3 per kWp, the mean lifetime energy cost will be comparable to that of energy from a gas-fired peaking plant. SMUD refers to this situation, in which PV finally becomes competitive without relying on external subsidies, as "sustained orderly development" [Holihan, 1997].

SMUD has two major advantages over Wisconsin utilities in profitably implementing grid-tied PV systems. The first is a favorable climate for solar power. Summers in central California are nearly cloudless and winters skies are often clear as well. The second advantage is simply that SMUD has a head start in using PV technology, helping to reduce the costs of installation and system administration. As module prices continue to fall, however, PV may prove to be economical in Wisconsin. Other factors which could potentially aid PV's penetration of the grid-tied market are carbon taxes on utility generation and rising fuel prices, particularly for natural gas.

CHAPTER 3

Photovoltaic Models

In any simulation scheme involving photovoltaic systems, one important choice is the selection of a mathematical PV model. This model should predict how PV current and voltage will vary with ambient temperature and illumination conditions. PV simulation programs have been written for years, and during this time many models have been developed. A variety of schemes in which a PV is treated as an equivalent circuit have been summarized by Townsend [2].

This chapter begins with a qualitative overview of the physics involved in the photovoltaic conversion process. The mathematical bases for three PV models are then introduced, along with comparison analyzing the relative merits of these models. Three main criteria are considered in evaluating the models. The first is versatility: what range of PV modules and systems can the model handle? Accuracy is the second issue: what is the physical basis and how closely can the model replicate manufacturers' data? The final issue is computational speed. This criterion is of secondary importance for this work, although it may be more critical for other applications.

Speed may be an important issue in applications in which a PV is coupled directly to a load such as water pump and/or employs battery storage. Simulating such systems involves simultaneously finding the current-voltage characteristics for a PV and another device, often requiring extensive iteration between the two. Grid-tied applications employing a maximum power point tracking device (MPPT), however, do not require that the program iterate between the PV and another device. This work deals only with modeling grid connected building-integrated PV systems, so using a relatively slow-running is not a major concern.

Some simulations for maximum power tracking systems do not determine current-voltage relationships in a PV array. Instead, it is assumed that the PV has some baseline

efficiency for converting sunlight into electricity at reference conditions. This efficiency may vary with insolation level and module temperature. Sandia National Laboratory's PV Forum software uses such a scheme[1]. However, neglecting IV calculations may result in some loss of accuracy if maximum power performance does not vary linearly with temperature or radiation. The maximum power behavior of amorphous photovoltaics such as the Millennia PV line from Solarex may display such nonlinearity. [4].

The so-called "four parameter" model is a widely used model with a semi-physical basis. Discussed by Beckman and Townsend [2], this model treats a PV as an irradiance-dependent current source connected in parallel with a diode and in series with a resistor and the load. The four parameters appearing in the IV equations are the light current I_L, the series resistance R_s, and two diode characteristics I_o and γ. These parameters are not measurable quantities and are not generally included in manufactures' data. As a result, they must be determined from systems of IV equations at various operating points; these points are taken from catalog data. One important consideration is that this model does not accurately reproduce the IV characteristics of amorphous silicon PV modules. Eckstein incorporated the four parameter model into a TRNSYS component [3].

The final system evaluated here is a five-parameter model that adds a shunt resistance R_{sh} to the four-parameter scheme described above. The second resistance makes the five parameter model more computationally intensive and also calls for an additional piece of catalog data. However, this model has the significant advantage of being applicable to both crystalline and amorphous PVs. In this work, Eckstein's code for the four-parameter model was modified to account for the fifth parameter.

3.1 Band Structure, p-n Junctions, and the Photovoltaic Effect

A brief description of the physics behind photovoltaics is helpful in understanding the origin of the equivalent circuits used to model these devices. Photovoltaic cells are semiconductor devices; the vast majority of commercial PVs are fabricated from silicon.

A PV cell may consist of a single crystal, a number of smaller crystals (polycrystalline), or it may lack crystal structure all together (amorphous). Other semiconducting materials such as gallium arsenide are employed in PVs for extraterrestrial or sun concentrator applications, but this description will concern a silicon PV cell.

In a solid material, not all electrons are necessarily bound to a particular atom. Unbound electrons occupy a group of energy states known collectively as the **conduction band**. In the presence of an electric field, these electrons will respond by moving against the field, producing an electric current. Metals contain many conduction band electrons and thus have very low electrical resistivity. Semiconductors contain orders of magnitude fewer conduction electrons than do metals, but their numbers are still significant. Those electrons which are bound to atoms in states farthest from the nucleus are called **valence electrons**, and they collectively form the **valence band**. A key point is that under certain circumstances electrons may jump from the valence band to the conduction band or vice versa.

A silicon atom contains four valence electrons, and in a crystal each valence electron contributes to a chemical bond linking the silicon atom to one of its neighbors. The following diagram is a two-dimensional illustration of this arrangement:

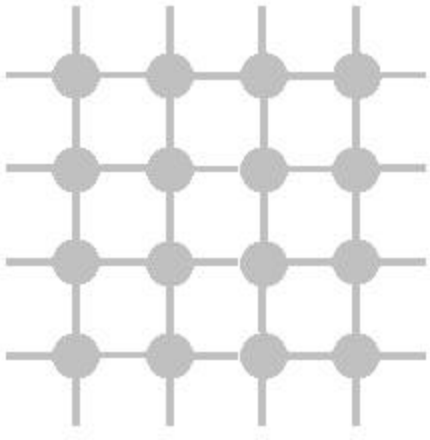

Figure 3.1-1: Two-dimensional crystal lattice

In a process called **doping**, specific impurities are added to the silicon lattice. An **n-type dopant** (n for “negative”) is an atom with one more valence electron than silicon; the most common example is phosphorus. This extra electron cannot fit into the crystal lattice and is forced into the conduction band. A **p-type dopant** (for "positive") such as boron has one fewer valence electron than does silicon. In this case, one chemical bond is absent from the regular lattice arrangement. This missing bond is referred to as a valence band **hole**. Conduction band electrons are more energetic than valence band electrons. Thus, a conduction electron will “fall” into the valence band to fill a hole and release some energy in the form of light or atomic vibrations, if given the chance. The effect of n-type and p-type dopants on the silicon lattice structure is shown in this diagram:

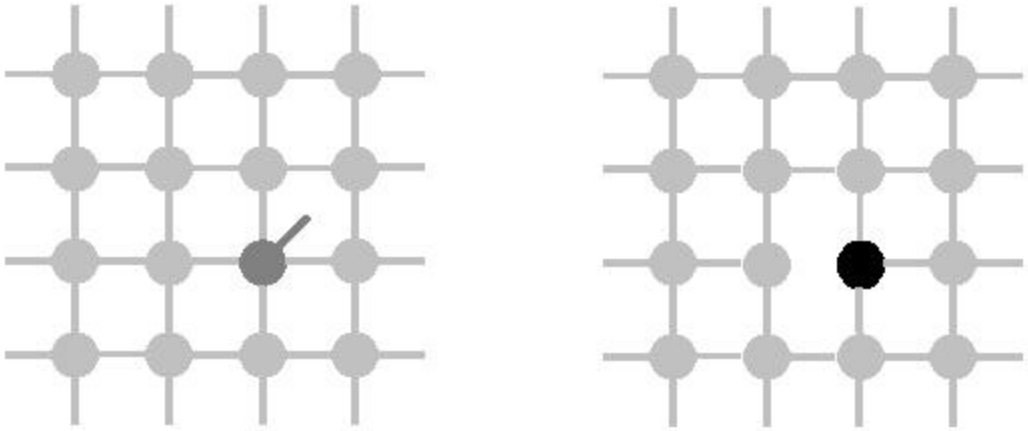

Figure 3.1-2: n-Type (left) and p-Type (right) Dopants

A **p-n junction** is formed when n-type and p-type semiconductors are placed in contact. In such a device, some of the excess conduction electrons in the material quickly migrate to the p-type material to fill in valence holes. This gives rise to a strong, permanent electric field in the immediate vicinity of the junction, as shown below:

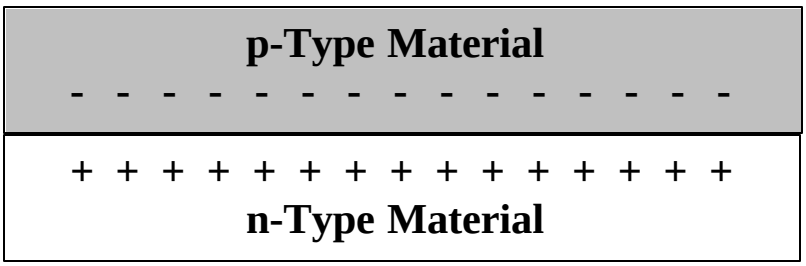

Figure 3.1-3: A p-n Junction

p-n junctions are commonly employed in diodes as current rectifiers. If a diode is placed in a circuit, current will flow freely from the n-type to p-type material. However, very little current can flow in the opposite direction even if driven by a very strong voltage. Light-emitting diodes and diode lasers (used in CD players) are designed to produce near infrared or visible light when electrons drop from the conduction band to fill valence holes.

A PV cell is essentially a large diode that produces a voltage when exposed to incident light. It may be considered to be a light-emitting diode "run backward;" the analogy is similar to a heat engine and a refrigerator. The **semiconductor bandgap** is the difference in energy between valence and conduction bands. It is a material-dependent property; in undoped silicon it has a value of 1.12 electron-volts or 1.79×10^{-19} joules. An incident photon with at least this much energy may interact with a valence electron in the p-type material, forcing it up into the conduction band. Any photon with a wavelength less than about 1100 nm has sufficient energy to initiate this reaction. This wavelength corresponds to radiation in the near infrared portion of the spectrum.

If the PV cell is connected to a load in a completed circuit, the new conduction band electron will be repelled by the excess negative charge in the p-type side of the PV cell. It travels through the circuit, producing a current through the load.

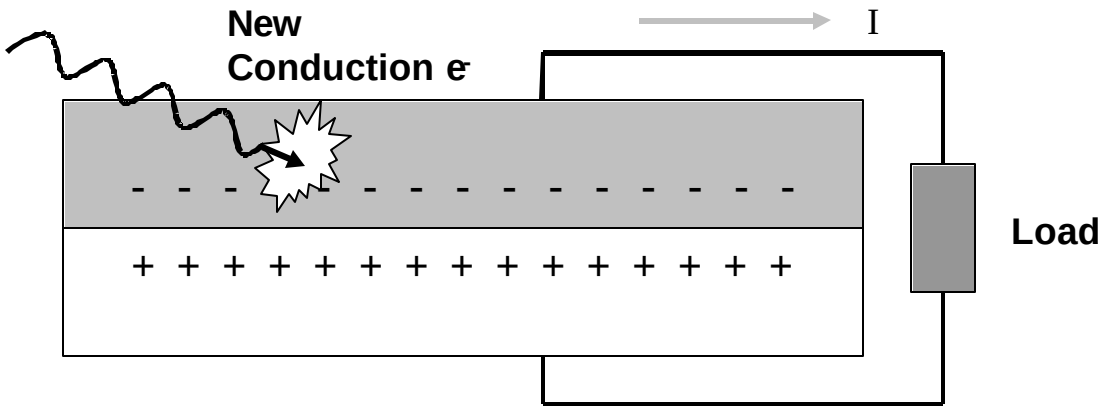

Figure 3.1-4: The Photovoltaic Effect – Incident Light Moves an electron from the Valence Band to the Conduction Band

3.2 Four-Parameter Photovoltaic Model: Equations and Solution Techniques

The behavior of the four-parameter PV model is described by Beckman and Townsend [2,5] and incorporated into a TRNSYS component by Eckstein [3]. This section summarizes the derivation of the model equations as well as the numerical techniques employed by Townsend and Eckstein in solving them. The model assumes that an "ideal" PV may be modeled as an irradiance-dependent current source in parallel with a diode. The diode provides a means for some current to be shunted across the load without actually reaching it. Physically, this is equivalent to a photoelectron falling back into a valence hole before leaving the semiconductor material; if this occurs the electron can no longer contribute to useful current. Since a PV is a large p-n junction, its current-shunting behavior may be reasonably approximated with a diode. In addition to the photocurrent source and diode, a single resistor is added to the model to account for ohmic losses as current travels through the PV. The equivalent circuit in this model is as shown in Figure 3.2-1:

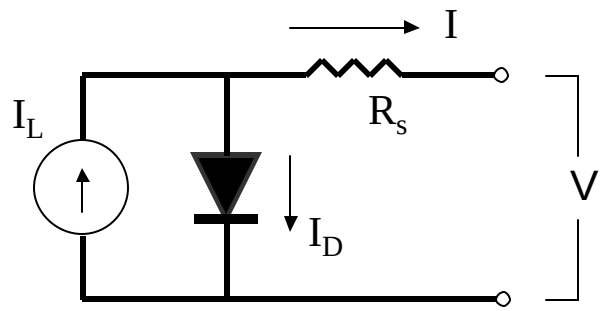

Figure 3.2-1: Equivalent Circuit in the Four-Parameter Model

Here, I and V represent the current and voltage at the load. The useful power generated by the PV is the product of these two quantities. The photocurrent I_L is proportional to the irradiance on the PV. The diode current I_D may be written in terms of the diode reverse saturation current I_o and a diode parameter γ:

$$I_D = I_o\left[\exp\left(\frac{q}{gkT_c}(V + IR_s)\right) - 1\right] \qquad \text{Eq. 3.2-1}$$

The nomenclature in this expression is as follows:

g	dimensionless diode curve-fitting factor, with a minimum possible value equal to the number of cells in series in the module N_s
I_D	diode current (A)
I_o	reverse saturation current; the current that will flow "backward" through the diode if subjected to a large reverse bias (A)
k	Boltzmann constant: 1.381×10^{-23} J/K
q	electron charge: 1.602×10^{-19} C
R_s	module series resistance (Ω)
T_c	cell temperature (K)
V	voltage across the PV module (V)

In an ideal diode, the curve-fitting factor γ is equal to 1. Similarly, γ is equal to the number of cells in series N_s in an ideal PV module. Imperfections in any real PV cause γ

to be larger, but it is helpful to employ N_s as a lower bound [2]. The photocurrent may be added to the above diode current expression to determine the total current through the load:

$$I = I_L - I_o\left[\exp\left(\frac{q}{gkT_c}(V + IR_s)\right) - 1\right] \qquad \text{Eq. 3.2-2}$$

This expression defines the IV characteristics for the four-parameter model. Note that the reverse saturation current I_o may be written in terms of material characteristics and temperature [2]:

$$I_0 = DT_c^{\,3}\exp\left(\frac{-qe}{AkT_c}\right) \qquad \text{Eq. 3.2-3}$$

The constant A is γ divided by the number of cells wired together in series in the module, N_s.

$$A = \frac{g}{N_s} \qquad \text{Eq. 3.2-4}$$

D is constant and ε is the semiconductor bandgap energy, 1.12 eV for silicon. A, the "diode completion factor," is dimensionless quantity with a minimum value of 1.

Two of the model parameters, R_s and γ, are assumed to be constant. However, the other two parameters are functions of the PV operating conditions. I_o changes with temperature and I_L is a function of incident radiation. Given reference values of 298 K and 1000 W/m^2, I_o and I_L are determined as follows:

$$\frac{I_L}{I_{L,ref}} = \left(\frac{T}{T_{ref}}\right)^3 \qquad \text{Eq. 3.2-5}$$

$$I_L = I_{sc,ref} \frac{G}{G_{ref}}$$ Eq. 3.2-6

Equation 3.2-2 may be used to predict the current-voltage behavior of the model at any temperature and radiation conditions, assuming that the values of the four parameters $I_{L,ref}$, $I_{o,ref}$, γ, and R_s are known. However, these are not easily measured physical quantities and are not available from manufacturer's data. Therefore, they must be evaluated from other information that can be easily obtained from the manufacturer. A system of four equations is necessary to solve for these values. The four equations are all derived from the general IV expression 3.2-2. Three of these result from substituting values into the equation at the reference open circuit, short circuit, and maximum power point conditions as follows:

$$0 = I_{L,ref} - I_{o,ref}\left[\exp\left(\frac{qV_{oc,ref}}{gkT_{c,ref}}\right) - 1\right]$$ Eq. 3.2-7

$$I_{sc,ref} = I_{L,ref} - I_{o,ref}\left[\exp\left(\frac{qI_{sc,ref}R_s}{gkT_{c,ref}}\right) - 1\right]$$ Eq. 3.2-8

$$I_{mp,ref} = I_{L,ref} - I_{o,ref}\left[\exp\left(\frac{q}{gkT_{c,ref}}\left(V_{mp,ref} + I_{mp,ref}R_s\right)\right) - 1\right]$$ Eq. 3.2-9

The reverse saturation current I_o for any diode is a very small quantity, on the order of 10^{-5} or 10^{-6} amperes. This minimizes the impact of the exponential term in Eq. 3.2-8, so it safe to assume that the photocurrent equals the short circuit current:

$$I_{L,ref} \approx I_{sc,ref}$$ Eq. 3.2-10

Eq. 3.2-7 may then be solved for I_o. This value for I_o, along with I_L from Eq. 3.2-10, may be substituted into Eq. 3.2-9. Some algebra then yields:

$$\gamma = \frac{q\left(V_{mp,ref} - V_{oc,ref} + I_{mp,ref} R_s\right)}{kT_{c,ref} \ln\left(1 - \frac{I_{mp,ref}}{I_{sc,ref}}\right)} \qquad \text{Eq. 3.2-11}$$

At this point the problem has been reduced to a system with two unknowns (R_s and γ) and one equation. An additional expression involving information available from the manufacturer is necessary to find the remaining two parameters. Townsend [2] has shown that the temperature coefficient of open circuit voltage may be used to provide an additional equation. Eq. 3.2-7 may be solved for the open circuit voltage $V_{oc,ref}$. Substituting Eq. 3.2-5 into this expression and then differentiating with respect to temperature yields the following (after some algebra)*:

$$\left.\frac{\partial V_{oc}}{\partial T}\right|_{ref} = \mu_{voc} = \frac{\gamma k}{q}\left[\ln\left(\frac{I_{sc,ref}}{I_{o,ref}}\right) + \frac{T_c \mu_{isc}}{I_{sc,ref}} - \left(3 + \frac{qe}{AkT_{c,ref}}\right)\right] \qquad \text{Eq. 3.2-12}$$

For any particular value of R_s, γ may be determined explicitly from Eq. 3.2-11. Then γ is substituted into Eq. 3.2-12 to determine the open-circuit voltage temperature coefficient. At the correct value of R_s and γ, the catalog value should match the analytical value. Eckstein's four-parameter TRNSYS component uses a numerical bisection method to solve for series resistance value that forces the left and right sides of Eq. 3.2-10 to be equal. The upper limit for R_s is that value such that A = 1. The lower limit for R_s is 0; it does not make physical sense to define a negative series resistance.

As mentioned above, R_s and γ are assumed to be constants which do not change with radiation or temperature. However, the other two* parameters in the model, I_o and I_L, are

* Again, the 1 in Eq. 3.2-5 was neglected in this calculation. Beckman [6] has shown numerically that the changes in the IV curve which result when the 1 is neglected are insignificant.

not constant. Once their reference values, are known, Eckstein's TRNSYS component determines I_o and I_L at each simulation timestep using Eqs. 3.2-5 and 3.2-6. Voltage is an input for the TRNSYS type, so the general IV expression, Eq. 3.2-2, is employed to find the operating current. Since this equation is implicit in *I*, Newton's method is used to solve for the current numerically.

3.3 Efficiency Coefficient Model

The four parameter model discussed above may be used to determine current as a function of load voltage. Being able to predict current-voltage characteristics is essential for modeling remote PV systems which are directly coupled to a load or battery. Of course, one may use this model's IV curve to determine the maximum operating power at given conditions. For grid-tied applications such as those studied in this work, the maximum power is actually the only important result. This opens the possibility of using a model that determines the maximum operating power directly without considering the IV characteristics. Such a scheme would be mathematically and computationally simpler than the four-parameter model.

The module efficiency is defined as the ratio of useful electrical power output to incident solar power.

$$h \equiv \frac{P_{mp}}{GA} \qquad \text{Eq. 3.3-1}$$

G represents insolation in W/m^2 and *A* is module area in m^2. Manufacturers may quote a "reference efficiency." This is simply the efficiency of the module at reference testing conditions, generally an insolation of 1000 W/m^2 and a module temperature of 25 C. The maximum power may be given as the product of current and voltage at the maximum power point, so the reference efficiency can be expressed as:

$$h_{ref} \equiv \left(\frac{V_{mp} I_{mp}}{G_{ref} A} \right)_{T=T_{ref}} \qquad \text{Eq. 3.3-2}$$

The reference efficiency of terrestrial PV modules ranges from about 0.03 for small amorphous battery charging modules to 0.14 for the best monocrystalline modules.

The efficiency coefficient model is based on two important assumptions. The first assumption is that the efficiency is independent of the intensity of incident radiation. For light levels greater than about 400 W/m^2 this assumption appears to be fairly accurate. It breaks down at lower levels, but accurate modeling is less important at these low levels since little useful output is produced anyway. The validity of this "radiation-independent efficiency" assumption will be discussed in more detail at the end of this section. The second assumption is that the efficiency varies linearly with temperature, and that the constant of proportionality for this relationship may be determined from catalog data.

Given these assumptions, the chain rule of calculus may be used to determine the derivative of efficiency with respect to temperature:

$$\frac{dh}{dT} = \frac{dh_{ref}}{dT} = \frac{1}{G_{ref} A} \frac{d}{dT} \left(V_{mp} I_{mp} \right) = \frac{1}{G_{ref} A} \left(I_{mp} \frac{dV_{mp}}{dT} + V_{mp} \frac{dI_{mp}}{dT} \right) \qquad \text{Eq. 3.3-3}$$

Unfortunately, the temperature coefficients of V_{mp} and I_{mp} are not generally available from catalog data. However, they may determined from μ_{Voc} and μ_{Isc} if every point on the IV curve is assumed to translate linearly with a temperature change. In other words, a change in temperature from reference conditions will cause the IV curve to "stretch" or "contract" in both the *I* and *V* directions, but the overall form of the curve will not change. For instance, consider that the operating temperature drops below the reference temperature of 25 C. In this case V_{oc} will increase and I_{sc} will decrease, and the rest of the curve will follow. This idea is illustrated in Figure 3.3-1; the magnitude of the change has been exaggerated for the sake of clarity:

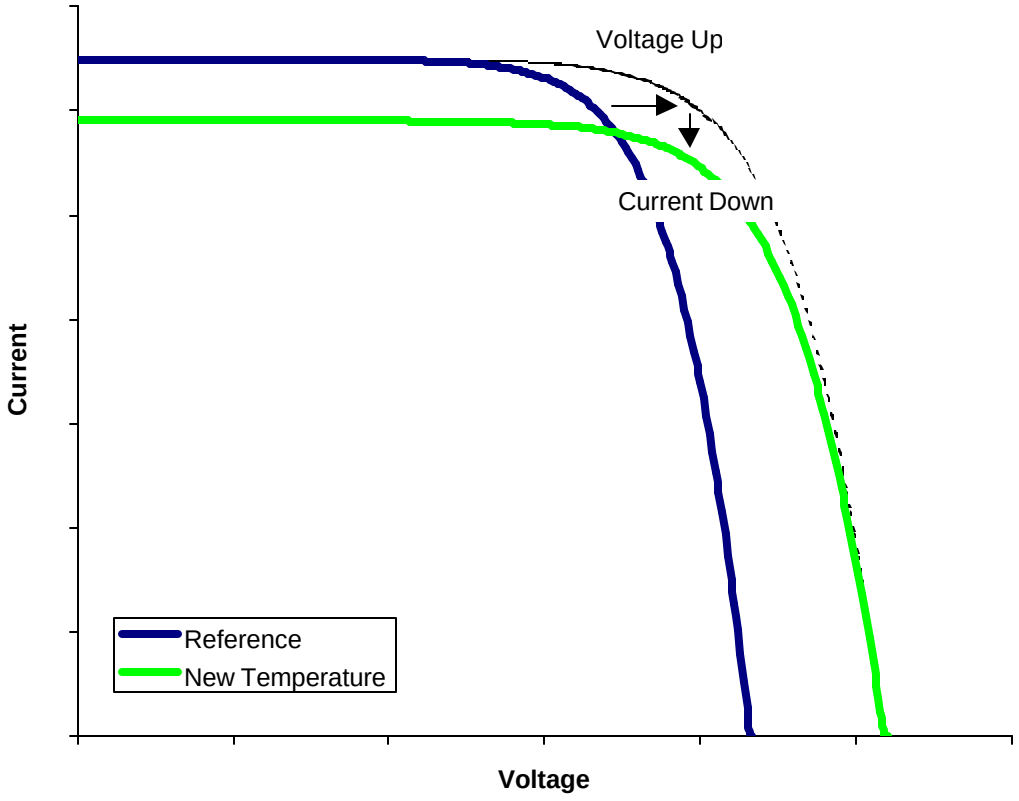

Figure 3.3-1: The IV Curve "Stretches" as Temperature Moves from the Reference Value

If the whole curve scales with temperature in this manner, we may use the following relations to find the temperature coefficients of V_{mp} and I_{mp}:

$$\frac{dV_{mp}}{dT} = \frac{V_{mp,ref}}{V_{oc,ref}} \frac{dV_{oc}}{dT} = \frac{V_{mp,ref}}{V_{oc,ref}} m_{Voc} \qquad \text{Eq. 3.3-4}$$

$$\frac{dI_{mp}}{dT} = \frac{I_{mp,ref}}{I_{sc,ref}} \frac{dI_{sc}}{dT} = \frac{I_{mp,ref}}{I_{sc,ref}} m_{Isc} \qquad \text{Eq. 3.3-5}$$

Substituting these expressions into Eq. 3.3-3 produces the following result for the temperature dependence of efficiency:

$$\frac{dh}{dT} = \frac{1}{G_{ref} A} V_{mp,ref} I_{mp,ref} \left(\frac{m_{Voc}}{V_{oc,ref}} + \frac{m_{Isc}}{I_{sc,ref}} \right) \qquad \text{Eq. 3.3-6}$$

Using Eq. 3.3-6 and the definition of efficiency produces the following expression for maximum power output as a function of T and G:

$$P_{\max} = \frac{G}{G_{ref}} V_{mp,ref} I_{mp,ref} \left[1 + \frac{dh}{dT} \left(T - T_{ref} \right) \right] \qquad \text{Eq. 3.3-7}$$

All of the quantities in this expression may be obtained from catalog data. Manufacturer's specifications for the Siemens SR100 crystalline module were used to compare the efficiency coefficient model with the four-parameter model. Figure 3.3-2 illustrates the temperature dependence in the two models:

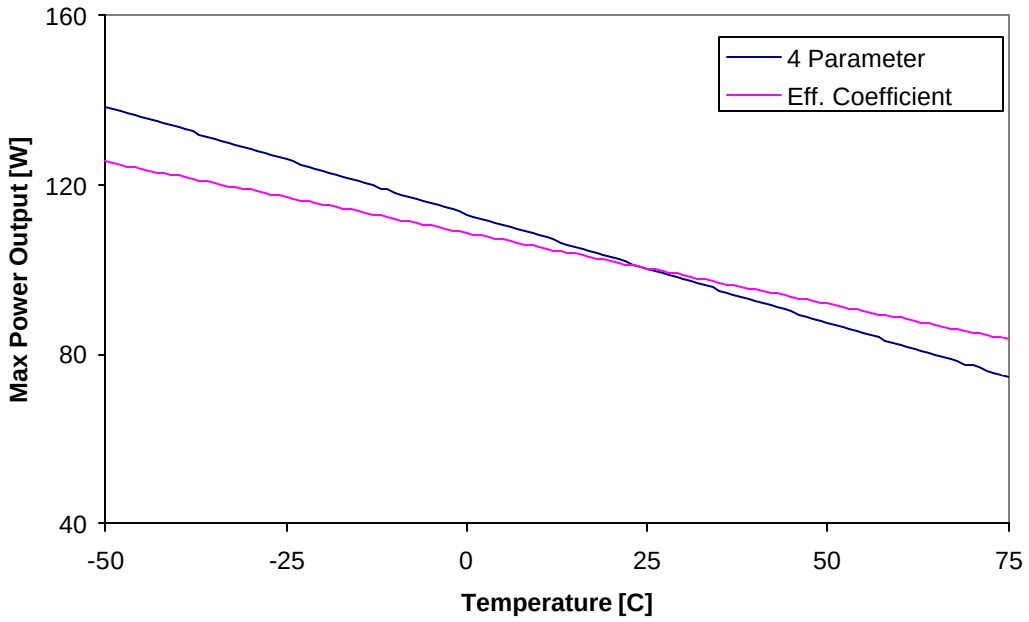

Figure 3.3-2: Temperature Dependence of Maximum Power in Four Parameter and Efficiency Coefficient Models

Both models produced maximum power outputs which are essentially linear with temperature, although the four parameter model predicts a slightly larger temperature

dependence. This suggests that the IV curves generated by the four-parameter model do not obey the temperature behavior illustrated in Figure 3.3-1.

The efficiency coefficient model also assumes that η does not change with insolation. Although the efficiency coefficient model does not calculate the efficiency directly, the four parameter model makes no such assumption. A comparison of the two models, again using the Siemens SR100 catalog data, produced the results shown in Figure 3.3-3.

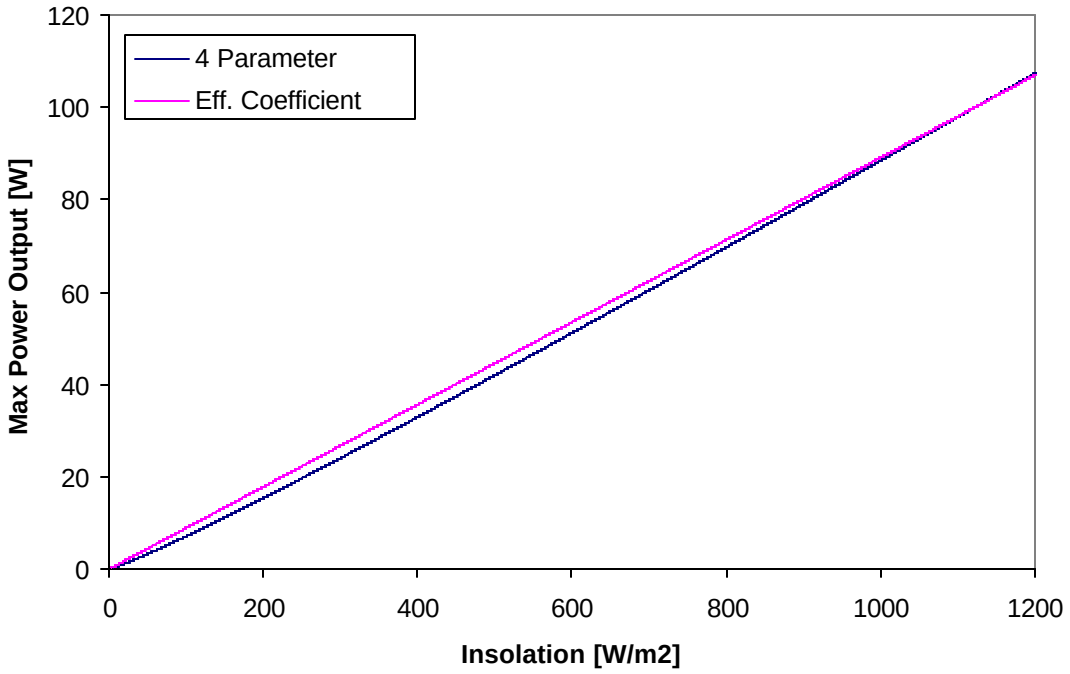

Figure 3.3-3: Insolation Dependence of Maximum Power in the Efficiency Coefficient and Four Parameter Models

Below the reference insolation of 1000 W/m^2 the efficiency coefficient model predicts slightly greater output than the four parameter model. In the four parameter model the efficiency is slightly less than in the efficiency coefficient model at low insolation levels. Graphing the efficiency directly presents this result more clearly, as shown in Figure 3.3-4:

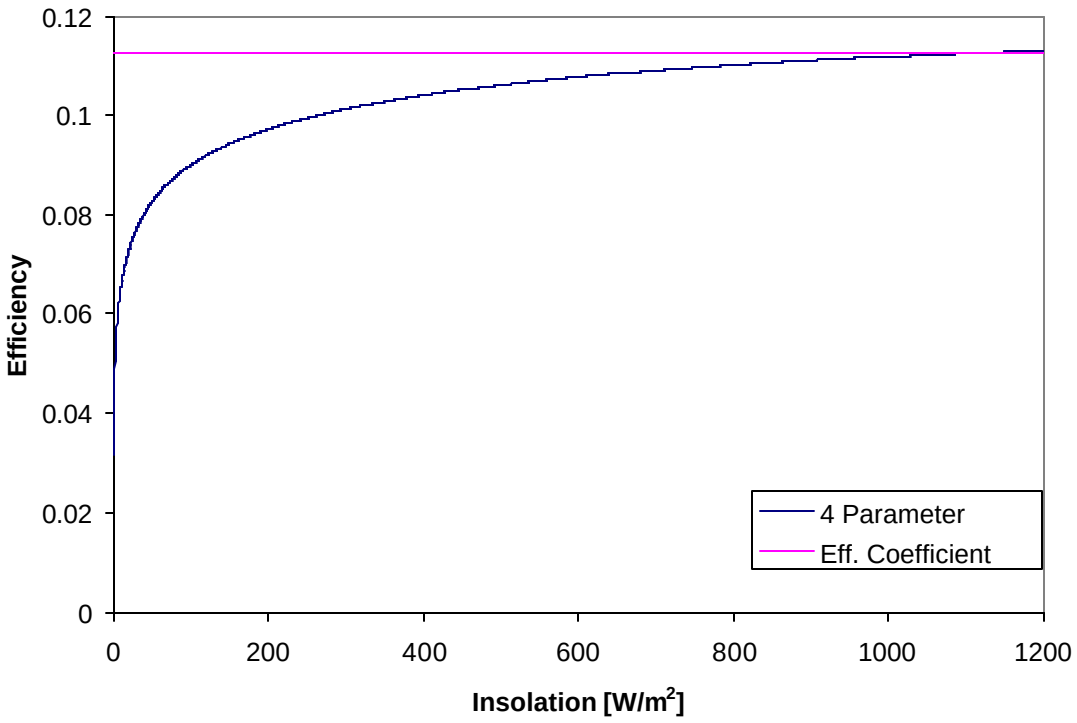

Figure 3.3-4: Insolation Dependence of Efficiency in the Four Parameter and Efficiency Coefficient Models

It is clear that at low insolation levels the efficiency coefficient overestimates the PV performance. At first glance, this graph suggests that the efficiency coefficient model may be too inaccurate to consider as a simulation option. However, above 600 W/m^2 or so, where most PV energy output actually occurs, the two models agree fairly closely. Actual simulation results provide a more valid basis for judgement. Year long simulations were run for the two models using TMY data from four locations. In each case a single Siemens SR100 was modeled, facing south with a slope equal to the location latitude. The results are shown in Table 3.3-1.

	Four Parameter Model	h Coefficient Model
Washington DC	152 kWh	157 kWh
Madison, WI	154 kWh	158 kWh
Miami, FL	170 kWh	179 kWh
Albuquerque, NM	244 kWh	247 kWh

Table 3.3-1: Simulation Results for Four Parameter and Efficiency Coefficient Models

In each case the efficiency coefficient model predicted 1% to 5% more energy production than the four parameter model. The two models agree most closely for Albuquerque because in this sunny climate radiation levels are generally higher than at the other locations. Figure 3.3-4 shows that the efficiency coefficient model agrees most closely with the four parameter at high radiation levels.

3.4 Five - Parameter Photovoltaic Model

The four-parameter model has been implemented into many TRNSYS programs, and it reliably predicts the performance of single crystal and polycrystalline PV arrays. The four parameter model assumes that the slope of the IV curve is flat at the short-circuit condition:

$$\left(\frac{dI}{dV}\right)_{v=0} = 0 \qquad \text{Eq. 3.4-1}$$

However, this assumption is not generally valid for amorphous photovoltaics. The short-circuit IV slope is finite and negative, so the four-parameter model cannot reproduce IV characteristics typical of amorphous silicon. A modification is necessary to broaden the model to include amorphous PVs.

The "five-parameter model" introduces a second resistor in the PV equivalent circuit. This electrical behavior of the PV is represented in the following diagram:

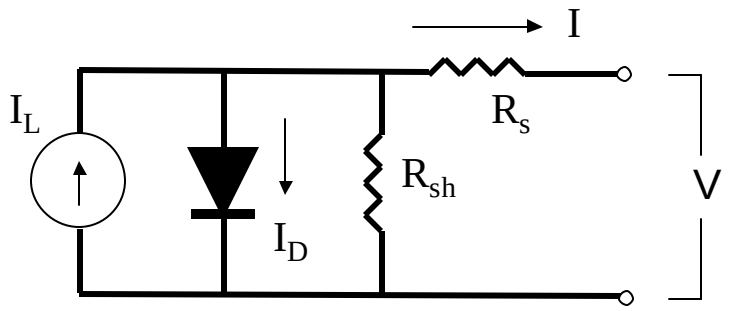

Figure 3.4-1: Equivalent Circuit in the Five-Parameter Model

A shunt resistance R_{sh} has been added to the standard four parameter model. The magnitude of the IV slope at short-circuit is related inversely to the shunt resistance. As R_{sh} approaches infinity, this arrangement becomes identical to the four-parameter model. Thus, all the equations employed in the five-parameter model reduce to those in the simpler four parameter scheme for very large values of R_{sh}.

The IV equation for the five-parameter model is:

$$I = I_L - I_o\left[\exp\left(\frac{q}{gkT_c}(V + IR_s)\right) - 1\right] - \frac{V + IR_s}{R_{sh}} \qquad \text{Eq. 3.4-2}$$

3.5 Determining the Shunt Resistance

Adding the shunt resistance of course introduces another unknown value into the model. Like I_L, I_o, γ, and R_s, the shunt resistance is not an easily-measured physical quantity. Thus, it must be determined from information available from the manufacturer. The primary effect of the shunt resistance on the IV characteristic is to change the short-circuit slope. Thus, it is logical to use the measured value of this slope to back out a value for R_{sh}. The short-circuit slope is *not* a value which is generally included in the list of catalog specifications. However, it is possible to approximate this value if the IV curve is available. This is often the case for amorphous modules.

In order to determine the the mathematical relationship between the short-circuit slope and the shunt resistance it is first necessary to differentitate the IV expression Eq. 3.4-2 with respect to voltage. Performing the differentiation, setting V to 0 and I to $I_{sc,ref}$ yields:

$$m = -\frac{q}{kgT_{c,ref}} I_{o,ref} (1 + R_s m) \exp\left(\frac{q}{kgT_{c,ref}} I_{sc,ref} R_s \right) - \frac{(1+m)R_s}{R_{sh}} \qquad \text{Eq. 3.5-1}$$

where the variable m is equal to the short-circuit slope $\left(\frac{dI}{dV} \right)_{v=0}$ Solving this expression for R_{sh} produces:

$$R_{sh} = \frac{-(1+m)R_s}{m + \frac{q}{kgT_{c,ref}} I_{o,ref} (1 + mR_s) \exp\left(\frac{q}{kgT_{c,ref}} I_{sc,ref} R_s \right)} \qquad \text{Eq. 3.5-2}$$

A difficulty with this expression is that, in addition to the short-circuit slope, it includes the parameters γ and R_s which cannot be explicity written in terms of the manufacturers' parameters. Thus, solving for these values simultaneously would involve a computationally intensive two-stage iteration scheme. Fortunately, Beckman [6] has suggested that this expression may be simplified with the approximation:

$$R_{sh} \approx \frac{-1}{\left(\frac{dI}{dV}\right)_{V=0}} \qquad \text{Eq. 3.5-3}$$

To test the validity of this approximation several sample IV curves with different shunt resistances values were produced using the five-parameter model. An EES program was written for this purpose; EES will readily solve the implicit and nonlinear IV equation. The values for the other four parameters had been previously determined using the four-parameter model for a Siemens 100SR crystalline module as follows:

R_s	=	0.1101 Ω
γ	=	64.65
I_L	=	6.50 A
I_o	=	0.00001429 A

The resulting IV curves are shown in Figure 3.5-1:

The resulting IV curves are shown in Figure 3.5-1.

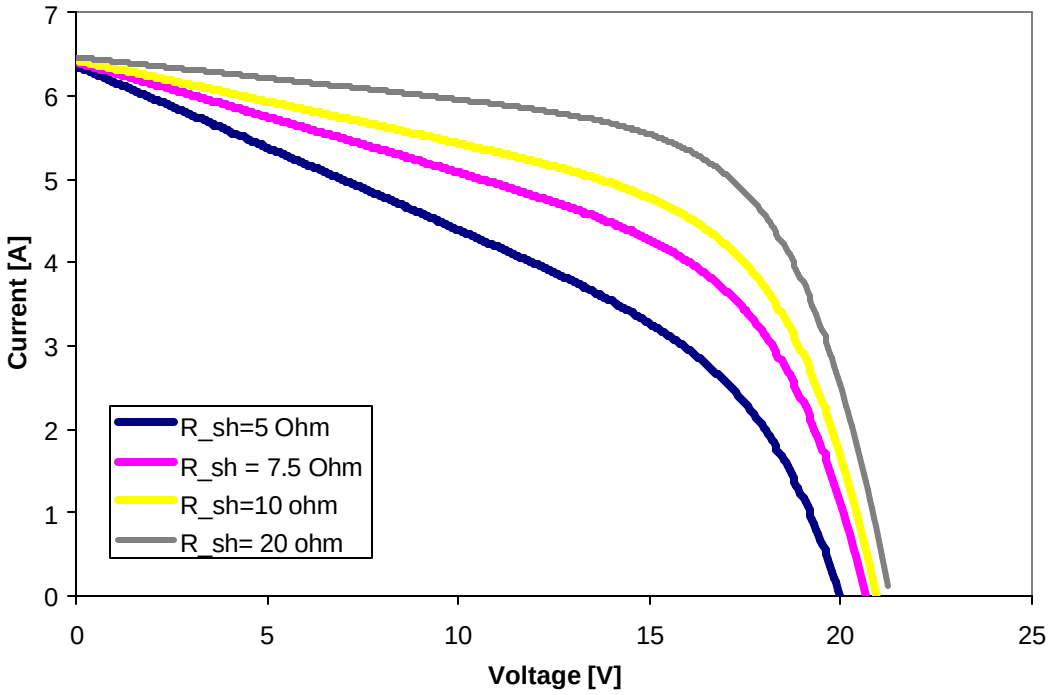

Figure 3.5-1: Shunt Resistance and IV Curve Shapes

These values were used simply as an example of realisitic parameters. When combined with a finite shunt resistance they no longer represent a real module. However, this test is intended only to varify Eq. 3.5-3, not to predict the behavior of a particular PV. It is clear that the short-circuit slope of the curve becomes more shallow as the shunt resistance increases. To see if it is truly an inverse relationship as Eq. 3.5-3 asserts, the numerical derivative of each IV curve was determined as a function on voltage. The results are shown in Figure 3.5-2.

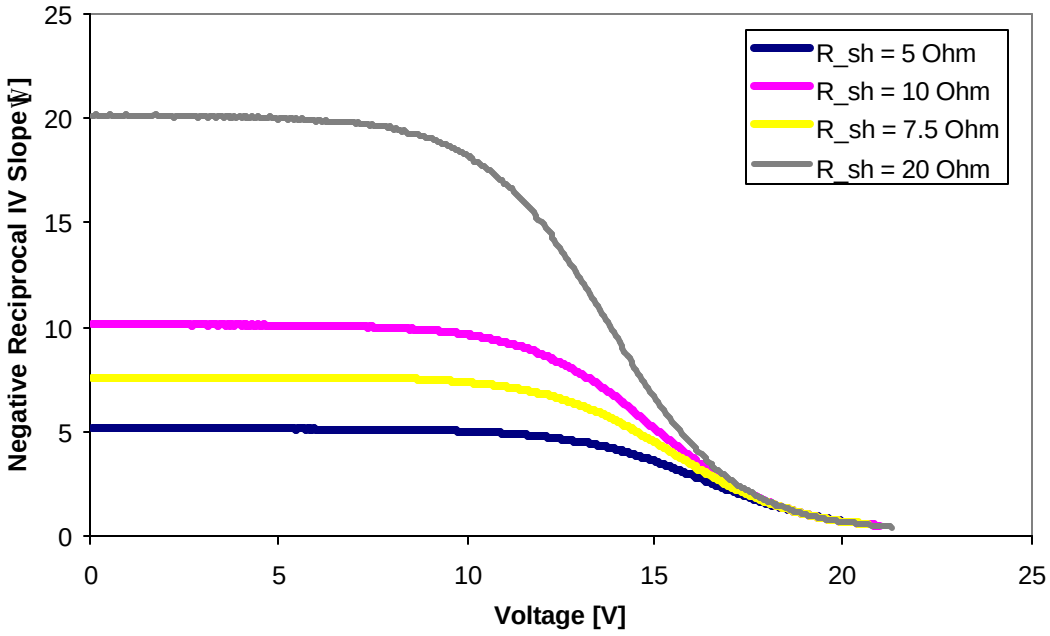

Figure 3.5-2: Effect of Shunt Resistance on the IV Slope in the Five Parameter Model

At the open-circuit condition, the negative inverse slope matches closely with the shunt resistance. Thus, it is safe to assume that Eq. 3.5-2 may be simplified to Eq. 3.5-3 in the five-parameter model.

3.6 Isolating $I_{L,ref}$, $I_{o,ref}$, R_s, and γ from the Equations of the Five Parameter Model

This section explains the algebra by which $I_{L,ref}$, $I_{o,ref}$, and γ are isolated from a system of IV equations at various operating conditions. The series resistance R_s must be determined numerically; Sections 3.7, 3.8, and 3.9 discuss various apsects of the computation techniques employed to find R_s. The fifth parameter, R_{sh}, is determined directly from the short-circuit slope of the IV curve as explained in Section 3.5. The methodology introduced here is essentially the same as that employed by Townsend and Eckstein. Adding of a fifth parameter changes the equations significantly.

At open-circuit, short-circuit, and maximum power point conditions respectively, the five parameter IV equation becomes:

$$0 = I_{L,ref} - I_{o,ref}\left[\exp\left(\frac{q}{\gamma k T_{c,ref}} V_{oc,ref}\right) - 1\right] - \frac{V_{oc,ref}}{R_{sh}} \qquad \text{Eq. 3.6-1}$$

$$I_{sc,ref} = I_{L,ref} - I_{o,ref}\left[\exp\left(\frac{q I_{sc,ref} R_s}{\gamma k T_{c,ref}}\right) - 1\right] - \frac{I_{sc,ref} R_s}{R_{sh}} \qquad \text{Eq. 3.6-2}$$

$$I_{mp,ref} = I_{L,ref} - I_{o,ref}\left[\exp\left(\frac{q}{\gamma k T_{c,ref}}\left(V_{mp,ref} + I_{mp,ref} R_s\right)\right) - 1\right] - \frac{V_{mp,ref} + I_{mp,ref} R_s}{R_{sh}} \qquad \text{Eq. 3.6-3}$$

The factor of one outside the exponential is very small compared to the exponential itself and is neglected in the following analysis. In addition, the exponential term itself may be neglected at the short-circuit condition; the voltage drop across the diode is due only to the small series resistance factor since the load voltage is absent. With these two assumption, Eq. 3.6-1 may be rearranged to solve for the reference photocurrent $I_{L,ref}$.

$$I_{L,ref} = I_{sc,ref}\left(1+\frac{R_s}{R_{sh}}\right) \qquad \text{Eq. 3.6-4}$$

The shunt resistance is generally much larger than the series resistance so that the resistance makes only a small contribution to Eq. 3.6-4. However, it is included as it does not complicate the anlysis.

Neglecting the 1, Eg. 3.6-2 may be solved for the reference reverse saturation current:

$$I_{o,ref} = \frac{I_{L,ref} - \frac{V_{oc,ref}}{R_{sh}}}{\exp\left(\frac{q}{kgT_{c,ref}}V_{oc,ref}\right)} \qquad \text{Eq. 3.6-5}$$

Again negelcting the 1, Eq. 3.6-5 result is substitued for $I_{o,ref}$ in the maximum power point expression Eq. 3.6-3. Solving for γ then yields:

$$g = \frac{\left(q\left(V_{mp,ref} - V_{oc,ref} + I_{mp,ref}R_s\right)\right)}{kT_{c,ref}\ln\left(\frac{I_{L,ref} - I_{mp,ref} - \frac{V_{mp,ref} + I_{mp,ref}R_s}{R_{sh}}}{I_{sc,ref} - \frac{V_{oc,ref}}{R_{sh}}}\right)} \qquad \text{Eq. 3.6-6}$$

At this point an additional equaition is need since there are four unknowns and only three equations. As in the four-parameter case, the catalog value that is employed in the additional equation is the temperature coefficient of open-circuit voltage. Taking the analytical derivative of Eq. 3.4-2 and using Eq. 3.2-3 for the temperature dependence of I_o yeilds the following:

$$\frac{\partial V_{oc}}{\partial T} = m_{Voc} = \frac{m_{Isc} - \frac{I_{o,ref}}{T_c}\left(3 + \frac{qe}{AkT}\right)\exp\left(\frac{q}{klT_{c,ref}}\right)}{\frac{q}{klT_{c,ref}} I_{o,ref} \exp\left(\frac{q}{klT_{c,ref}} V_{oc,ref}\right) + \frac{1}{R_{sh}}} \qquad \text{Eq. 3.6-7}$$

3.7 Mathematical Behavior of the Series Resistance

At this point the problem has been reduced to a system of four unknowns ($I_{o,ref}$, $I_{L,ref}$, γ, and R_s) and four equations (3.6-4, 3.6-5, 3.6-6, and 3.6-7). Eqs. 3.6-4, 3.6-5, and 3.6-7 express $I_{o,ref}$, $I_{L,ref}$, and γ explicitly in terms of R_{sh}, R_s, and known manufacturer's values. Eq. 3.7 gives R_s as an *implicit* function of the temperature coefficient of open-circuit voltage. It is not possible to isolate R_s due to the transcendental nature of this equation, so R_s must be found numerically. At the correct value for R_s the analytical voltage coefficient given in Eq. 3.6-7 will equal the value given in the catalog. In planning the numerical solution scheme it is important to understand qualitatively how the analytical voltage coefficient varies with R_s. Townsend [2] states that for the four-parameter model the value of the voltage coefficient increases with series resistance. This assertion was tested with the five-parameter model for an amorphous silicon module, the Solarex SA-5. EES was employed to determine the analytical voltage coefficient as a function of R_s. Values for all the other parameters were constrained by the given values of R_s and the catalog data. Figure 3.7-1 shows the results.

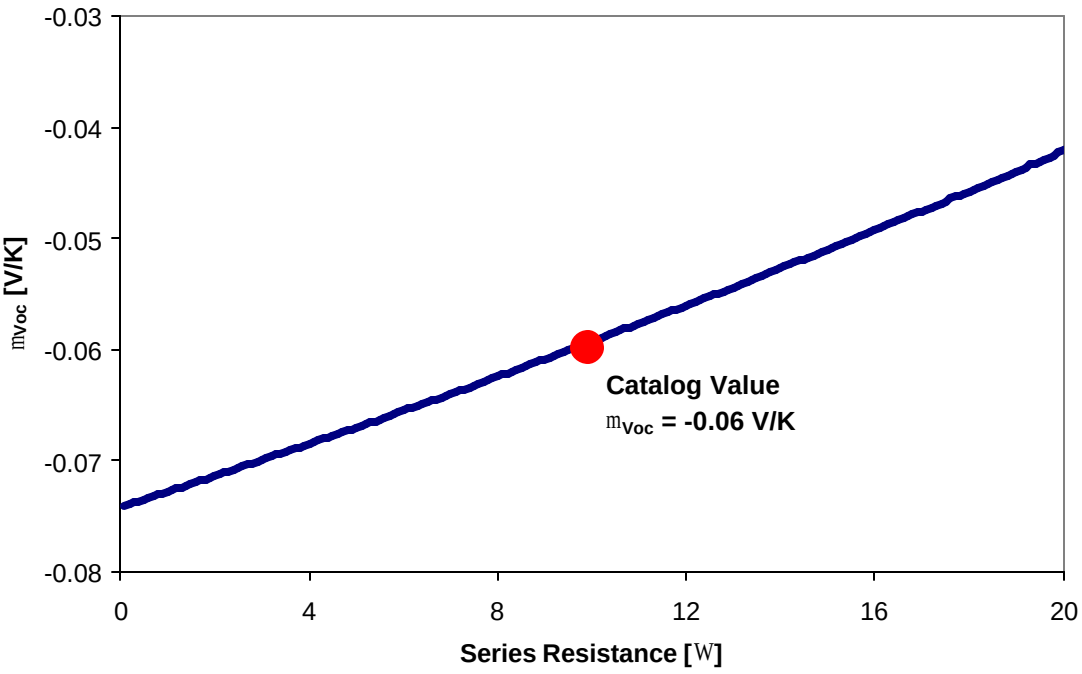

Figure 3.7-1: Analytical Voltage Coefficient vs. Series Resistance

From Figure 3.7-1 it appears that μ_{Voc} does increase montonically with R_s. Thus, a numerical scheme for converging on the proper guess value of R_s should increase the guess value with each iteration that μ_{Voc} is less than the catalog value. However, this function in monotonic only within a limited range. Figure 3.7-2 shows the *difference* between the analytical value and the catalog value of μ_{Voc} as a function of R_s.

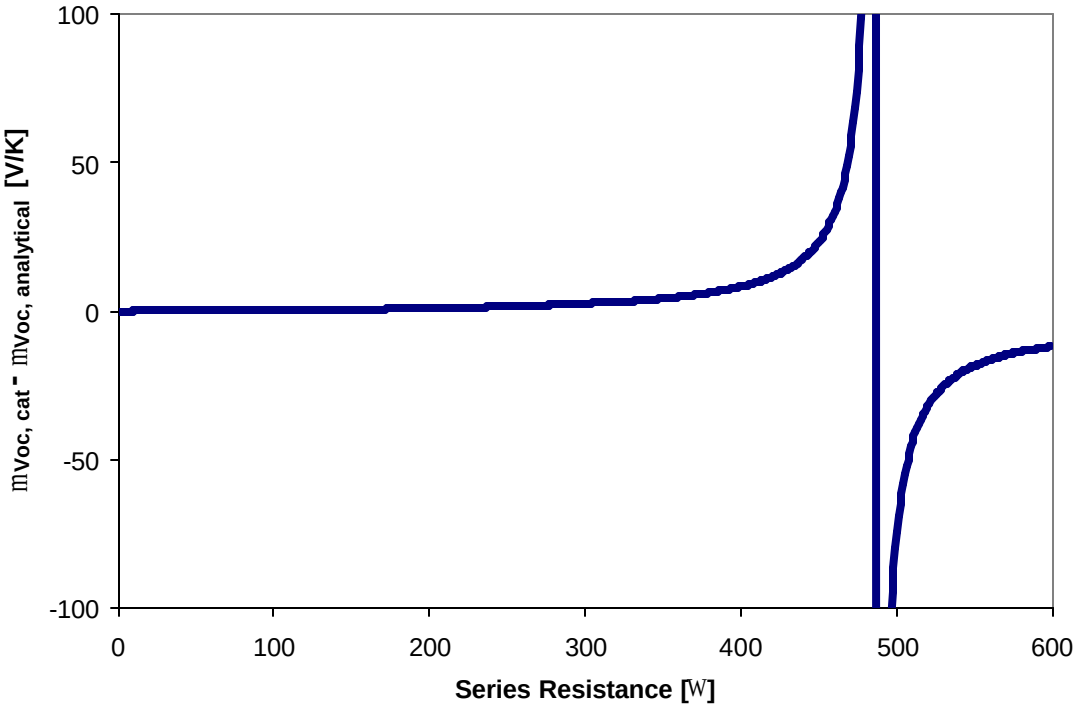

Figure 3.7-2: Error in Analytical Voltage Coefficient vs. Series Resistance

The voltage coefficient diverges near R_s = 480 Ω. In order to use an iterative method in which each guess is made larger or smaller based on the sign of the error of the last guess, it is necessary that all guesses for R_s stay below this discontinuity. This point might be a reasonable upper bound for R_s. The reason for this divergence can be seen from examining the expression for the voltage coefficient:

$$\frac{\partial V_{oc}}{\partial T} = m_{Voc} = \frac{m_{Isc} - \frac{I_{o,ref}}{T_c}\left(3 + \frac{qe}{AkT}\right)\exp\left(\frac{q}{klT_{c,ref}}\right)}{\frac{q}{klT_{c,ref}} I_{o,ref} \exp\left(\frac{q}{klT_{c,ref}} V_{oc,ref}\right) + \frac{1}{R_{sh}}} \qquad \text{Eq. 3.7-1}$$

The expression becomes very large as the denominator approaches 0. At the discontinuity, it is clear that

$$\frac{1}{R_{sh}} = -\frac{q}{k l T_c} I_o \exp\left(\frac{q}{k l T_c} V_{oc}\right) \qquad \text{Eq. 3.7-2}$$

$I_{L,ref}$ and $I_{o,ref}$ are both always positive quanities, as is the exponential, so the only way that this equation can hold true is if γ is negative. However, a negative value for γ is not physcially meaningful as it implies that the current through the diode actually decreases with the voltage drop across it. It is interesting to note how R_s effects γ, holding the other parameters constant.

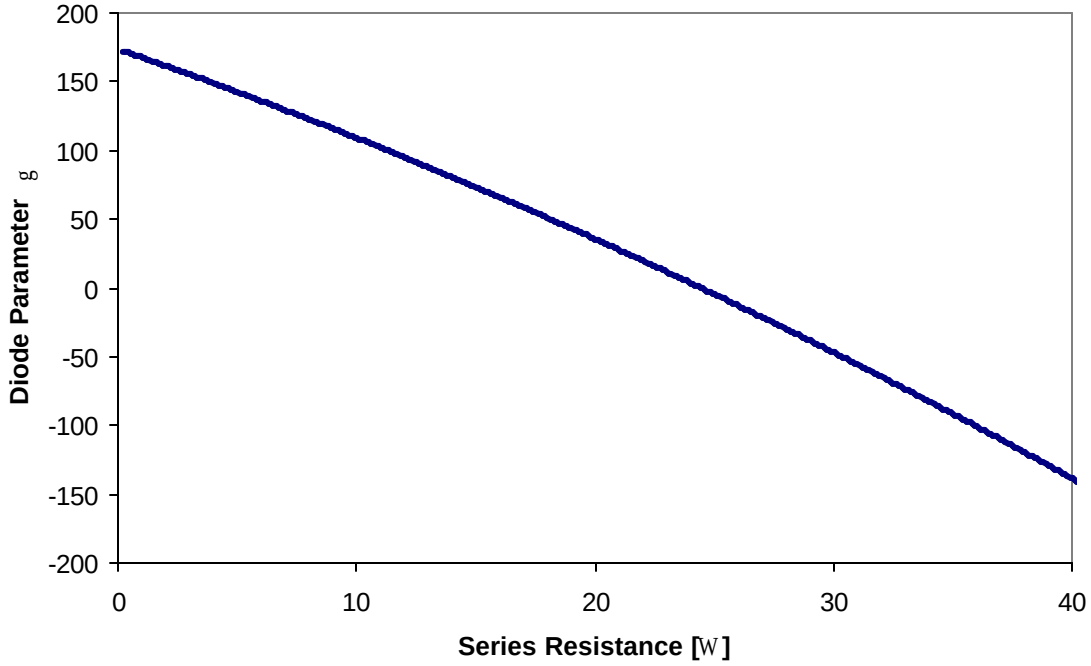

Figure 3.7-3: Relation Between Diode Parameter g and Series Resistance

This graph shows that g becomes negative at series resistance of about 24 Ω. Of course, this value is much less than R_s = 480 Ω, the point at which the voltage coefficient approaches infinity.

Townsend [2] has pointed out that the minimum physically meaningful value for γ is where the diode completion factor A is equal to unity. In this case,

$$g_{\min} = N_s \qquad \text{Eq. 3.7-3}$$

where N_s is the number of cells in series in the module. For the Solarex SA-5, $N_s = 30$. It is evident from Figure 3.7-3 that the maximum possible value for R_s is about 19 Ω.

3.8 Bounding R_s in the Iterative Numerical Scheme

It has been shown that physical constraints require that the series resistance parameter R_s be greater than zero and less than the value such that $\gamma = N_s$. R_s cannot be written explicitly as a function of γ, however, so the upper bound must be determined numerically. Newton's method is employed to find this upper bound. In Eq. 3.6-6, γ is given as an explicit function of R_s. Thus, at the correct upper bound for the series resistance, the following objective equation must hold true:

$$F = 0 = N_s - \frac{\left(q\left(V_{mp} - V_{oc} + I_{mp}R_{s,upper}\right)\right)}{kT_c \ln(C)} \qquad \text{Eq. 3.8-1}$$

where

$$C = \frac{I_L - I_{mp} - \dfrac{V_{mp} + I_{mp}R_{s,upper}}{R_{sh}}}{I_{sc} - \dfrac{V_{oc}}{R_{sh}}}$$

The derivative of F with respect to $R_{s,upper}$ is:

$$F' = -\frac{q}{kgT_c}\left(\frac{I_{mp}}{\ln(C)} - CI_{mp}R_{s,upper}\ln^2(C)\right) \qquad \text{Eq. 3.8-2}$$

Starting with an initial guess of 1 Ω, each value of R_s is chosen from the results of the previous iteration such that

$$R_{s,upper,new} = R_{s,upper,old} - \frac{F\left(R_{s,upper,old}\right)}{F'\left(R_{s,upper,old}\right)} \qquad \text{Eq. 3.8-3}$$

3.9 Implicit Solution for R_s

The previous two sections have addressed the physical and mathematical importance of bounding guesses for R_s and developed a method for determining these bounds. This section outlines the algorithm for finding R_s once the initial bounds are known. The method is essentially like that employed by Eckstein [3] except of course that the equations have changed because of the addition of a fifth model parameter. An initial guess for the series resistance taken to be the mean of the upper and lower bounds. Eqs. 3.6-4, 3.6-5, 3.6-6 are used to determine I_L, I_o, and γ. (The fifth parameter, R_{sh}, is determined once directly from catalog data and does not depend on R_s.) μ_{Voc} is determined according to Eq. 3.6-7, and this result is compared to the value given in the catalog. If analytical value is too low, then the lower bound is set equal to the present guess for R_s. If it is too large, the upper bound is set equal to the present guess. A new guess is then determined by averaging the new set of bounds. This scheme continues until R_s converges. Figure 3.9-1 illustrates the solution scheme.

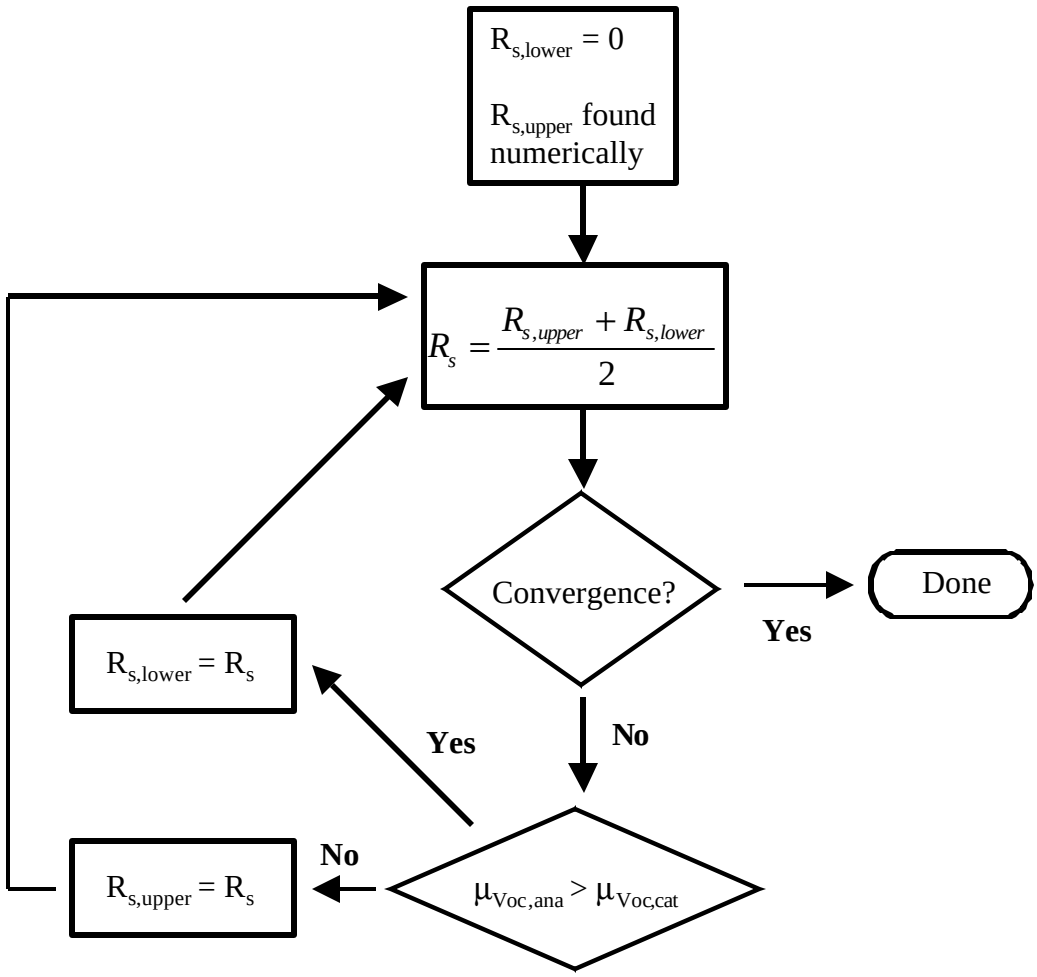

Figure 3.9-1: Flowchart Illustrating Algorithm to Determine R_s in Five Parameter Model

3.10 Variations in I_o and I_L Under Operating Conditions

Once the values for the five parameters are known, the general IV expression (Eq. 3.4-2) may be employed to find the operating current for any given load voltage. γ, R_{sh}, and R_s are assumed to be constant properties of the module, independent of temperature and radiation. However, it is important to remember that I_L and I_o are not constant; the values determined from Eqs. 3.6-4 and 3.6-5 are only valid for the reference conditions of T_c =

298 K and G = 1000 W/m^2. Thus, these two parameters must be recalculated at each timestep based on their reference values and the ambient conditions. The NOCT method is used to determine the cell temperature T_c [2]. As with the four parameter model, the photocurrent is assumed to be proportional to the incident radiation:

$$I_L = I_{L,ref}\left(\frac{G_{ref}}{G}\right) \qquad \text{Eq. 3.10-1}$$

By manipulating Eq. 3.2-3, the temperature dependence of the reverse saturation current may be expressed as:

$$I_o = \left(\frac{T_c}{T_{c,ref}}\right)^3 \exp\left[\left(\frac{qe}{Ak}\right)\left(\frac{1}{T_{c,ref}} - \frac{1}{T_c}\right)\right] \qquad \text{Eq. 3.10-2}$$

3.11 Finding I_{sc} and V_{oc} Under Operating Conditions

The short circuit current and open-circuit voltage are useful quantities for some applications, and the TRNSYS program automatically calculates them at each timestep. In addition, V_{oc} is employed as an upper bound in a search routine to determine the voltage at the maximum power point; this will be discusses in a later section. Determining I_{sc} is trivial; it is determined directly from I_L by rearranging Eq. 3.6-4. V_{oc} may be found from Eq. 3.6-5, although an explicit solution is not possible. (It may be found explicitly in the four-parameter model, however.) A search routine similar to that used to find R_s is employed to converge on a value for V_{oc}. The initial lower bound is 0 V, while the initial upper bound taken conservatively to be 150% of $V_{oc,ref}$. (Under operating conditions except for the most extreme climates, V_{oc} will not vary from $V_{oc,ref}$ by more than 20%.)

3.12 Numerical Method for Solving the IV Equation

As with upper bound for the series resistance, the TRNSYS subroutine employs Newton's method to find the current for any given voltage. Eq. 3.4-2 is manipulated to form an objective function:

$$F = 0 = I_L - I_o\left[\exp\left(\frac{q}{gkT_c}\left(V + I_{guess}R_s\right)\right) - 1\right] - \frac{V + I_{guess}R_s}{R_{sh}} - I_{guess} \qquad \text{Eq. 3.12-1}$$

The derivative with respect to I_{guess} is

$$F' = -1 - \frac{I_o R_s q}{kgT_c}\exp\left(\frac{q}{gkT_c}\left(V + I_{guess}R_s\right)\right) - \frac{R_s}{R_{sh}} \qquad \text{Eq. 3.12-2}$$

3.13 Method for Locating the Maximum Power Point

Under any operating condition there exists a unique maximum power point; this is the location along the IV curve where the power output of the PV is maximized. Building-integrated photovoltaic systems almost always employ a maximum power point tracker; this device provides a constantly varying load which forces the PV to operate at its optimal power point. All simulations in this study assume that the PV output is at its maximum power point.

The power is simply the product of current and voltage. At the maximum power point, the derivative of power with respect to voltage must be zero:

$$0 = \frac{dP}{dV} = \frac{d}{dV}\left(IV\right) = I + V\frac{dI}{dV} \qquad \text{Eq. 3.13-1}$$

Like the current itself, the derivative $\frac{dI}{dV}$ is an implicit function of voltage. At any given voltage, it may be found readily using Newton's method. The objective function F and its derivative with respect to $\left(\frac{dI}{dV}\right)_{guess}$ are:

$$F = -\left(\frac{dI}{dV}\right)_{guess} - \frac{I_o q}{kgT_c}\exp\left(\frac{q}{gkT_c}(V + IR_s)\right)\left(1 + R_s\left(\frac{dI}{dV}\right)_{guess}\right) - \frac{1}{R_{sh}} - \frac{R_s}{R_{sh}}\left(\frac{dI}{dV}\right)_{guess}$$

Eq. 3.13-2

$$F' = -1 - \frac{I_o q}{kgT_c}\exp\left(\frac{q}{gkT_c}(V + IR_s)\right)R_s\left(\frac{dI}{dV}\right)_{guess} - \frac{R_s}{R_{sh}}$$

Eq. 3.13-3

A bisection search routine (like that for R_s and V_{oc}) is employed to solve Eq. 3.13-1. The initial bounds for the maximum power point voltage are 0 and V_{oc}. If a guess for voltage is too low, $\frac{dP}{dV}$>0 and the lower bound is set equal to the present guess value for the next interation. Likewise, the upper bound is set equal to the guess value if $\frac{dP}{dV}$<0.

3.14 Incidence Angle Modifier

The percentage of incident radiation absorbed by a solar collector or photovoltaic module is a function of incidence angle. At large angles of incidence, a greater portion of incident radiation is reflected away rather than absorbed. King [19] gives an empirical correlation for the reflectance of glass front PV modules as a function of incidence angle. The correlation of King is as follows:

$$IAM = 1 - \left(1.098x10^{-4}\right)\theta - \left(6.267x10^{-6}\right)\theta^2 + \left(6.583x10^{-7}\right)\theta^3 - \left(1.4272x10^{-8}\right)\theta^4$$

Eq. 3.14-1

θ ιs the angle of incidence; at normal incidence θ is 0. *IAM* stands for "incidence angle modifier" and gives the ratio between radiation absorbed by the PV and the radiation that would have been absorbed at normal incidence. Figure 3.14.1 graphs the inc idence angle modifier correlation.

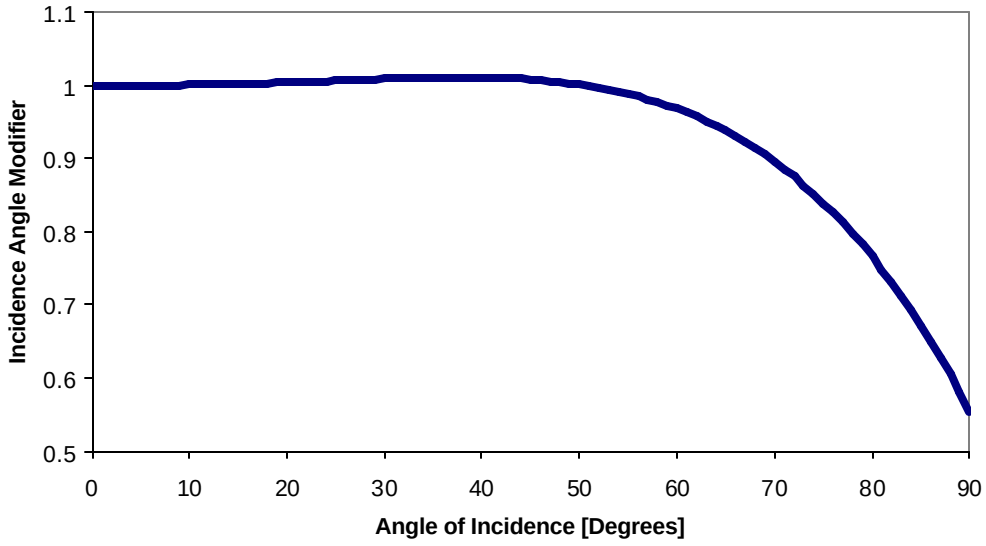

Figure 3.14-1: Incidence Angle Modifier Correlation

Al-Ibrahim has noted that the glass cover roughness varies between PV modules. However, he has shown experimentally that the roughness of the glass does significantly affect the dependence of reflectance on the incidence angle [20].

Of course, it is necessary to know the angle of incidence in order to use the correlation described above. The TRNSYS solar radiation processor (Type 16) calculates the incidence angle for the beam component of the radiation. However, the absorptance ratio cannot be found directly from this angle since doing so would neglect the diffuse and ground-reflected components of the radiation. Beckman and Duffie [5] ha ve compiled additional correlations to determine the "effective incidence angle" for diffuse and

ground-reflected radiation. These effective angles are functions only of collector or PV slope. The effective angles are then used as arguments in Eq. 3.14-1 to calculate absorptance ratios for diffuse and ground-reflected radiation. The effective angle correlations are:

$$q_{eff,diff} = 59.7 - 0.1388b + 0.001497b^2 \qquad \text{Eq. 3.14-2}$$

$$q_{eff,gnd} = 90 - 0.5788b + 0.002693b^2 \qquad \text{Eq. 3.14-3}$$

A total effective insolation may then be calculated by summing the individual components of radiation and multiplying them by their separate absorptance ratios.

$$I_{T,eff} = I_{T,b}IAM_b + I_{T,d}IAM_d + I_{T,g}IAM_g \qquad \text{Eq. 3.14-4}$$

Simulations were run for four US locations to examine how including the incidence angle modifier affects annual PV output. TMY (Typical Meteorological Year) data was used for each location. Each simulation has a length of one year and employs a single amorphous Solarex MST-56 module facing south with a slope equal to the latitude. The results are as follows:

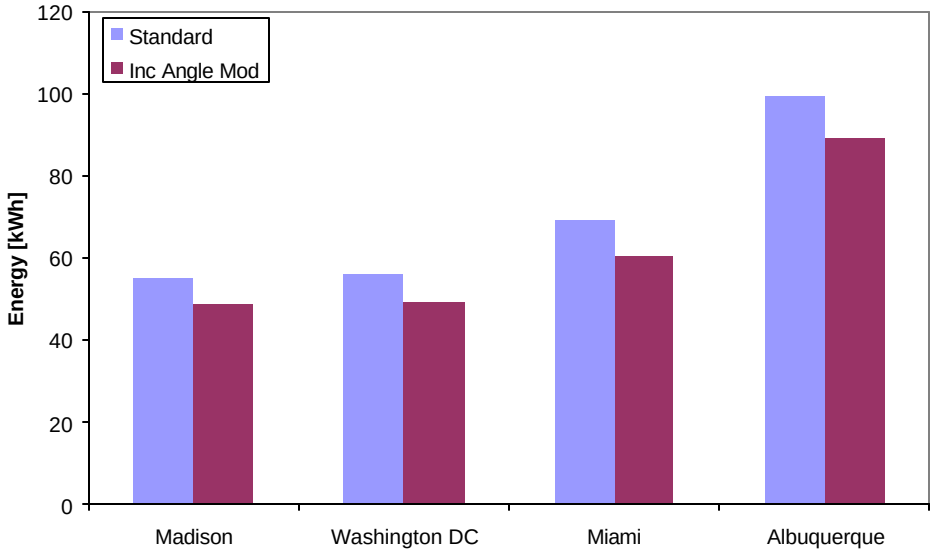

Figure 3.14-2: Simulation Results Employing the Incidence Angle Modifier

In each case, including the incidence angle modifier reduced the annual energy production by roughly 10%.

3.15 Testing the Five-Parameter Model

In general, photovoltaic devices exhibit better performance at lower temperatures. In a climate such as the Midwest with significant seasonal variations in temperature, the PV conversion efficiency may vary by 15% or more from winter to summer. μ_{Isc}, the temperature coefficient of short-circuit current, is a positive quantity; short-circuit performance actually improves as the temperature goes up. However, at most operating conditions including the maximum power point, this effect is outweighed by a drop in open-circuit voltage. Thus, the overall derivative of maximum power with respect to temperature is a negative quantity.

The temperature dependence of the five parameter model was examined for two amorphous modules, the Solarex SA-5 and Solarex MST-56. These results are compared to selected points read from manufacturers' IV curves. The selected points are *not* experimental data but rather are taken from small catalog graphs. At an irradiance of 1000 W/m^2, the IV curves for the SA-5 at 25 C, 50 C, and 75 C are as shown in Figure3.15-1.

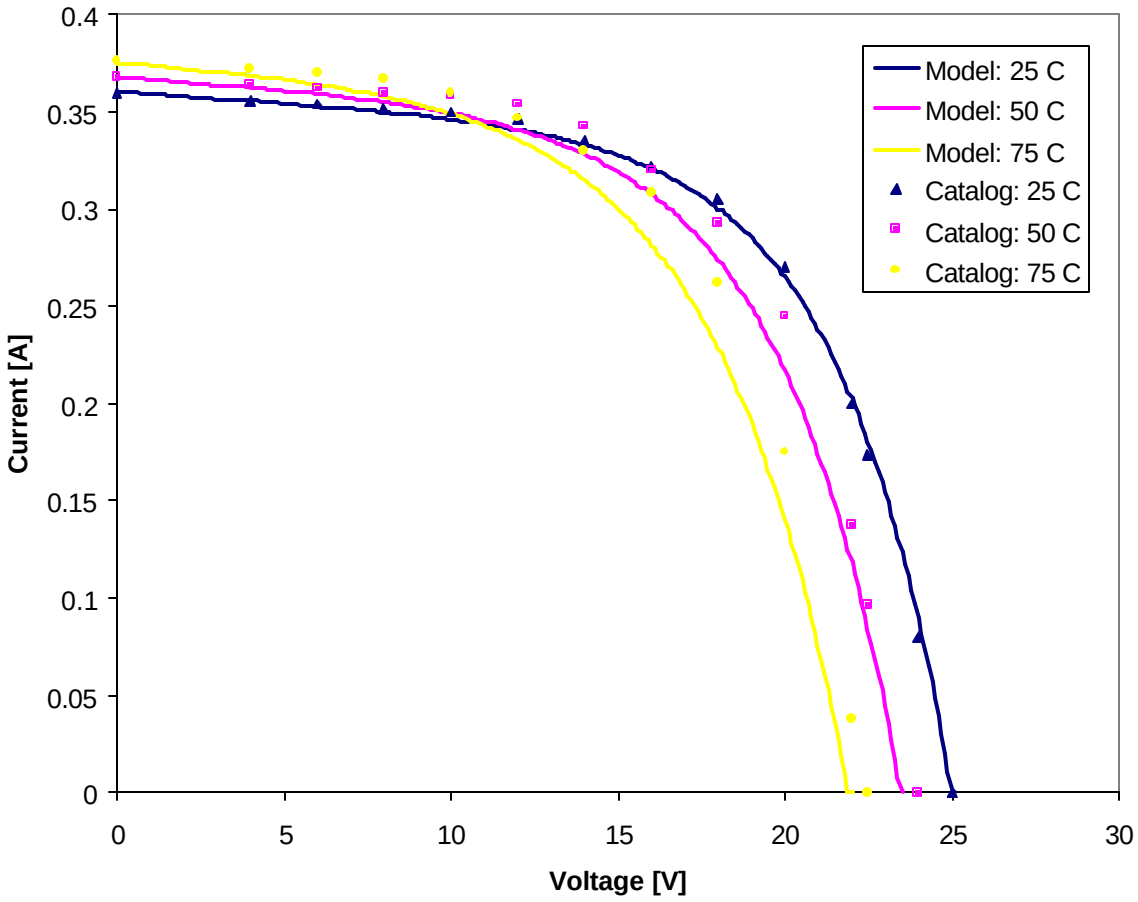

Figure 3.15-1: Catalog Data and Model IV Curves for Solarex SA-5

The model agrees closely with the catalog data for voltages below about 12 V. Beyond about 15 V, the model begins to underpredict the current significantly. At a current of 0.2 A, the model underpredicts the catalog results by about 1 V at each temperature.

For grid-tied applications, it may be useful to graph power rather than current as a function of voltage. This aids is visualizing the difference in peak power between the model and catalog:

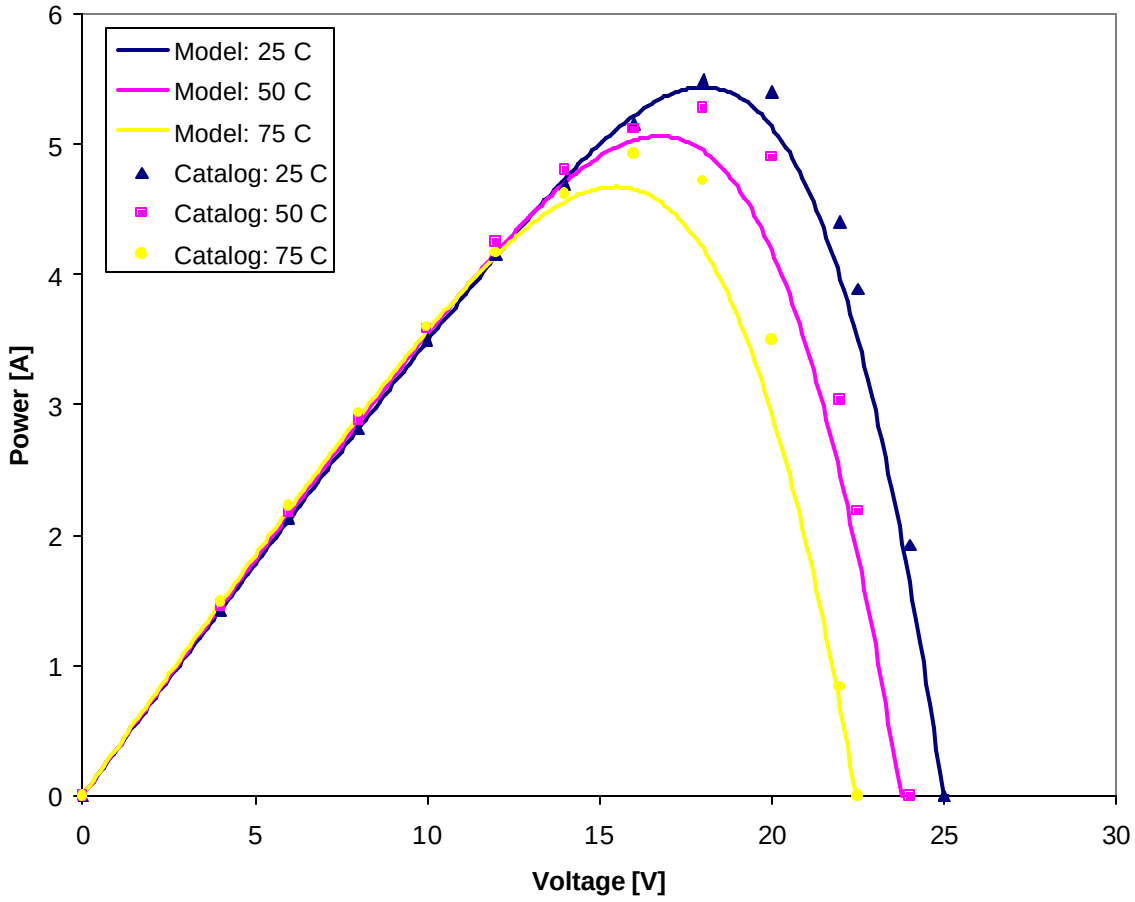

Figure 3.15-2: Catalog Data and Model Power-Voltage Curves for Solarex SA-5

As with current, the predicted power agrees closely with the catalog curve below about 13 V. At the maximum power points for 25 C and 50 C, the catalog and model differ by about 0.25 W. The discrepancy is greater for the 75 C curve, however: about 0.4 W.

Experimental IV points were not available to validate the model; such data would clearly be preferable to using catalog data. It is notable that the values for V_{oc}, I_{sc}, and the maximum power point given in the specifications list were inconsistent with the IV curve presented in the catalog. In modeling the IV curve, these values were taken from the catalog curve rather than the specifications list. These parameters for the SA-5 are compared in Table 3.15-1.

Table 3.15-1: Specifications List and Catalog IV Curve for Solarex SA-5

	I_{sc}	V_{oc}	***Max Power Point***
Specs List	0.380 A (minimum)	23 V (minimum)	15 V, 0.340 A (min)
Read from IV Curve	0.358 A	25.0 V	15 V, 0.325 A

The discrepancies are significant and suggest that the IV curves in the catalog may be not extremely accurate. Experimental data would clearly provide a better test of the model. The table value of 15 V for the maximum power point was used in the model, and reading from the catalog IV curve implied a maximum power point current of 0.325 A. However, Figure 3.15-2 shows that even according to the catalog curve the maximum power point occurs as at about 18 V for test conditions (25 C). Again reading from the catalog, this point corresponds to a maximum power point current of 0.300 A. Running the model a second time using this new value for the maximum power point produced the results shown in Figures 3.5-3 and 3.5-4.

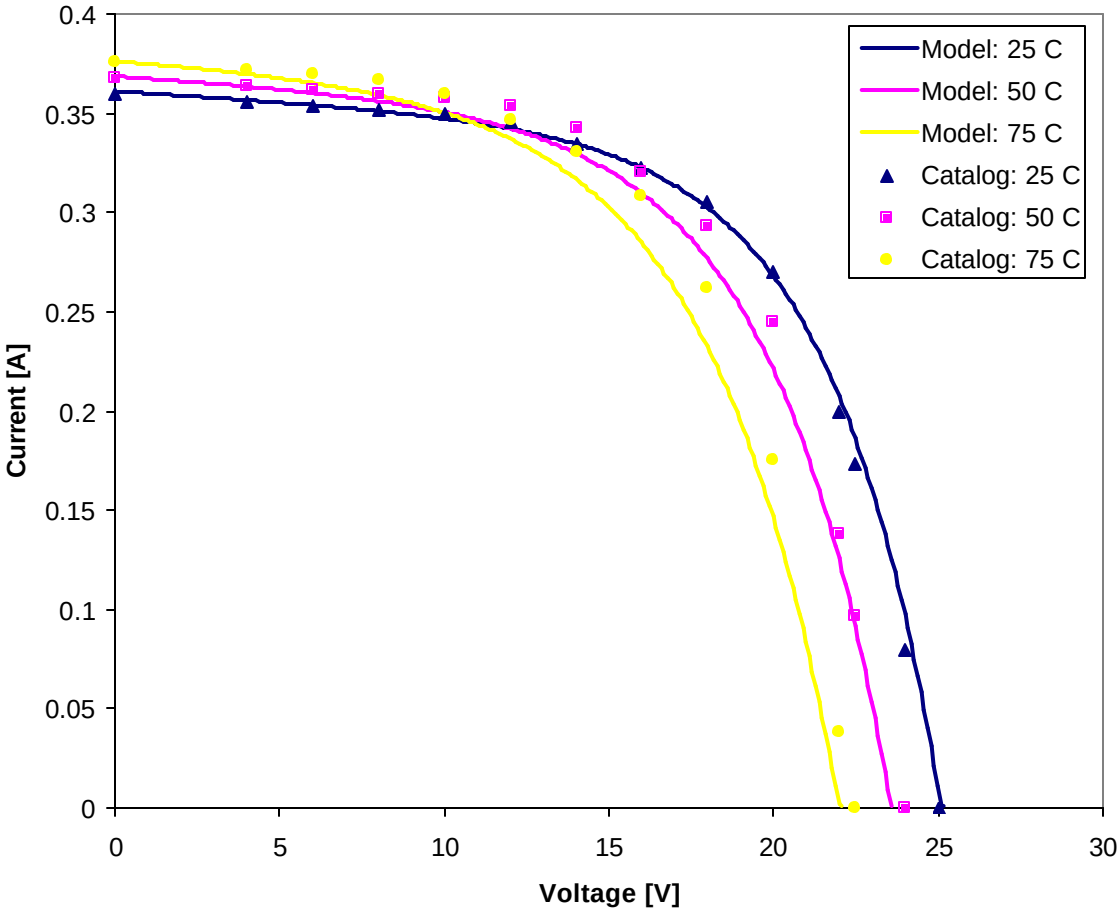

Figure 3.15-3: Catalog Data and Model IV Curves for Solarex SA-5, taking catalog IV value of V_{mp} = 18 V

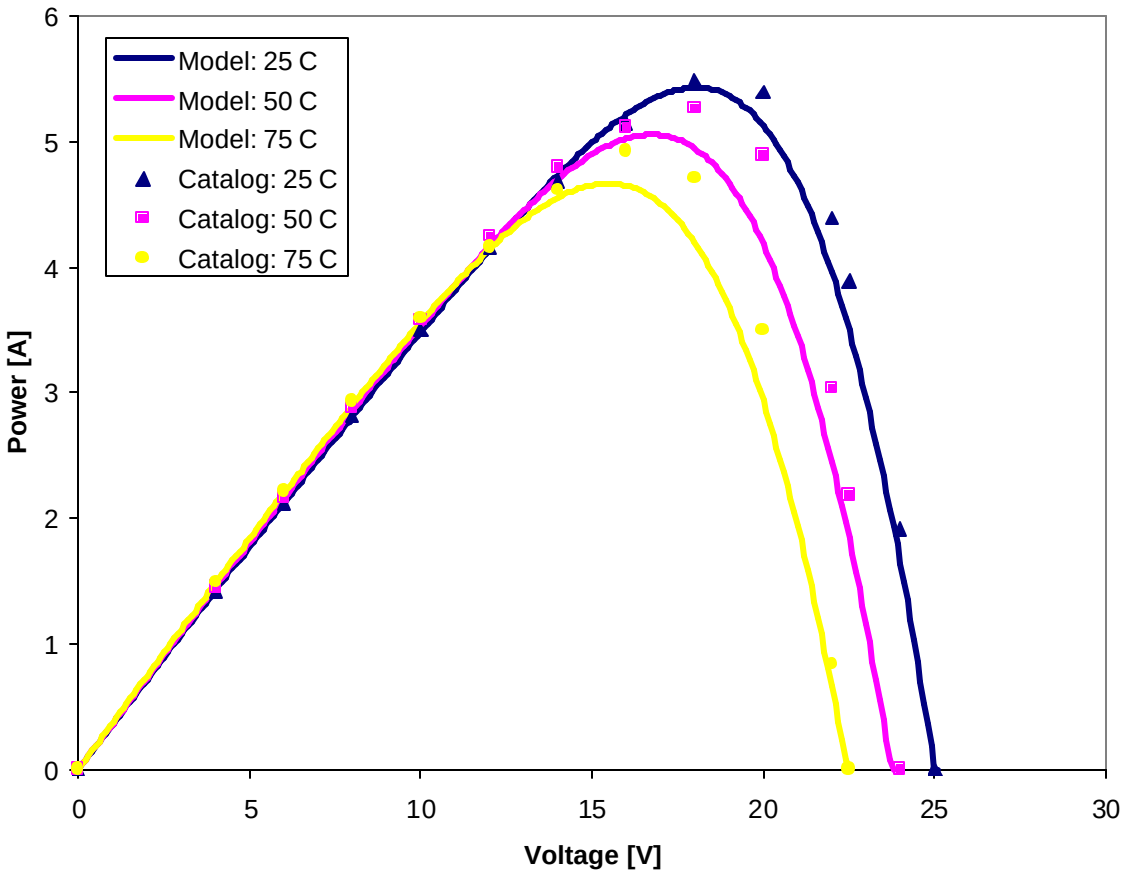

Figure 3.15-4: Catalog Data and Model Power-Voltage Curves for Solarex SA-5, taking catalog IV value of V_{mp} = 18 V

Changing this maximum power point value in the model improves the agreement with the catalog data substantially, particularly for the 25 C reference temperature curve. Not surprisingly, this alteration moves the maximum power voltages in the model to correspond much more closely with those in the catalog. At maximum power the model still underpredicts the catalog currents by about 0.2 W for the 50 C and 75 C curves.

The temperature dependence and catalog comparison for the Solarex MST-56, another amorphous module, are shown in Figure 3.15-5 :

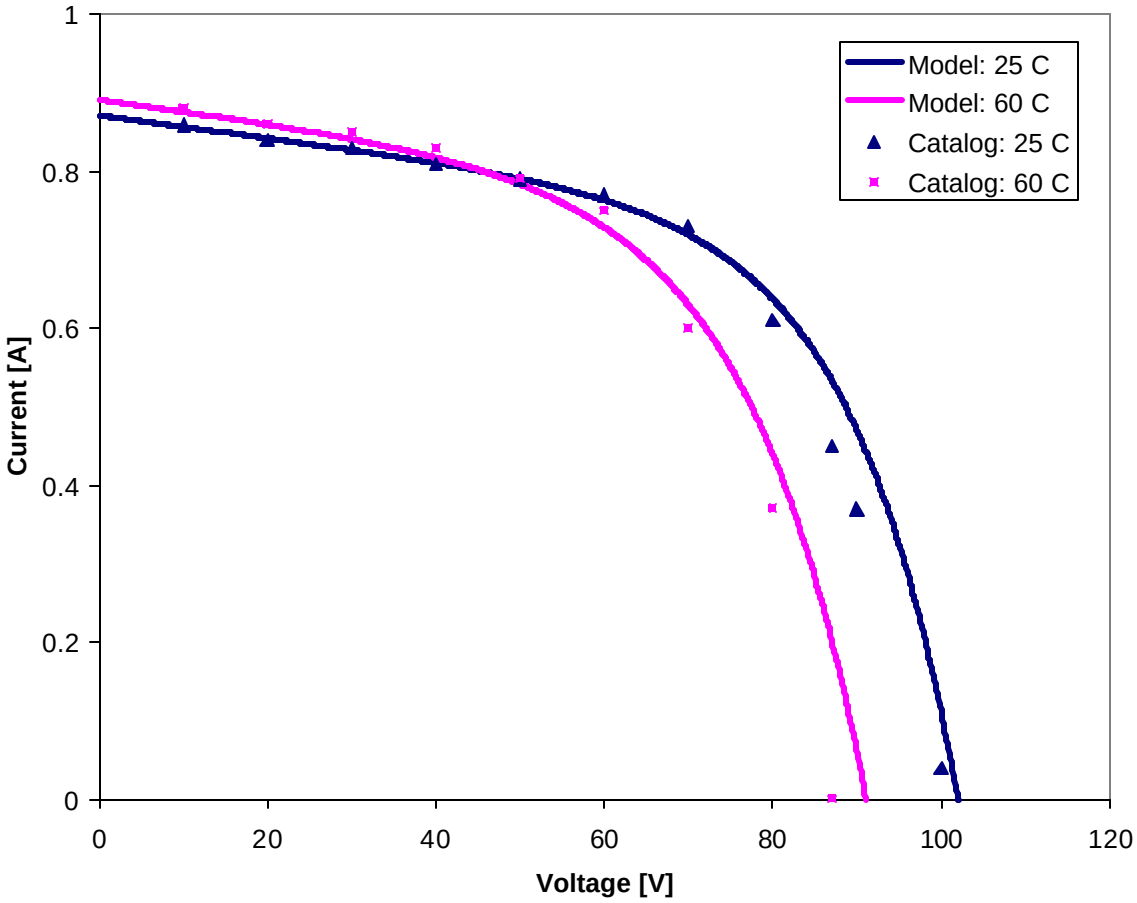

Figure 3.15-5: Catalog Data and Model IV Curves for Solarex MST-56

Figure 3.15-6 shows the power-voltage characteristics for the MST-56 at 25 C and 60 C.

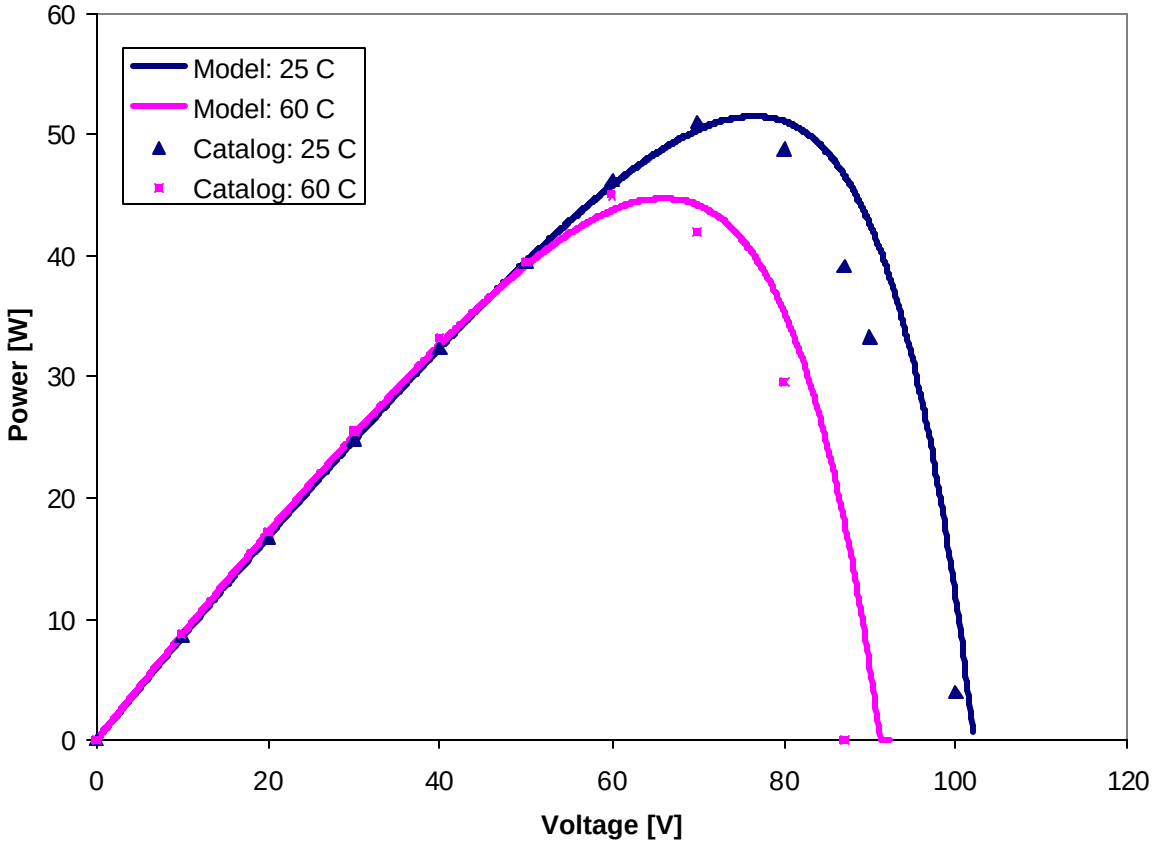

Figure 3.15-6: Catalog Data and Model Power-Voltage Curves for Solarex MST-56

Again, the model seems to perform well at low voltages including the short-circuit condition. It also seems to be fairly consistent around 70 V, the vicinity of the maximum power point. At larger voltages the model overpredicts the performance of the PV slightly. (For the SA-5, the five-parameter model underpredicts the current.) This overprediction is particularly evident for the 60 C case at the open-circuit condition. The five-parameter model underestimates the detrimental effect of increasing temperature on this PV. The catalog value of V_{oc} (-0.4 V/K) was used for the model. This agrees closely with the value of V_{oc} implied by the catalog IV curve; the problem is not simply a case of inaccurate values in the specs list. The model attempts to match the analytical and catalog values for V_{oc} at reference conditions, however, so this result is surprising. One explanation could be the V_{oc} actually changes with temperature. To examine this

possibility, the open-circuit voltage was determined using the model for a wide range of temperatures: the results are given in Figure 3.15-7:

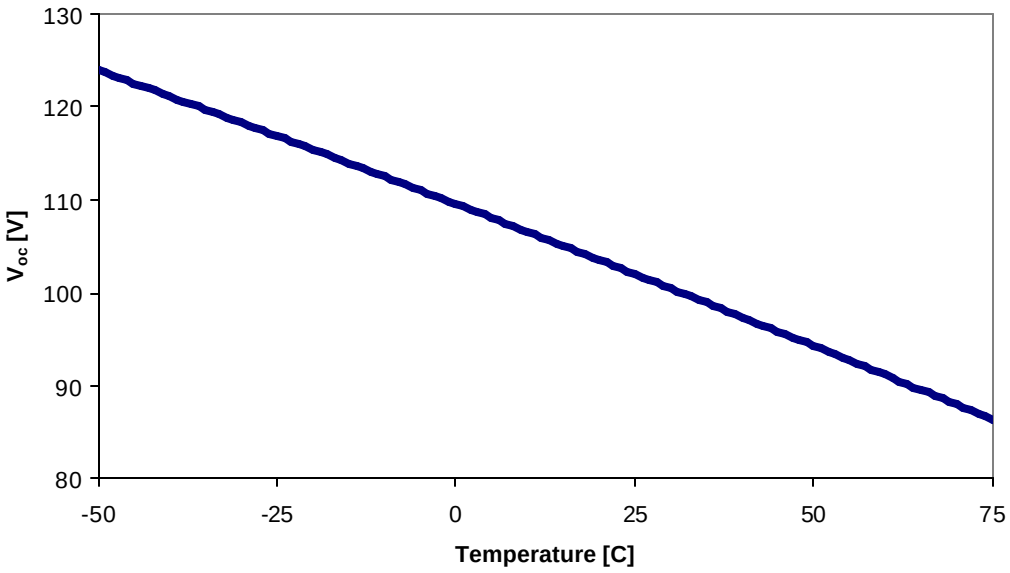

Figure 3.15-7: Model Open-Circuit Voltage vs. Temperature for Solarex MST-56

This function appears to be quite linear, suggesting that μ_{Voc} does not change much with temperature. Figure 3.15-8 gives two values for μ_{Voc} as functions of temperature. One is determined by numerically differentiating the function in Figure 3.15-7. The other is the analytical value from Eq. 3.6-6.

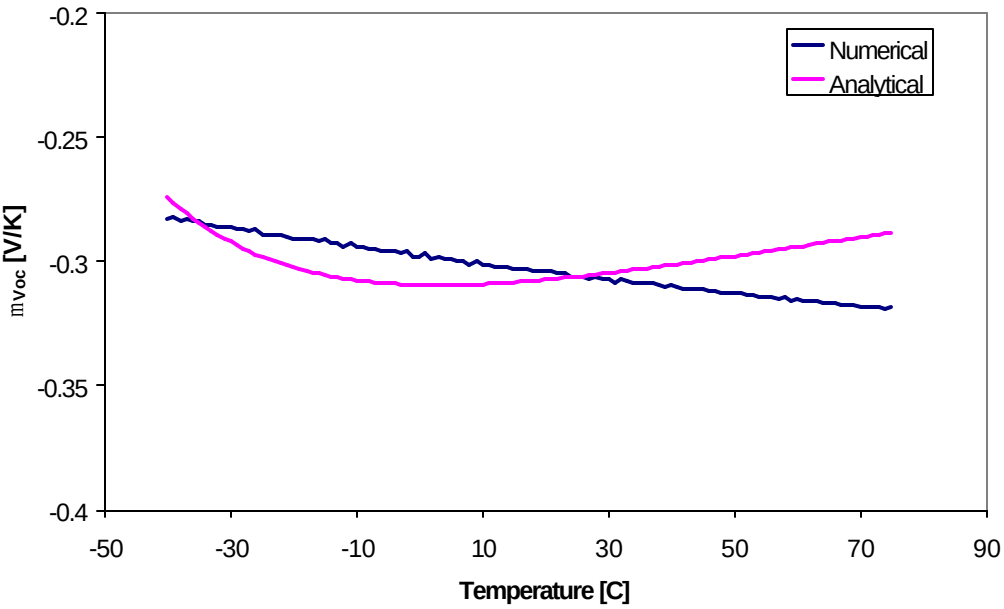

Figure 3.15-8: Analytical and Numerical m_{Voc} vs. Temperature for Solarex MST-56

Over the range of operating temperatures (about –30 C to 70 C) the two coefficients are roughly –0.3 V/C. The reason that these values do not agree precisely is that the short-circuit current coefficient μ_{Isc} is assumed to be constant in Eq. 3.6-6; this assumption may not be completely valid. However, the model determines R_s such that the analytical value of μ_{Voc} should match the catalog value at reference conditions; this is clearly not the case.

The reason for this is that the lower bound imposed on R_s prevents it from reaching a value where the coefficients can agree. R_s for this module is very small, 0.00045 Ω. The value is actually "pinned" by the constraint that R_s cannot become negative. A negative series resistance is clearly not physically meaningful. However, a test was run allowing R_s to drop below zero; perhaps this would improve the models agreement with the catalog data. When the lower bound constraint on the series resistance was removed, the model converged on R_s = -41.66 Ω. In this case μ_{Voc} agrees much more closely with the given value of –0.4 V/K, as shown in Figure 3.15-7.

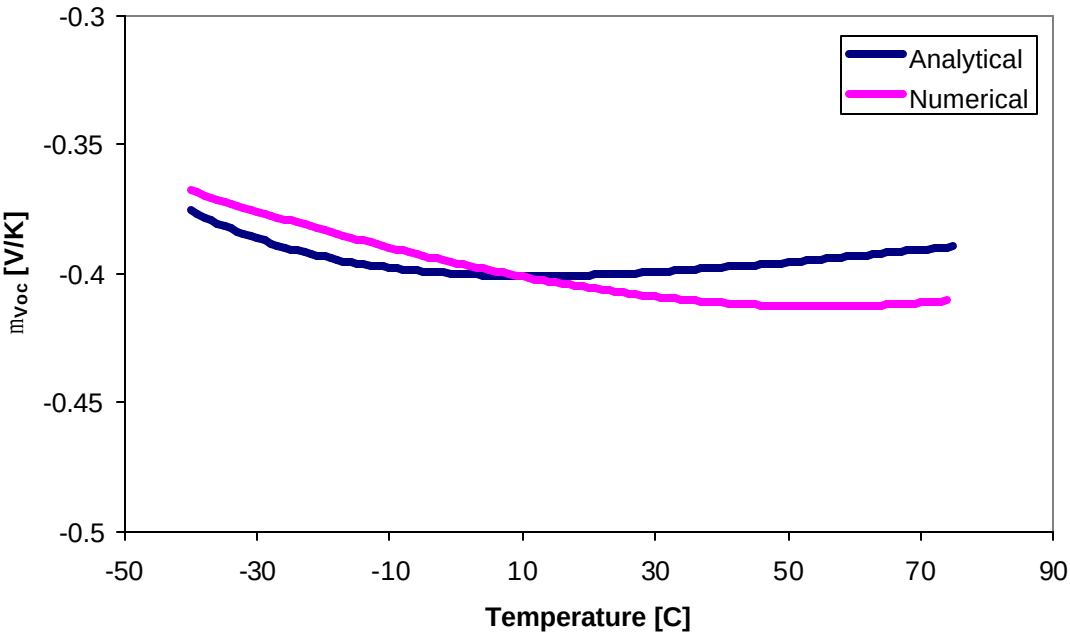

Figure 3.15-9: Analytical and numerical m_{Voc} values, allowing R_s to become negative

The IV and power-voltage curves are shown in Figures 3.15-10 and 3.15-11.

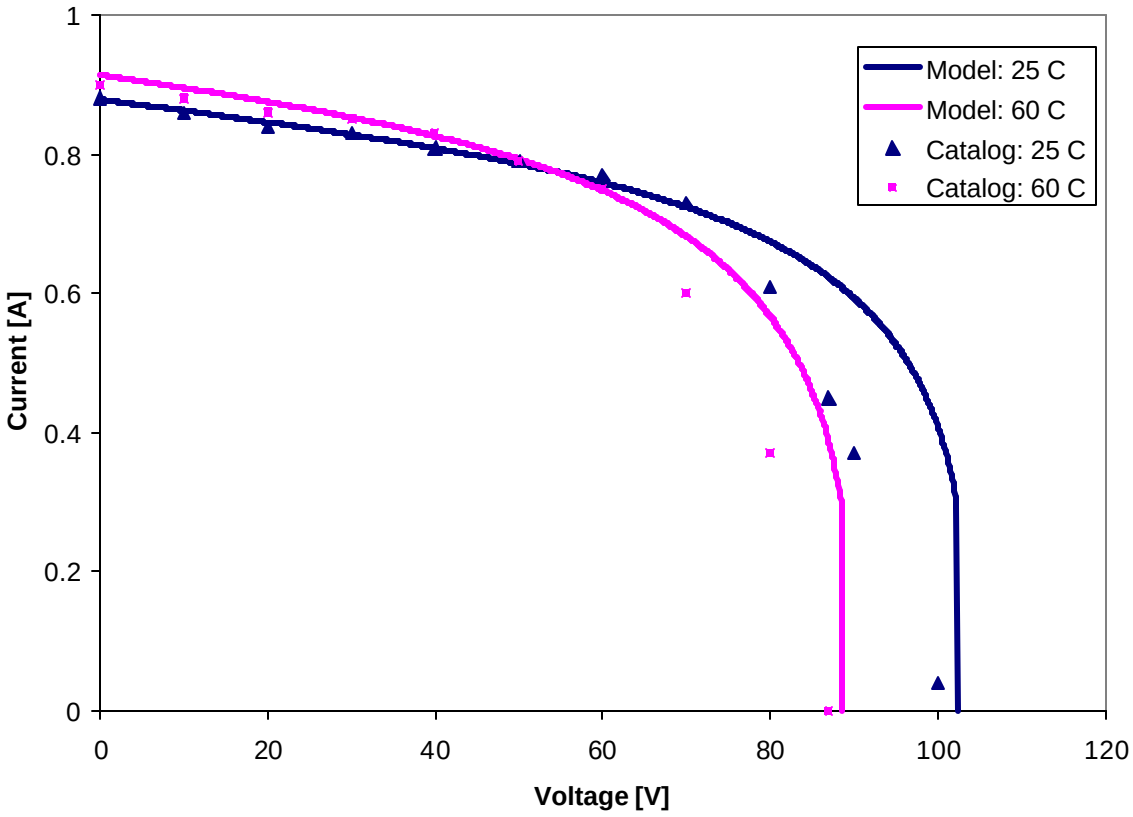

Figure 3.15-10: Catalog Data and Model IV Curves for Solarex MST-56, Allowing R_s to Become Negative

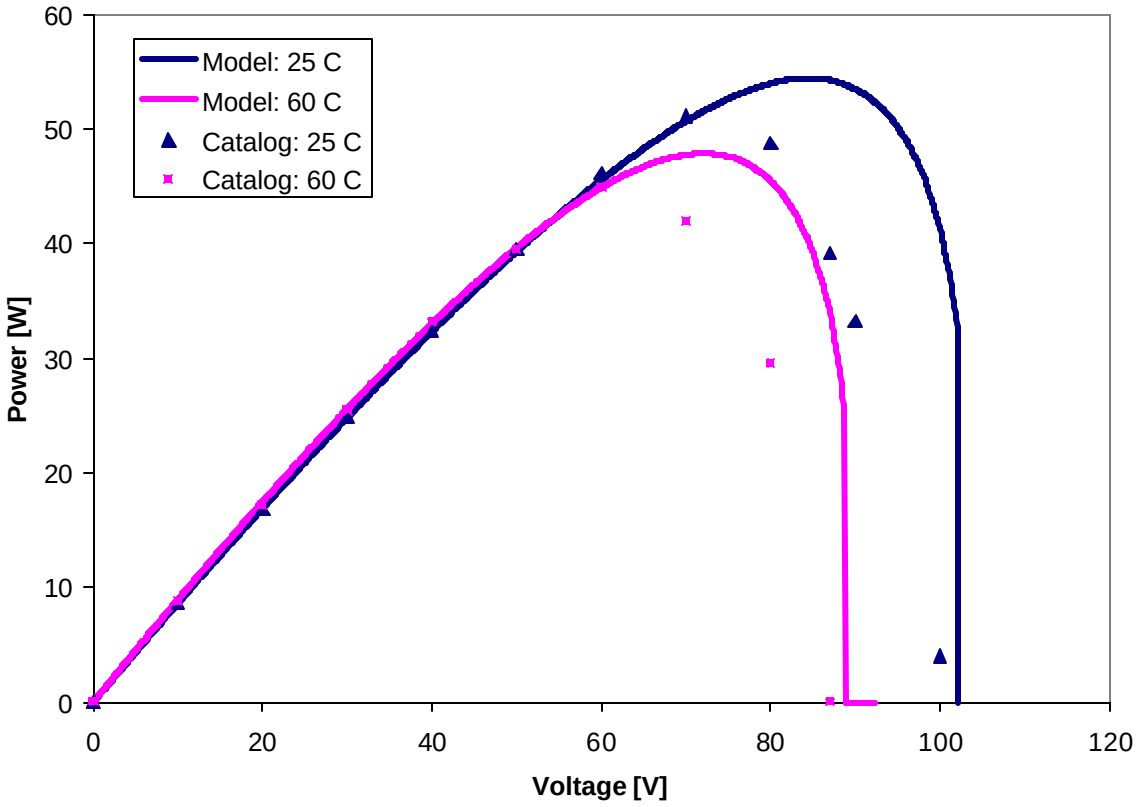

Catalog Data and Model Power-Voltage Curves for Solarex MST-56, Allowing R_s to Become Negative

Allowing R_s to fall below zero to match the voltage coefficient clearly does not help the model. Not surprisingly, the temperature effect on V_{oc} is improved, but the model fails to predict current and power accurately above 60 V for either temperature. Based on this result, it seems that the physical constraint of requiring a non-negative series resistance is justified.

As with the SA-5, there is some inconsistency between the specifications list and points shown on the catalog IV curve. Values for I_{sc}, V_{oc}, and I_{mp} were taken from the manufacturer's IV curves rather than from the catalog specs list. The differences are illustrated in Table 3.15-2.

Table 3.15-2: Discrepancies in Catalog IV Curve Values and Catalog Specifications List

	I_{sc}	V_{oc}	*Max Power Point*
Specs List	0.871 A	102 V (minimum)	73 V, 0.761 A (min)
Read from IV Curve	0.88 A	101 V	73 A, 0.70 A

The maximum power point voltage of 73 V given in the specifications list is consistent with that read from the power-voltage graph generated from the catalog IV curve. As discussed above, the largest disagreement between the model and catalog for this module is the effect of temperature on open-circuit voltage.

3.16 "Parameter Optimization" to Determine I_L, I_o, g, and R_s

The method described above to solve for I_L, I_o, γ, and R_s relies on algebraic relationships between these parameters derived from the general IV equation. An alternate approach is simply to find values for the parameters that minimize the error in model IV predictions. A TRNSYS program to perform similar parameter optimization for refrigeration equipment was developed by Rabehl and Reichler[7]. EES was employed for the error minimization program in this work. EES has the capability to numerically minimize a specific variable with respect to up to ten degrees of freedom. In this case the variable to be minimized is the sum of the squares of the differences between a set of catalog IV data and corresponding points along an IV curve generated by the model. Each "difference" is just a geometric distance between a catalog point and model point in the IV plane. All the currents and voltages are normalized to their open circuit and short circuit values; this assures that current and voltage will be weighted equally in finding the difference between two points. For N pairs are data, the total error to be minimized may be expressed as

$$e_{total} = \sum_{j=1}^{N} \left(\frac{I_{\mathrm{mod},j}}{I_{sc}} - \frac{I_{cat,j}}{I_{sc}} \right)^2 + \left(\frac{V_{\mathrm{mod},j}}{V_{oc}} - \frac{V_{cat,j}}{V_{oc}} \right)^2 \qquad \text{Eq. 3.16-1}$$

Values for I_{mod} and V_{mod} were read from manufacturers' IV curves for the Solarex SA-5 and MST-56 modules. The SA-5 catalog includes curves for three temperatures and the MST-56 includes two. A key issue in using this method is finding an appropriate point on the model IV curves to compare to each catalog point. One possibility is to match voltages; a model current is calculated for each catalog voltage and compared to the current on the catalog IV curve. In this case the voltage term in Eq. 3.16-1 drops out, leaving only a squared difference in currents. This method is simple and intuitive. However, it may not lead to model IV curves that match the catalog data as closely as possible. The reason for this is that at high voltages approaching V_{oc} the slope of the IV curve is quite large. This means that even if there is very little geometric distance between a catalog curve and a model curve, there may be large differences between currents at a particular voltage in this region. Thus, the optimization scheme will preferentially match the model and catalog data at high voltages at the expense of regions near the short circuit current.

A better method is to choose each I_{mod} and V_{mod} so that these points lie along the same "resistance line" as I_{cat} and V_{cat}. Normalizing with respect to I_{sc} and V_{oc}, this condition may be expressed as

$$\frac{V_{\mathrm{mod},j}}{I_{\mathrm{mod},j}} = \frac{V_{cat,j}}{I_{cat,j}} \qquad \text{Eq. 3.16-2}$$

Figures 3.16-1 and 3.16-2 compare these two methods, illustrating how matching voltage rather than resistance lines overemphasizes differences between the model and the catalog data for high voltage values.

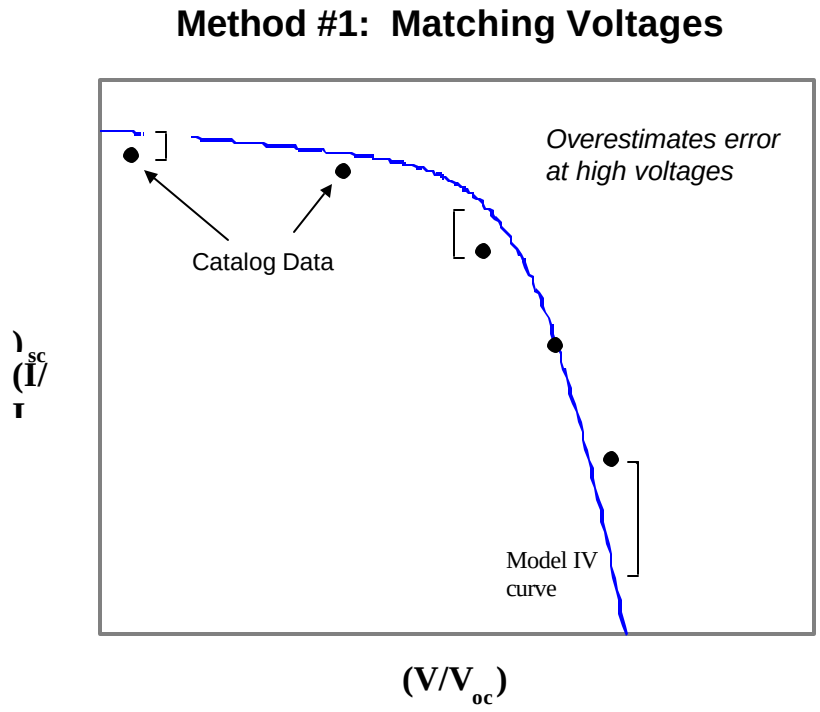

Figure 3.16-1: Matching Voltages to Optimize Paramteters Exaggerates High Voltage Error

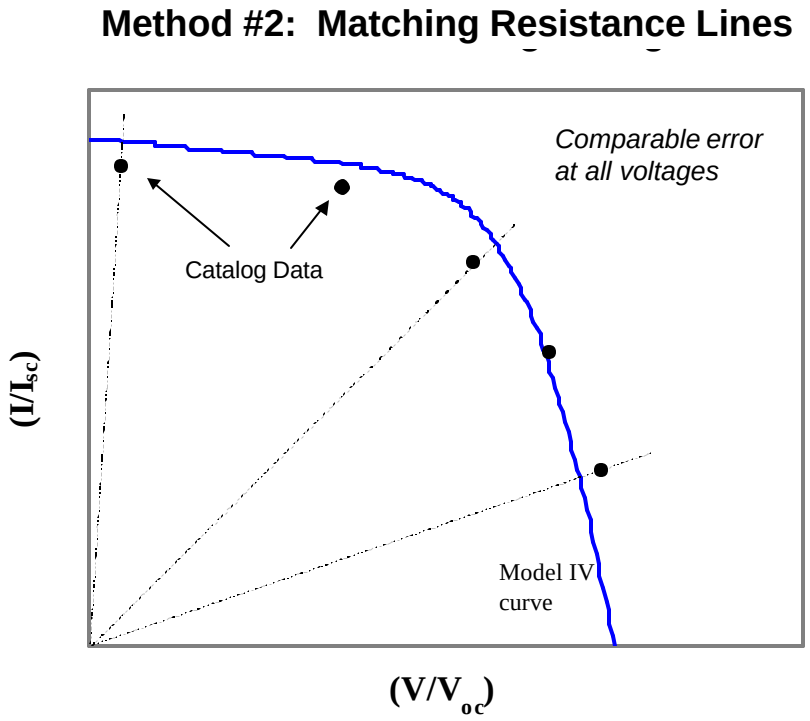

Figure 3.16-2: Matching Resistance Lines Evaluates Error on Geometric Distance Between Model and Catalog IV Curves

The parameter optimization method was first tested using a large number of points along the three IV curves for the Solarex SA-5. 14, 13, and 12 data points were used at 25 C, 50 C, and 75 respectively. With a total of 39 catalog data points, this method produced an excellent fit at all three temperatures, as Figures 3.16-3 and 3.16-4 show.

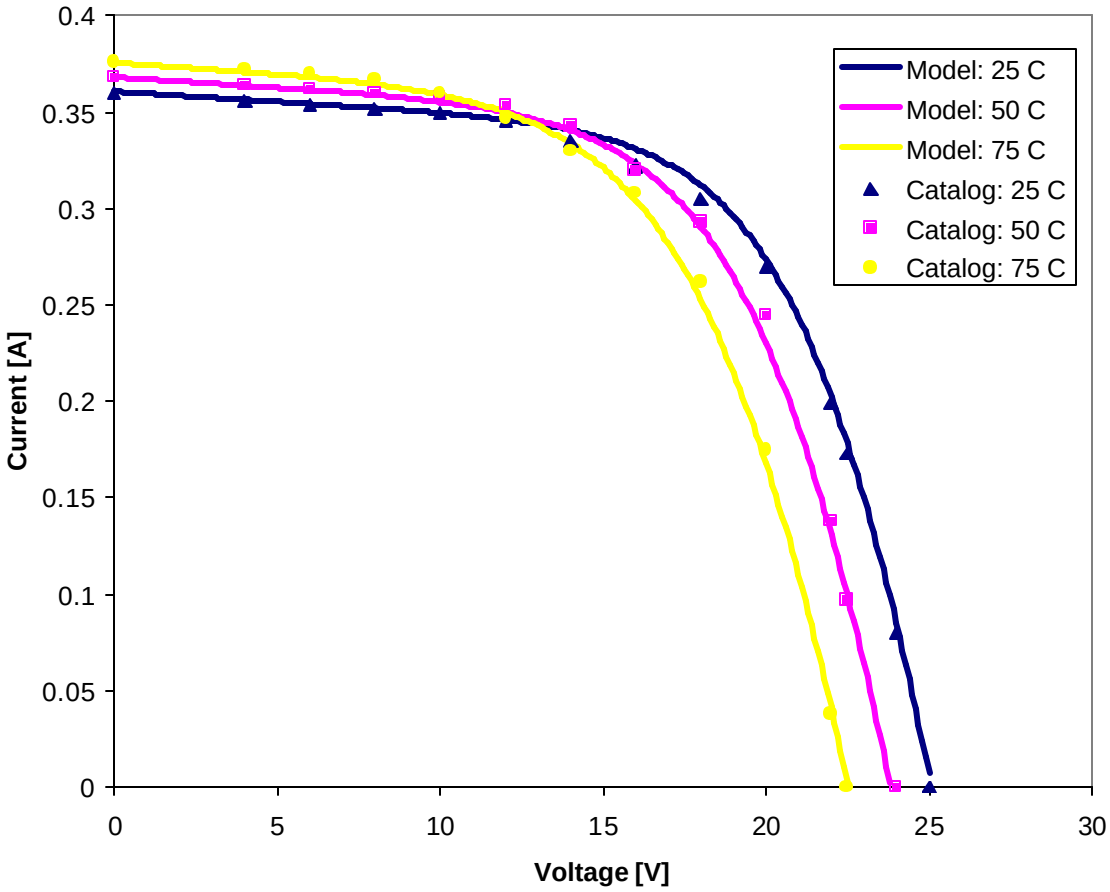

Figure 3.16-3: Catalog Data and Model IV Curves For Solarex SA-5 Using Parameter Optimization Scheme (39 Points)

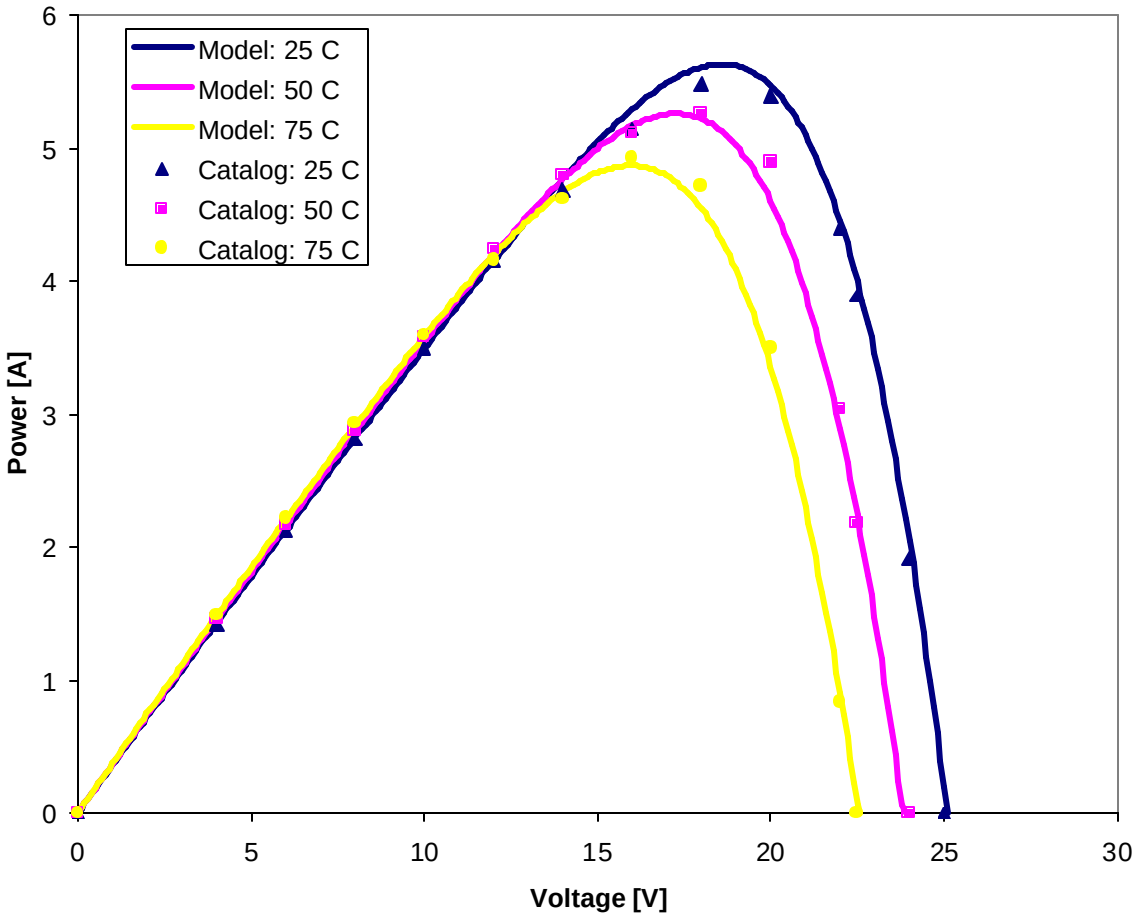

Figure 3.16-4: Catalog Data and Model Power-Voltage Curves For Solarex SA-5 Using Parameter Optimization Scheme (39 Points)

In some cases this many points may not be available, so it is interesting to see if the parameter optimization routine will still work well when fitting fewer points. The program was run again using a total of nine points, three at each temperature. The results are encouraging, producing curves nearly identical to those generated using 39 catalog points. Figures 3.16-5 and 3.16-6 illustrate the parameter optimization for nine points.

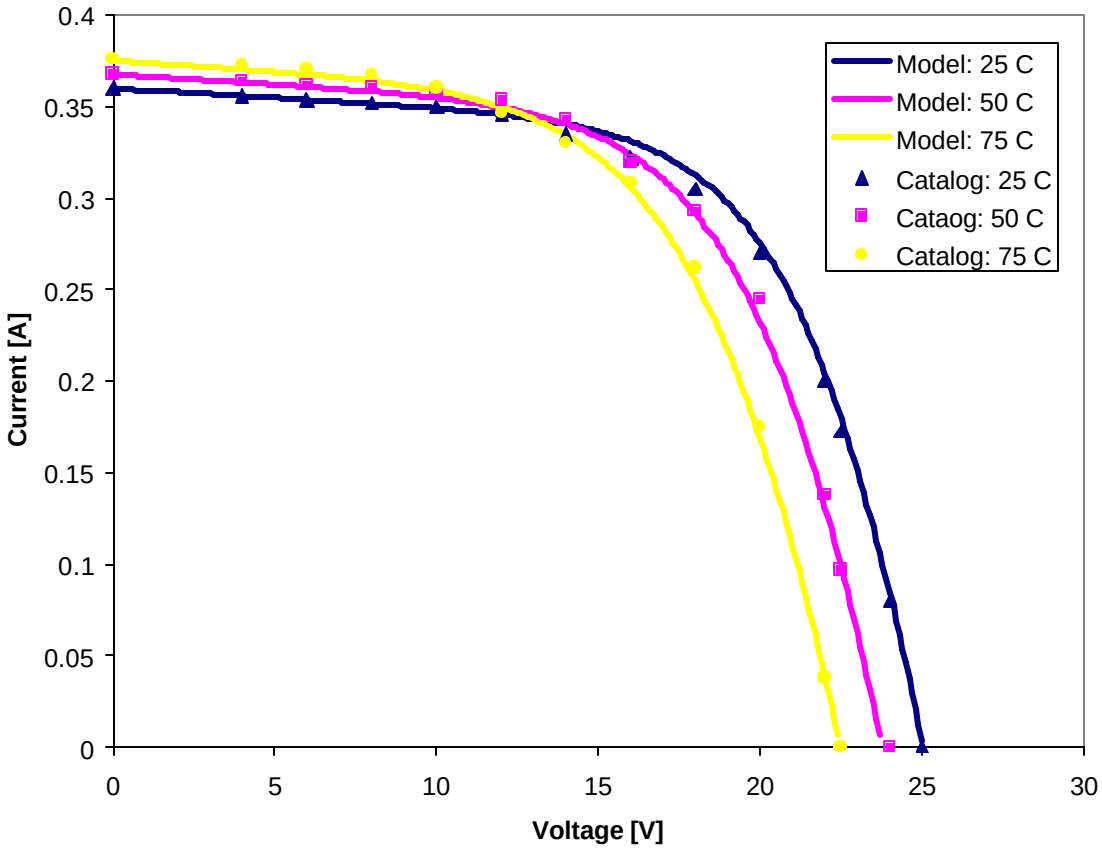

Fig 3.16-5: Catalog Data and Model IV Curves For Solarex SA-5 Using Parameter Optimization Scheme (9 Points)

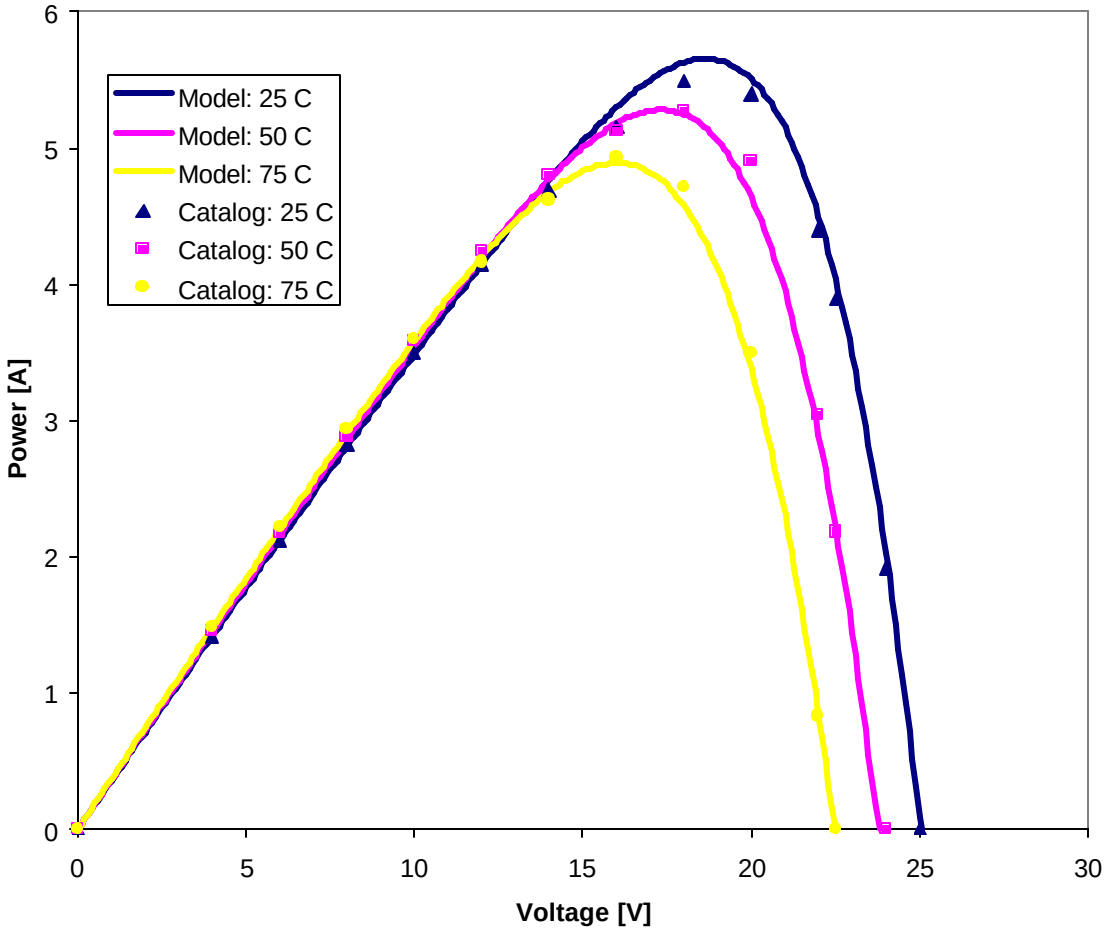

Fig 3.16-6: Catalog Data and Model Power-Voltage Curves For Solarex SA-5 Using Parameter Optimization Scheme (9 Points)

For the SA-5 parameter optimization clearly provides a viable alternative to iterating to find R_s and then solving for the other parameters algebraically. Unfortunately, the EES program to optimize the parameters for the Solarex MST-56 failed to converge using three data points at each of two temperatures. An additional point for each temperature was added between the maximum power point and open-circuit voltage point but this did not change the result. The algebraic parameter solution method did not produce wholly satisfactory results for the MST-56 either; correctly matching μ_{Voc} produced a negative series resistance and very poor fit at

voltages greater than the maximum power point. It may be that the five parameter IV relation described by Eqn. 2-20 does not adequately describe the behavior of this module.

3.17 Summary of Model Parameters at Reference Conditions

For the SA-5, the values of the five parameters I_L, I_o, R_{sh}, R_s, and γ at reference conditions are given in Tables 3.17-1 and 3.17-2 for various methods of calculation. The physical significance of these values is limited as they cannot be compared to measurable quantities. Their accuracy should be evaluated by comparing the IV curves they produce to experimental or catalog IV data.

Table 3.17.1: Parameter Values for Solarex SA-5

Method	I_L	I_o	g	R_s	R_{sh}
Algebraic iteration: V_{mp} = 18 V as given in specs list	0.3600 A	2.02×10^{-4} A	131.3	2.75×10^{-4} Ω	1000 Ω
Algebraic iteration: V_{mp} = 15 V as implied by catalog IV curve	0.3631 A	2.55×10^{-6} A	82.5	8.68 Ω	1000 Ω
Parameter optimization: 39 data points	0.3623 A	7.25×10^{-6} A	90.9	4.838 Ω	1000 Ω
Parameter optimization: 9 data points	0.3615 A	7.30×10^{-6} A	90.8	4.382 Ω	1000 Ω

Table 3.17.2: Parameter Values for Solarex MST-56

Method	I_L	I_o	g	R_s	R_{sh}
Algebraic iteration: R_s required to remain positive	0.8710 A	1.81×10^{-4} A	478.6	4.46×10^{-4} Ω	714.3 Ω
Algebraic iteration: R_s allowed to drop below zero	0.8202	9.33×10^{-3} A	926.8	-41.66 Ω	714.3 Ω
Parameter optimization: 6 data points	**Failed to Converge**				
Parameter optimization: 8 data points	**Failed to Converge**				

3.18 Insolation Effects in the Five-Parameter Model

In any PV both I_{sc} and V_{oc} decrease at low insolation levels. I_{sc} is roughly linear with insolation; this is reflected in the model by setting the photocurrent I_L to be proportional to insolation. V_{oc} does not drop off as quickly, although changes in this quantity are also significant. These effects are reflected in the five-parameter model, as illustrated in Figure 3.18-1 and 3.18-2.

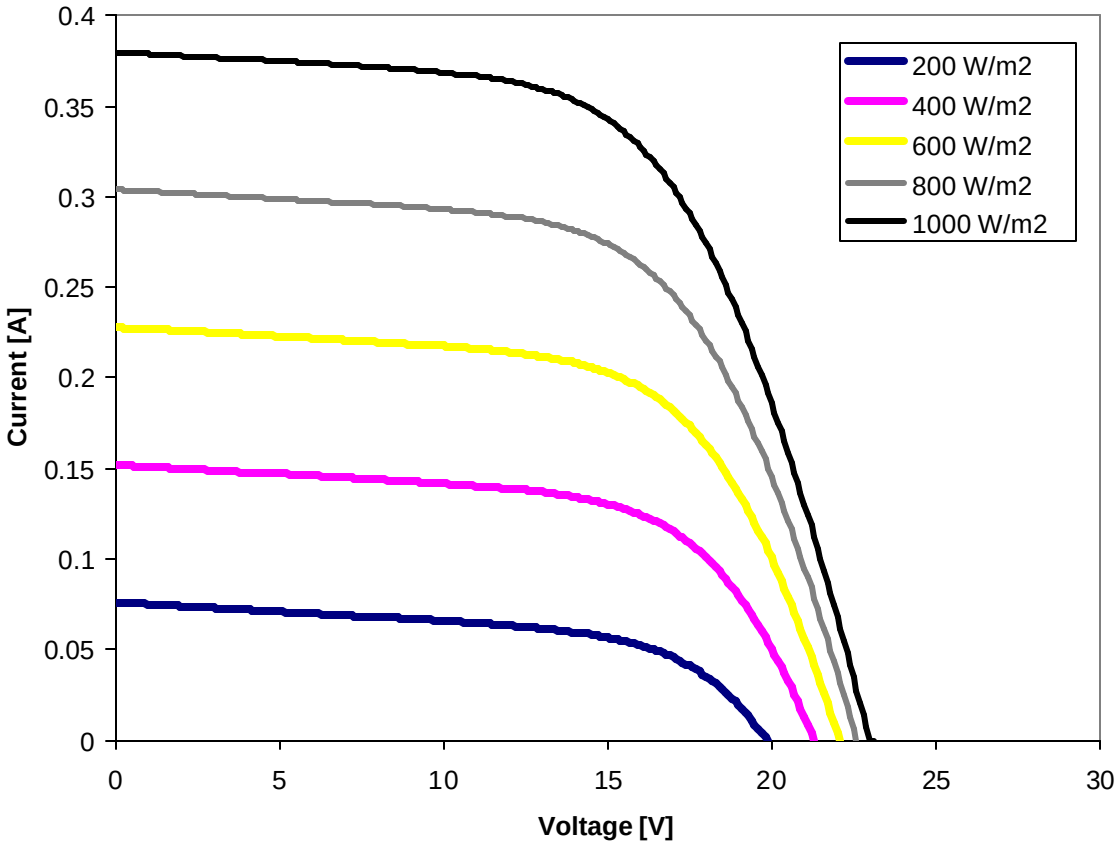

Figure 3.18-1: Model IV Curves for Solarex SA-5 at Five Insolation Levels

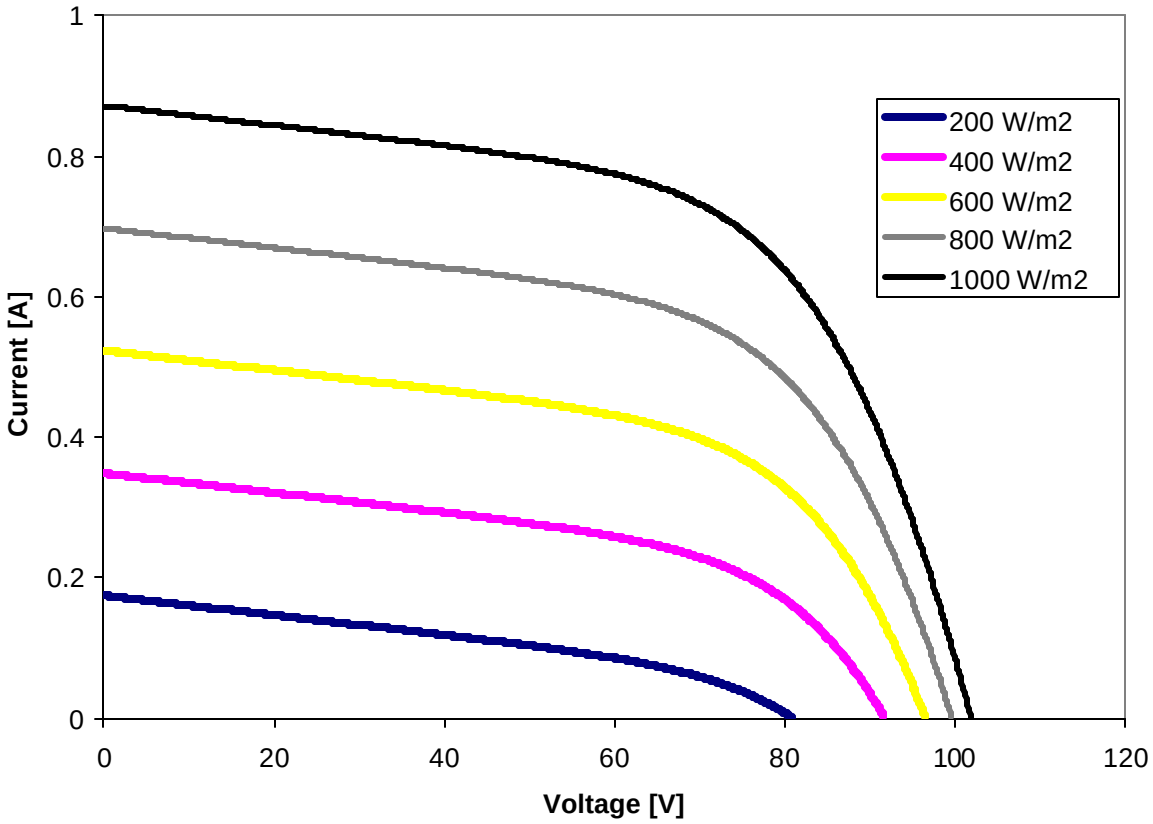

Figure 3.18-2: Model IV Curves for Solarex MST-56 at Five Insolation Levels

3.19 Computational Speeds of the Three Models

A final consideration in selecting a PV model is computational speed. The primary thrust of this work is estimating the economic potential for BIPV systems in Wisconsin. For this application computational speed is not a high priority since programming, data analysis, and documentation require much more time than actually running the simulations. However, a secondary goal is to produce stand-alone software for analyzing BIPV systems. Computational speed is more critical for this application.

Three "bare-bones" TRNSYS simulation decks were written to compare the speeds of the three models. Each deck includes only five PV arrays (four parameter, efficiency coefficient, or five parameter), five radiation processors, and a TMY data reader. The simulation length was set to one year with hour-long timesteps. The decks were run on a 200 MHz Intel Pentium Pro machine. The computational time necessary to run each model is given in Table 3.19.1.

Table 3.19-1: Computational Times with 200 MHz Pentium Pro

PV Model	***Computational Time***
Efficiency Coefficient	8 sec
Four Parameter	9 sec
Five Parameter	24 sec

It is surprising to see that the efficiency coefficient model is only marginally faster than the four parameter model. Given its relatively unsophisticated calculations and broad assumptions, a 10% improvement in computational over the four-parameter model does not justify its use in simulations for this work. The five parameter model is about three times slower, although it still runs this test in well less than a minute. For both Wisconsin economic analysis and stand-alone software development the five parameter model appears to be acceptably quick. The advantage of the five parameter model lies in its ability to simulate amorphous modules. For single crystal and polycrystalline modules its results are identical to those of the four parameter model. For the of sake speed, the

developed software actually employs the five parameter model only for amorphous modules. The four parameter model is used for single crystal and polycrystalline modules. Simulations in which a PV is coupled directly to a load require far more current-voltage iterations than grid-tied applications in which the PV unit is only called once per timestep. Thus, the slower speed of the five-parameter model may pose more of an obstacle for direct-coupled simulations.

3.20 Conclusion

This chapter addresses the basic physics of photovoltaic devices qualitatively and discusses issues involved in simulating their performance. A PV is formed by "doping" a semiconductor material such as silicon with impurities that change the electronic structure of the crystal lattice. If an incident photon of sufficient energy reacts with an electron in the PV material, the electron may be knocked loose from its atomic orbit. Such an electron is free to contribute to an electric current. A permanent electric field in the PV forces this photoelectron through a load, where it can perform useful work.

Three PV modeling schemes are introduced: the efficiency coefficient model, the four parameter model, and the five parameter model. The first of these, the efficiency coefficient model, determines the maximum power out of the PV without calculating its current-voltage coefficients. This limits its use to applications in which only the maximum power output is desired; it cannot be employed in simulations of direct-coupled PV systems. The efficiency coefficient assumes that the conversion efficiency of any PV is linear with operating temperature and independent of insolation. Neither of these assumptions is precisely correct. However, under most operating conditions they are reasonable approximations. The advantages of the efficiency coefficient lie in its speed and simplicity, although this works calls for the use of a more sophisticated model.

The four parameter model, developed largely by Townsend [2] and implemented into TRNSYS by Eckstein [3], has been used extensively in PV simulation work. It treats the PV as an equivalent circuit consisting of a current source, a diode, and a single resistor.

The "four parameters" consist of the current source strength, the resistance, and two diode curve-fitting parameters. These values are not physically measurable quantities and cannot be obtained directly from catalogs. However, they may be determined numerically from numbers readily available in a PV specifications list. This model is only slightly slower than the efficiency coefficient scheme. In addition, it is not suitable to determine the IV characteristics of amorphous PVs. Unlike the efficiency coefficient model, it has a semi-physical basis and does not make simplifying assumptions about the insolation and temperature-dependent behavior of the PV.

The final system, the five-parameter model, was implemented into a TRNSYS component for this work. It is based on an equivalent circuit like that in the four parameter model, although a second resistance is added. The model is able to simulate amorphous as well as single crystal and polycrystalline PVs. For single crystal and polycrystalline modules, however, the equations employed in this model reduce to those in the four-parameter model. Two methods of calculating the five parameters from catalog data are discussed. The "algebraic iteration" method iterates to determine a value for R_s such that the analytical coefficient of open circuit voltage matches the catalog value. The other parameters may be found explicitly from R_s at each iteration. In the "Parameter Optimization" method, an EES program minimizes the differences between points on a model IV curve and catalog data to find optimal values for the parameters. This method produces an excellent fit for the Solarex SA-5 but fails to converge for the Solarex MST-56. Running the five parameter model takes about three times longer than the four parameter model, although it is still acceptably fast for this work. The TRNSYS simulations detailed in the following chapter employ the four parameter model for single crystal and polycrystalline modules and the five parameter model with algebraic iteration for amorphous PVs.

CHAPTER 4

PHANTASM Simulation Program

PHANTASM (PHotovoltaic ANalysis and TrAnsient Simulation Method), developed for this work, is a tool for estimating the electrical energy production of grid-tied building integrated photovoltaic systems. Based on these results, the program also calculates a customer's monetary savings. This program employs TRNSYS, an energy simulation package developed at the UW Solar Energy Laboratory. PHANTASM was run using 1990 weather, load, and utility data for Milwaukee to estimate the feasibility of large-scale BIPV implementation in Wisconsin. The results of these simulations are discussed in Chapters 6 and 7.

This chapter begins with an overview of the capabilities of TRNSYS. It then summarizes the methodology and calculations employed in the PHANTASM program and describes the new TRNSYS components included in the program. The PHANASM User's Manual explains the features and capabilities of the program in more detail [Fry, 1999]. Appendix A gives the TRNSYS code for PHANTASM. Fortran Code and descriptions for the new TRNSYS TYPEs are given in Appendix B.

4.1 TRNSYS, TRNSHELL, and TRNSED

The photovoltaic simulations in this work were developed using TRNSYS (short for Transient System Simulation.) TRNSYS is a general-purpose energy system simulation package developed at the Solar Energy Laboratory [Klein et. al, 1997]. A TRNSYS program consists of a number of components or "TYPEs," each of which represents a specific part of the system. A TYPE may be physical system element such as a chiller, tank, or photovoltaic module. Other TYPEs perform necessary calculations but do not represent an actual piece of equipment. An example is the TYPE 16 "radiation

processor" which determines the solar energy incident on a tilted surface. Other TYPEs are output components that write simulation data to disk or produce graphical results on-screen.

Each TYPE requires a specific set of parameters and inputs. Parameters are values describing the component which do not vary with time, such as the reference value for short-circuit current of a PV module. Inputs may change with time as the simulation progresses. For instance, the TRNSYS inputs for a PV component include incident radiation and ambient temperature. Each TYPE uses the values of its parameters and inputs to calculate outputs at every timestep. The physical system is defined by assigning the outputs of certain TYPES to be inputs of others, producing a system of differential and algebraic equations. TRNSYS iterates the system inputs numerically until all outputs reach a specified convergence tolerance.

Consider the following example of a TRNSYS deck modeling a simple PV system. This deck includes four TYPEs. The first is a TYPE 9 data reader that reads a weather data file from disk; this data file includes hourly values for ambient temperature T_a and total solar radiation I on a horizontal surface. The second is a TYPE 16 radiation processor. This component employs an empirical correlation to determine the total radiation incident on the tilted surface of the PV module. The third component is the TYPE 64 PV module itself. It uses various module parameters, ambient temperature, and incident radiation from TYPE 16 to calculate electrical power generation. Finally, a TYPE 25 "printer" writes the PV output to disk. Figure 4-1.1 illustrates the information flow in this sample program.

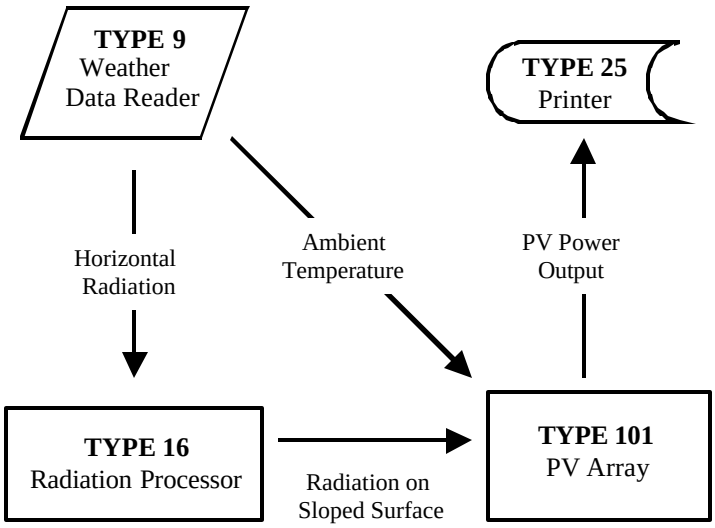

Figure 4-1.1: Simple TRNSYS PV program

Each TYPE is a Fortran subroutine that calculates outputs from inputs and parameters. TRNSYS provides a framework to link these subroutines together, along with numerical algorithms to solve the resulting system of equations. The source code for TYPEs in the standard component library may be modified as needed. In addition, new TYPEs may be developed for special applications. Seven new TYPEs were written for this work:

TYPE 3:	Utility Rate Schedule Calendar
TYPE 100:	Parallel Generation Rate Processor
TYPE 99:	Utility Rate Schedule File Writer
TYPE 96:	Efficiency Coefficient "Quick" PV Module
	(Evaluated in Chapter 3 but not used in final program)
TYPE 87:	Inverter
TYPE 98:	Economic Impact Evaluation
TYPE 123:	Sequential Simulation Summary

Two other non-standard TYPEs, developed by Thermal Energy System Specialists [1998], are included in the BIPV program:

TYPE 70: Grouped Parameter Replacement

TYPE 153: Load Data Reader

Finally, substantial modifications were made to Eckstein's TYPE 64 Four Parameter PV Module [1990] in developing the TYPE 101 Five Parameter PV Module.

TRNSYS decks are usually coded using TRNSHELL, a text editor. TRNSED is another, more intuitive user interface for TRNSYS. TRNSED uses buttons, pull-down menus, and number-entry fields to modify the components and parameters in a deck. One major advantage of TRNSED is that it allows users to quickly modify, run, and analyze TRNSYS simulations without detailed knowledge of the TRNSYS language. PHANSTASM employs the TRNSED interface. It is intended for engineers and architects interested in quickly estimating the economic performance of PV systems. Figure 4.1-2 illustrates the a portion of the TRNSED input screen for the PHANTASM program.

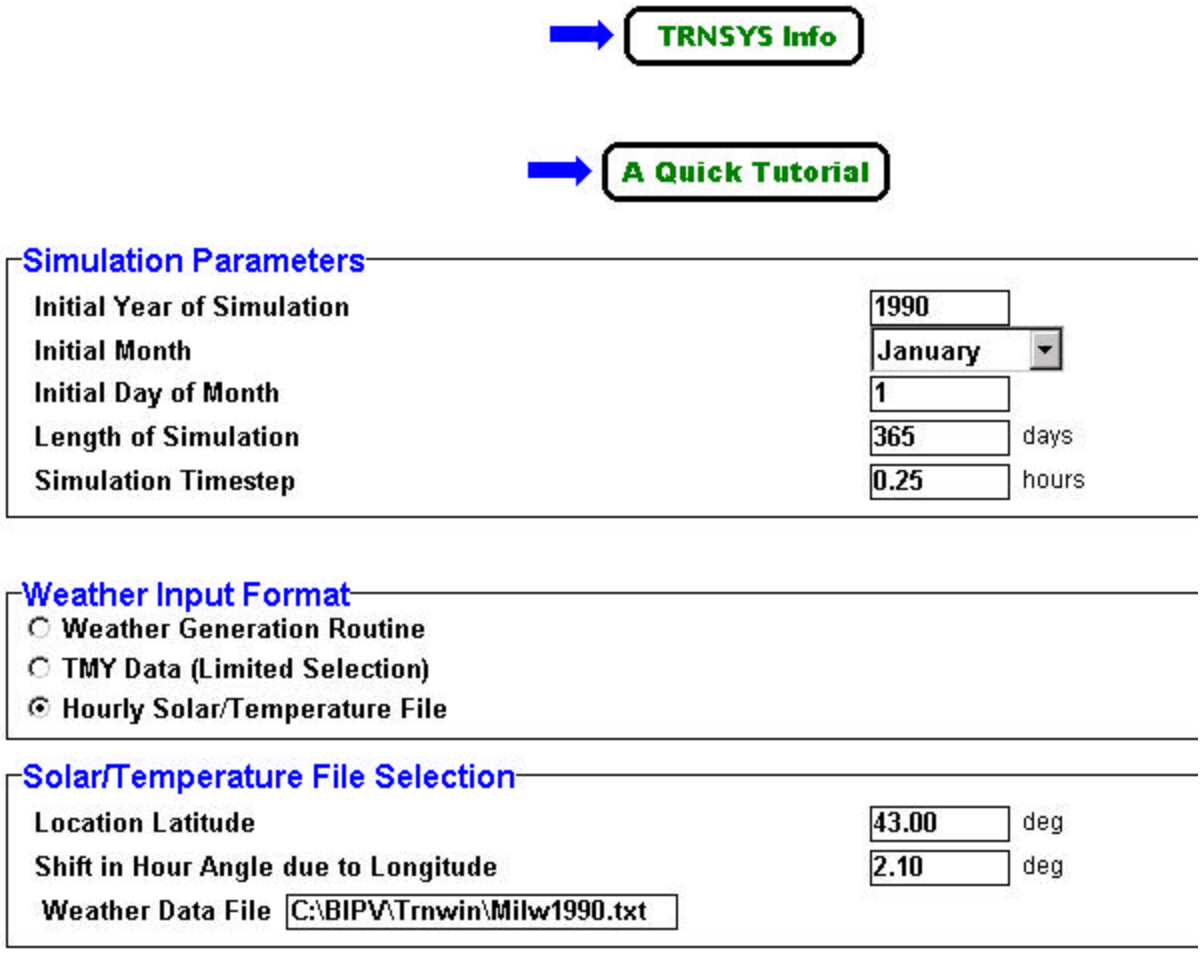

Figure 4.1-2: Portion of PHANTASM input screen

4.2 Overview of the PHANTASM Program

PHANTASM evaluates the physical performance of a BIPV system over any desired time period for which weather data is available. It also estimates the utility bill savings for the building owner. Three types of data are necessary to run a simulation: weather, building loads, and a utility rate schedule. A fourth data set, hourly utility demand obligation values, was used in this study to estimate the impact of BIPV systems on a utility. Chapter 5 discusses the data used in the Milwaukee simulations. All the

necessary information to run a simulation is summarized in Table 4.2-1. The table also shows where these data were obtained for the Milwaukee simulations.

Table 4.2-1: Input data for PHANTASM

Data	***Description***	***Source for Milwaukee Simulations***
PV System Parameters	Inverter information. Number, make, and orientation of PVs	Manufactures' catalog data
Weather	Temperature and solar radiation	Hourly solar data from NREL and temperature data from Commercial Cooling Load Library [12, 16]
Building Load	Total electrical load of building at each timestep	Records from Commercial Cooling Load Library [16]
Rate Schedule	Hourly and seasonal usage and demand rates for electric customers	Wisconsin Electric rate schedule brochure [14]

Weather data is necessary to determine the electrical performance of a PV system. This may be either statistically generated weather from a TYPE 54 Weather Generator or a file containing hourly values for temperature and solar radiation. 1990 data for Milwaukee was used for this study but any hourly weather data set may be used. A TYPE 16 Radiation Processor determines incident radiation on each PV array. The arrays themselves are represented by TYPE 101 Five Parameter Photovoltaics. Chapter 3 describes the calculations employed in TYPE 101. A TYPE 87 Inverter accounts for power conditioning losses. The total production of electricity at each timestep is the inverter output.

Determining a customer's savings due to PV-generated electricity is more involved than simply totaling up PV generation and multiplying by a constant price per unit of energy. There are two main complicating factors in this calculation. The first is that the price a utility charges for a kWh of electricity is not necessarily constant from one hour to the next. Rate schedules often include hourly and/or seasonal variations. The second complicating factor is that most commercial utility schedules include monthly (and

possibly annual) demand charges. A demand charge is based on a customer's largest instantaneous net power consumption over the course of the month. The demand charge is independent of the usage charge assessed for total energy consumption. Chapter 5 discusses rate schedules in more detail.

PHANTASM accepts building electrical loads from one of two sources. The first is the program SCHED.EXE developed by Thermal Energy Systems Specialists (TESS) [1998]. This program provides twenty-four "sliders" to define hourly loads and writes the load pattern to disk as a data file. The PHANTASM program includes a link to SCHED.EXE. A TYPE 153 Load Data Reader reads this file as the simulation runs. The slider input display is shown in Figure 4.2-1.

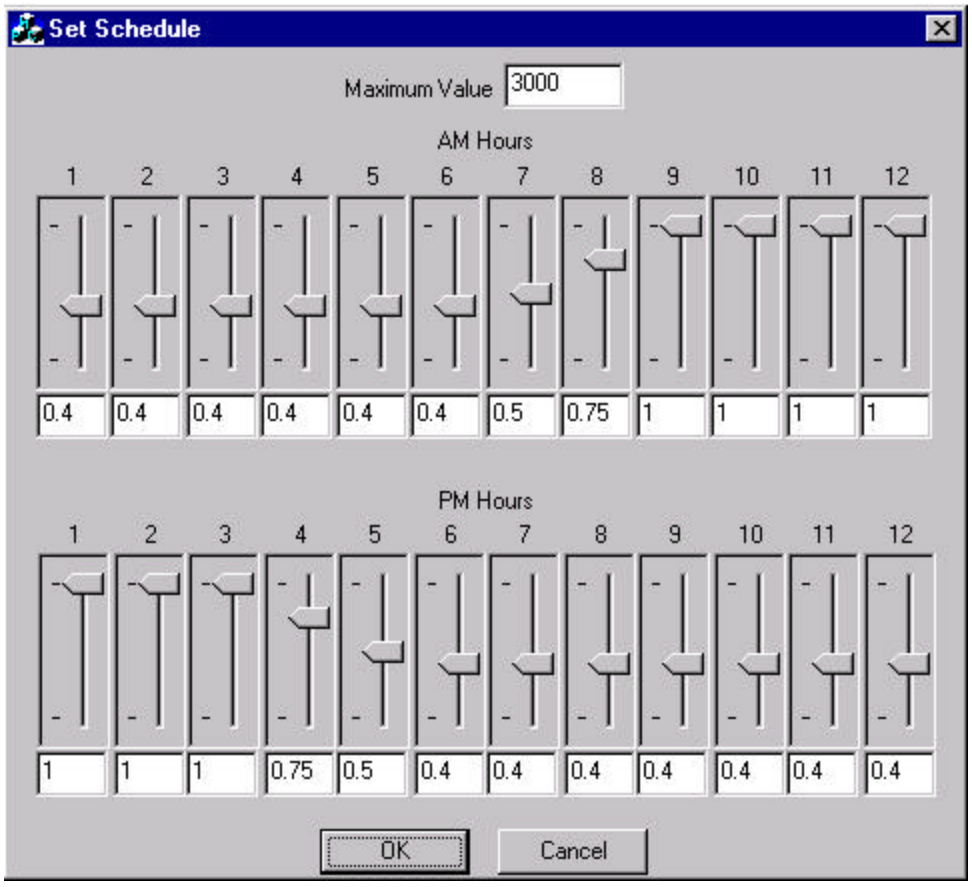

Figure 4.2-1: Graphical load input using SCHED.EXE

Alternately, a file containing load data over the course of a year may be read in from disk. Fifteen-minute load files from the Energy Center of Wisconsin Commercial Cooling Load Library [The Fleming Group, 1994] were used in the Milwaukee BIPV simulations.

Four new TYPEs were developed to calculate PV savings. These components may also be used in TRNSYS programs employing other types of renewable parallel generation. The first component is the TYPE 3 Utility Rate Schedule Calendar. This TYPE calculates the hour of day, day of week, and month at each simulation timestep. It also determines if the timestep falls on a weekend or holiday. These pieces of information are inputs for the TYPE 100 Utility Rate Schedule Processor. TYPE 100 reads a utility rate schedule file and uses the calendar to determine the usage and demand rates at each timestep. Cumulative energy usage and maximum demand are totaled for each month and written to two "utility bill" files. Twenty-four rate schedules for major Wisconsin utilities are saved as text files; the user may select a rate schedule from a pull-down menu on the TRNSED input screen. Alternatively, the user may create a new rate schedule. This file is written to disk by the TYPE 99 Utility Rate Schedule File Writer. At the end of the simulation a TYPE 121 Economic Evaluation component is called once. This component calculates one of four quantities and prints the results to a data file. Depending on the operating mode selected, TYPE 121 reports on payback time, break-even cost, profits (or losses), or return-on-investment.

Any of five TYPE 25 “Printers” write output files to disk. The TYPE 25 components produce tab-delimited text files detailing system performance at each timestep. A type 123 Sequential Simulation Summary writes a single-line summary giving savings and energy generation over the course of the simulation. This line is written at the bottom of an existing file without altering any data it may already contain; this component was developed to quicken the analysis of parametric studies. Finally, the user has the option of choosing between five TYPE 65 On-Line Displays which plot various aspects of system performance as the simulation runs. Turning off the on-line graphics causes the program to run slightly faster.

Figure 4-2.2 shows a flowchart summarizing the information exchange in the program. Output components are not included in the diagram.

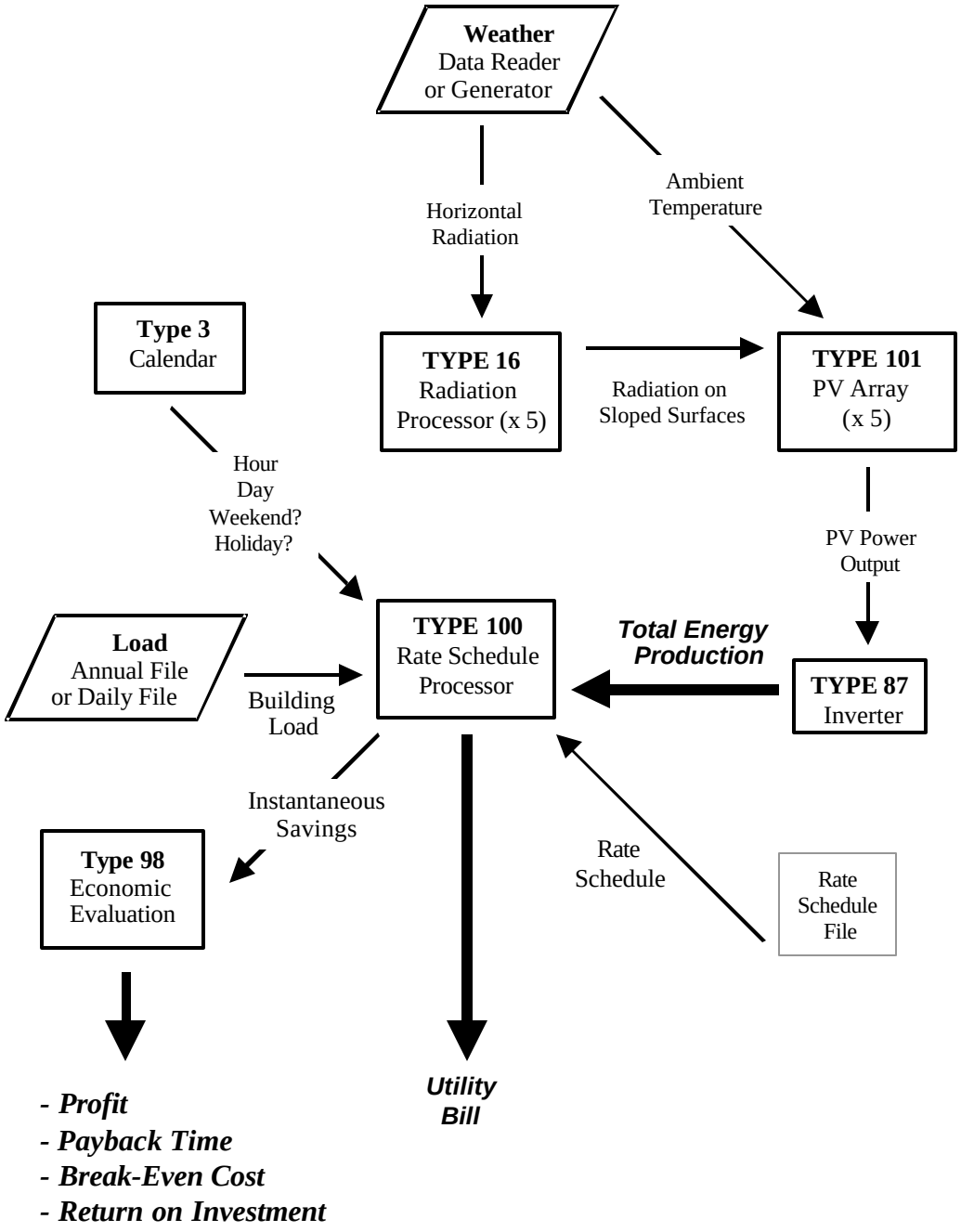

Figure 4-2.2: PHANTASM program flowchart

4.3 Weather Data

Weather may either be statistically generated at each timestep as the simulation runs or read from an hourly data file. The first option relies on the TYPE 54 Weather Statistical Weather Generator. This component produces hourly weather based on monthly averages for three quantities: horizontal radiation, temperature, and humidity ratio. TRNSYS includes these monthly quantities for over 200 North American cities, and any of these locations may be selected from the TRNSED input screen. The ground reflectance is not an output from TYPE 54, and the user will be prompted to enter a constant ρ_g value if weather generation is employed.

The program also supports two types of hourly weather files. The first is the standard TRNSYS TMY (Typical Meteorological Year) format. TMY data is compiled by NREL to represent climatic conditions in an ordinary year. The TMY database is discussed in further detail in Chapter 5. The user may select TMY data from one of four locations: Madison, Albuquerque, Miami, or Washington DC. As with statistically generated data, the user will be prompted to enter a constant value for ground reflectance when TRNSYS TMY data is selected. Other TMY data sets may be added if desired.

The second weather file format, referred to as "reduced NREL," was developed for this work and employed in the Milwaukee simulations. It includes hourly values for total horizontal radiation I and normal beam radiation I_{bn} at the present hour and following hour. In addition, the file contains entries for ground reflectance, ambient temperature, and relative humidity, and dewpoint temperature. (The dewpoint and relative humidity are not employed in calculations in the present version of the program, so zeros may be entered as placeholders if these values are unavailable.) The reduced NREL data format consists of 8760 rows of hourly data in eight tab-delimited columns as shown in Table 4.3-1:

Table 4.3-1: Format of "reduced NREL" data file

Column	***Quantity***	***Description***	***Units***
#1	I	Total radiation on a horzontal surface at present timestep	W/m^2
#2	I_{bn}	Beam radiation on a normal surface at present timestep	W/m^2
#3	I_{next}	Total radiation on a horizontal surface at next timestep	W/m^2
#4	$I_{bn,next}$	Beam radiation on a normal surface at next timestep	W/m^2
#5	T_{amb}	Ambient temperature	C
#6	R	Relative humidity	Unitless (0-100)
#7	T_{dp}	Dewpoint temperature	C
#8	ρ	Ground reflectance	Unitless (0-1)

4.4 PV System Calculations

A TYPE 16 Radiation Processor calculates the radiation incident on each PV array. The radiation processors in this program are configured to take total horizontal radiation and beam normal radiation as inputs. The beam radiation incident on each surface is calculated from these values. The diffuse radiation on each surface is determined using the "isotropic sky" method of Liu and Jordan [1960]. This method assumed that diffuse solar radiation emanates uniformly from all regions of the sky. Other diffuse radiation correlations, such as that developed by Perez [1988], account for increased sky radiation from regions near the horizon and solar disk. The Perez calculation was not employed in the BIPV program, however, because it occasionally generated unrealistically large "spikes" of radiation near dawn and dusk. The Liu and Jordan method gives a conservative estimate of PV output.

Both the weather data files and statistically generated data contain solar information in hourly increments. However, the Milwaukee simulations were run with a 15 minute timestep. TYPE 16 includes a "radiation smoothing" algorithm to interpolate solar radiation values at timesteps between the hourly data points. This algorithm employs a

quadratic fit between the previous hour, the present hour, and the next hour. This is why the new reduced NREL data format includes radiation values for both the present hour and the next hour.

The PV arrays themselves are represented in the program by TYPE 101 Five Parameter Photovoltaics. Chapter 3 describes the calculations employed in TYPE 101. For each array, the user may select one of seven manufacture's modules from a pull-down menu. The data for each of these modules (short-circuit current, temperature coefficient of voltage, etc.) are stored in text files which are accessed according to the menu selection. Alternately, the user may enter values for each of these parameters if the module desired for the simulation is not included in the list. The incidence angle modifier correlation described in Chapter 3 is included in TYPE 101, reducing solar absorption at large angles of incidence.

A TYPE 87 Inverter accounts for power conditioning losses. The TRNSED input screen allows the user the option of selecting a constant inverter efficiency or setting the efficiency to be a function of power. The user is also prompted to enter a maximum inverter capacity and an upper limit on excess PV power that may be sold to the utility. If efficiency is set to be a function of power, an efficiency curve is defined using the graphical input program SCHED.EXE. Efficiencies at eleven input powers ranging from 0 to the inverter capacity are written to a data file. At the beginning of the simulation this file is read by a TYPE 70 Grouped Parameter Replacement component. TYPE 70 resets the inverter parameters in the TRNSYS deck to account for the efficiency curve. When an inverter input power falls between the eleven points on the curve, TYPE 87 employs linear interpolation between points to find the efficiency. The output from TYPE 87 is the total PV system generation at each timestep.

4.5 Building Loads

PHANTASM provides two options for electrical loads. The first option is an hourly load schedule which repeats each day. SCHED.EXE is used to define the load at each hour. In this case the load is read by a TYPE 153 Load Data Reader developed by TESS [10]. The second option is to read a historical load data file from disk. Fifteen minute electrical load data for three commercial buildings were employed in the Milwaukee simulations. There are three important considerations in using load data files:

#1: *The interval between entries in this file must be equal to the simulation timestep.* A new load point is read at every timestep, so if the timestep does not equal the data interval the simulation time and load time will be mismatched.

#2: *Each entry in the load file must be integrated energy use in kWh over the data interval*. Unless the data interval is exactly one hour, using a file giving power consumption in kW will produce incorrect results.

#3: *The time of the first data point for the load should correspond to the end of the interval of integration for the first weather point.* Solar data in TMY files and weather from the NREL's hourly solar files are integrated energy values over hour-long intervals. The first interval in an annual NREL data set is from midnight to 1:00 AM. Thus, the first point in the building load file should occur at 1:00 AM. The first three points in the Cooling Load Library data set occur at 12:15 AM, 12:30 AM, and 12:45 AM, so these points were deleted before running the Milwaukee simulations.

4.6 Calendar and Utility Rate Processor

As mentioned above, the monetary savings from PV-generated electricity cannot be determined simply by multiplying energy production by a constant electrical rate. The customer's benefit from parallel generation at any time is dependent on both the utility rate schedule and the building load. Two new TYPEs were developed for calculating the value of parallel generation to a building owner. The first is the TYPE 3 Utility Rate Schedule Calendar. Utilities generally employ off-peak rates on weekends and holidays, and TYPE 3 determines when these periods occur. TYPE 3 outputs several "calendar quantities" at each timestep:

Output #1:	Hour of Day
Output #2:	Hour of Year: Int (Simulation Time)
Output #3:	Day of Year
Output #4:	Day of Week (0 = Sunday, 6 = Saturday)
Output #5:	Month (1-12)
Output #6:	Day of Month (1-31)
Output #7:	Weekend Flag (1 = YES, 0 = NO)
Output #8:	Holiday Flag (1 = YES, 0 = NO)

Calculating outputs #1, #2, #3, and #5 is fairly trivial, requiring only modular division. The day-of-week calculation was obtained from a website detailing electronic calendar algorithms [Montes, 1998]. The day-of-week formula is

$$Day-of-Week = \left(36 + d + \frac{5y}{4}\right) \bmod 7 \qquad \text{Eq. 4.6-1}$$

where

$$d = Day-of-Year$$

$$y = year - \frac{14 - month}{12}$$

The weekend flag is activated when *d* is equal to 5 or 6. The holiday flag is activated on certain days of the year. The default holiday list is:

#1	New Year's Day
#2	Martin Luther King Day
#3	Presidents' Day
#4	Memorial Day
#5	Independence Day
#6	Labor Day
#7	Columbus Day
#8	Veterans Day
#9	Thanksgiving
#10	Christmas Day

Easter is not included in this list because it always falls on a Sunday. Utilities generally use the same off-peak rates for weekends and holidays, so for rate schedule purposes Easter is no different from any other Sunday. Some holidays, such as Christmas, always fall on a particular date. It is not difficult to determine, for example, whether or not a particular timestep falls on Christmas. The date of some other holidays, such as Presidents' Day, changes from year to year. President's day occurs on the third Monday in February. The formula for finding these holidays is:

$$Date = 1 + 7(N - 1) + [(Day - DW) \bmod 7] \qquad \text{Eq. 4.6-2}$$

Here, *Day* is the day of the week for the holiday in question: 1 for Monday, 2 for Tuesday, and so on. *N* is the number of occurrence for that day in the month, so N is set to 3 when solving for the third Monday in the month. *DW* is the day-of-week of a specific date in the month:

$$DW = Day - of - Week[Year, Month, 1 + 7(N - 1)] \qquad \text{Eq. 4.6-3}$$

Day-of-Week for day number [1+7(N-1)] is found from equation 4.6-1. At the third Monday in February, the day-of-year in Eq. 4.6-1 is set to 46.

The second unit involved in savings calculations is the TYPE 100 Parallel Generation Rate Processor. Inputs include load in W, parallel generation rate in W, (PV generation in this program), and several calendar values from TYPE 3. The load schedule is read from a text file. This file contains information on hourly rates for usage and demand as well as off-peak rates for holidays and weekend and ratchet rates. The format of the rate schedule files is detailed Section 4.3 of the PHANTASM User's Manual [Fry, 1999]. TYPE 100 keeps track of the cumulative energy consumption and generation as well as the maximum load during each month for determining demand charges. Outputs from TYPE 100 at each timestep include net building load (load minus parallel generation), usage rate, excess generation sold back to the utility, and cumulative solar savings. TYPE 100 also prints a "utility bill" file to disk detailing monthly energy consumption and generation as well as usage, demand, and ratchet charges for that month. PHANTASM includes two TYPE 100 components so the user may compare utility bills for buildings with and without BIPV.

4.7 Evaluating Economic Parameters

After a simulation is complete, a TYPE 98 Economic Evaluation component is called to determine key economic parameters of the system. These calculations are based on the total utility bill savings over the course of a year as well as such parameters as interest rate, market discount rate, and system cost. TYPE 98 has four modes; in each mode it calculates a different economic characteristic and prints the results to a data file. Table 4.7-1 summarizes the output values for each mode as well as the data necessary to determine the output.

There are three key assumptions in each economic evaluation:

> #1: The PV system is purchased with cash. Interest rates on loans are not included in the calculations.

Table 4.7-1: Modes of operation for TYPE 98 Economic Evaluation

Ouput	***Necessary Information***
Payback Time N_p	- System cost C_S - First year operation and maintenance costs C_M - Inflation rate i - Market discount rate d
Breakeven System Cost C_{even}	- Period of economic evaluation N - First year operation and maintenance costs C_M - Inflation rate i - Market discount rate d
Profits P	- System cost C_S - Period of economic evaluation N - First year operation and maintenance cost C_M - Inflation rate i - Market discount rate d
Return-on-Investment d_{ROI}	- System cost C_S - Period of economic evaluation N - First year operation and maintenance cost C_M - Inflation rate i

#2: The annual rate of return on a typical investment is a known value equal to the market discount rate *d*. The discount rate reduces the effective value of future electrical savings.

#3: Operation and maintenance costs and utility rates increase with the inflation rate *i*.

All other things being equal, these assumptions predict that a PV system becomes more profitable as the inflation rate goes up. This is because future electricity purchases will become more expensive when inflation is high. On the other hand, a high market discount rate makes PV appear less profitable. A large value of *d* indicates a strong economy in which other investments are more enticing.

Beckman and Duffie discuss a method to evaluate the payback time of solar thermal systems [1991]. In the following expressions, N_p is the number of years that a solar investment takes to pay off.

$$N_p = \frac{\ln\left(\frac{C_S(i-d)}{FLC_F}+1\right)}{\ln\left(\frac{i+1}{d+1}\right)} \qquad \text{for } i \neq d$$

$$N_p = C_S \frac{i+1}{FLC_F} \qquad \text{for } i = d \qquad \text{Eq. 4.7-1}$$

FL is amount of fuel saved over the course of one year, and C_F is the cost per unit of fuel. Thus, the quantity FLC_F is the total value of the energy produced by the system over the course of the year. For a PV system, this value is replaced by the electrical savings C_E. In the BIPV program it is the value of electrical savings over the course of a year-long simulation. Subtracting the annual operation and maintenance cost C_M gives

$$N_p = \frac{\ln\left(\frac{C_S(i-d)}{C_E - C_M}+1\right)}{\ln\left(\frac{i+1}{d+1}\right)} \qquad \text{for } i \neq d$$

$$N_p = C_S\left(\frac{i+1}{C_E - C_M}\right) \qquad \text{for } i = d \qquad \text{Eq. 4.7-2}$$

The second mode of operation determines the break-even cost C_{even} of the PV system given a period of economic evaluation N. At the break-even cost, it will take to N years of operation for the investment to begin to be profitable. The breakeven cost is found by solving Eq. 4.7-2 for C_S. The result is shown in the following expressions, with the variable C_S replaced by $C_{even.}$

$$C_{even} = \frac{1}{(d-i)}\left(1-\left(\frac{1+i}{1+d}\right)^{N}\right)(C_E - C_M) \qquad \text{for } i \neq d$$

$$C_{even} = \frac{N}{1+i}(C_E - C_M) \qquad \text{for } i = d \qquad \text{Eq. 4.7-3}$$

TYPE 121's third mode of operation calculates the profits (or losses) for a PV investment after a period of N years. Given a system cost C_S, the profits after a given period of evaluation is found by subtracting C_S from the total value of energy savings over that period. A negative result indicates a loss rather than profit.

$$P = \left[\frac{1}{(d-i)}\left(1-\left(\frac{1+i}{1+d}\right)^{N}\right)(C_E - C_M)\right] - C_S \qquad \text{for } i \neq d$$

$$P = \left[\frac{N}{1+i}(C_E - C_M)\right] - C_S \qquad \text{for } i = d \qquad \text{Eq. 4.7-4}$$

The fourth mode of operation for TYPE 121 is solving for the system return-on-investment, or ROI. The ROI is the market discount rate at which the investment will pay off in N years. It is not possible to solve Eq. 4.7-2 explicitly for d, so TYPE 121 employs an iterative numerical scheme to determine the ROI. When d is equal to d_{ROI}, profits will equal exactly zero. TYPE 121 starts with an arbitrary guess value of 0.08 and solves Eq. 4.7-4. If the profits at this discount rate are positive, the d is increased by 0.01. If the profits are negative d is decreased by 0.01. The step size is halved on any iteration when P changes from negative to positive or vice versa. It is assumed that d has converged d_{ROI} when the relative change in P over one iteration changes by less than 0.5%.

4.8 Summary

The PHANTASM program is a TRNSYS package for examining the impact of photovoltaic parallel generation on the electric bills of grid-tied customers. This program employs TRNSED, a menu-based interface for TRNSYS. Detailed knowledge of the TRNSYS programming language is not necessary to define a BIPV system and estimate its physical and economic performance. Photovoltaic generation is determined from weather data and PV system parameters. These results are combined with a building load and utility rate schedule to calculate solar savings over the course of the simulation. The program accounts for hourly, daily, and seasonal variations in electric usage and demand rates. The user may choose from one of seven types of PV modules and 24 rate schedules from major Wisconsin utilities. New PVs and rate schedules may be added as needed.

CHAPTER 5

Simulation Data

The main thrust of this work is to evaluate, through simulation, the economic feasibility of implementing large-scale BIPV systems in Wisconsin. Four sets of location-specific data for Milwaukee were employed in the simulations. The first of these is weather data, including Milwaukee's hourly solar radiation and temperature in 1990. The second set of data is 1990 electrical loads for three commercial buildings in the Milwaukee area. These loads were obtained from the Energy Center of Wisconsin Commercial Cooling Load Library. The third data set consists of two commercial rate schedules from Wisconsin Electric, the power utility in Milwaukee. These schedules were taken from a Wisconsin Electric pamphlet [1998]. Finally, a fourth data set was used in examining the benefit of BIPV system to the utility. Wisconsin Electric's total hourly loads in 1990 were matched with PV generation to estimate the peaking reduction potential of BIPV. The utility load data were obtained from Ron Pugh of Wisconsin Electric's marketing department [1998]. This chapter discusses the contents of these four data sets and how they were put to use in running and evaluating the Milwaukee simulations.

5.1 Weather Data Format

The BIPV Simulation Program requires two types of hourly weather data: solar radiation and ambient temperature. Depending on the mode selected, the TYPE 16 TRNSYS radiation processor can accept several types of solar data as inputs. One of several correlations may be employed to determine total radiation incident on a tilted surface from a single radiation value the total radiation on a horizontal surface *I*. In general, however, more accurate results may be obtained by using two radiation values at each timestep. The BIPV Simulation

Program is configured to use the total horizontal radiation, I, and the beam radiation incident on a normal surface, I_{bn}.

The NREL website (www.nrel.gov) contains downloadable hourly radiation data for over 300 North American locations [1992]. Data are available for every year from 1961 until 1990. These files include 5 solar quantities, each averaged over hour-long data intervals. Table 5.5-1 summarizes these quantities.

Table 5.1.1: Data in NREL's hourly solar radiation files

Quantity	***Description***	***Units***
I_o	Extraterrestrial radiation on a horizontal surface	[W/m^2]
$I_{o,normal}$	Extraterrestrial radiation on a normal surface	[W/m^2]
I	Total radiation on a horizontal surface	[W/m^2]
I_d	Diffuse radiation on a horizontal surface	[W/m^2]
I_{bn}	Beam radiation on a normal surface	[W/m^2]

I and I_{bn} were copied from the NREL file into MILW1990.TXT, the data file supplying inputs for TRNSYS.

The extraterrestrial values I_o *and* $I_{o,normal}$ were not measured but rather were calculated from astronomical relationships. In addition, the terrestrial values I, I_d, *and* I_{bn} for Milwaukee and most other locations were not actually measured with a pyranometer. In Milwaukee they were calculated from observed sky cover and estimated optical depths. This procedure introduces an uncertainty in the data greater than the experimental error inherent in pyranometer measurements. The NREL file includes uncertainty estimates for I, I_d, and I_{bn}. The typical range is 9% to 13%, although in some cases they range from 13% to 18%. These uncertainties in the solar data are probably the dominant source of error in the Milwaukee simulations.

The program also requires hourly temperature values because PV performance is temperature dependent. Milwaukee temperature data at fifteen minute intervals are included in the Cooling Load Library. An Excel macro was written to pull out one value per hour; these hourly values were saved in the weather file to be read by the BIPV Simulation Program. In addition, the program reads in the ground reflectance ρ at each timestep. The Upper Midwest's ground reflectance exhibits significant monthly variation because of the high albedo of snow. Hourly ground reflectance observations were not available, so ρ was estimated at each month as shown in Table 5.1-2.

Month	***Ground Reflectance***
January	0.6
February	0.6
March	0.4
April	0.3
May	0.2
June	0.2
July	0.2
August	0.2
September	0.2
October	0.2
November	0.3
December	0.4

Table 5.1-2: Monthly estimates for ground reflectance

5.2 Analyzing the Weather Data

The Milwaukee simulations are case studies intended to evaluate the potential for large scale implementation of BIPV systems in Wisconsin. The lifetime of a PV system is much greater than a single year, and its performance will vary somewhat from year to year due to fluctuations in the weather. For this reason it is desirable to estimate how closely Milwaukee's 1990 weather represents an "average" year.

A useful tool in this analysis is the Typical Meteorological Year (TMY) data. TMY data sets are compiled by NREL and may be freely downloaded from their website. TMY data are available for each of the North American locations in the NREL database [NREL, 1992]. Each month of the "typical year" is taken directly from one of the years in the meteorological database. For instance, the January data for Milwaukee TMY is taken from January 1962 and the February data is from February 1966. The source year for each month of the "typical year" is selected based on two criteria. The first is how closely the data replicates the average weather for that month. The second is the reliability of the data. Thus, if the June weather data for two years are both fairly normal, the year with smaller data uncertainty would be chosen.

The TMY data were compared with the 1990 Milwaukee data from NREL (solar) and the Cooling Load Library (temperature and humidity) to estimate how closely 1990 corresponds to an average year. Using an unusually cloudy or clear year for simulation case studies will tend to underestimate or overestimate the feasibility of BIPV. Temperature trends will also influence the results to a much lesser extent. The daily clearness index K_T was calculated to quantify the cloudiness of each day. The clearness index is defined as

$$K_T = \frac{H}{H_o} \qquad \text{Eq. 5.2-1}$$

where H is the total daily solar radiation incident on a horizontal surface and H_o is the total horizontal extraterrestrial radiation. K_T values typically range from about 0.15 on rainy days to 0.7 on days with no clouds or haze. EES was used to determine hourly dewpoint temperatures from the Cooling Load Library dry-bulb temperatures and relative humidities at each hour. Excel macros were employed to determine K_T, daily average temperature $\overline{T}$, and daily average dewpoint $\overline{T}_{dp}$ for each 1990 day and TMY day. It is notable that the Milwaukee TMY data for October was taken from 1990, so it is safe to assume that October was not an exceptional month in 1990. Figures 5.2-1, 5.2-2 and 5.2-3 show the monthly averages of $\overline{T}$, $\overline{T}_{dp}$, and K_T values for the two data sets. In October the K_T values are identical. $\overline{T}$ and $\overline{T}_{dp}$ do not match exactly because NREL's temperature and humidity values in TMY were taken independently of the Cooling Load Library data.

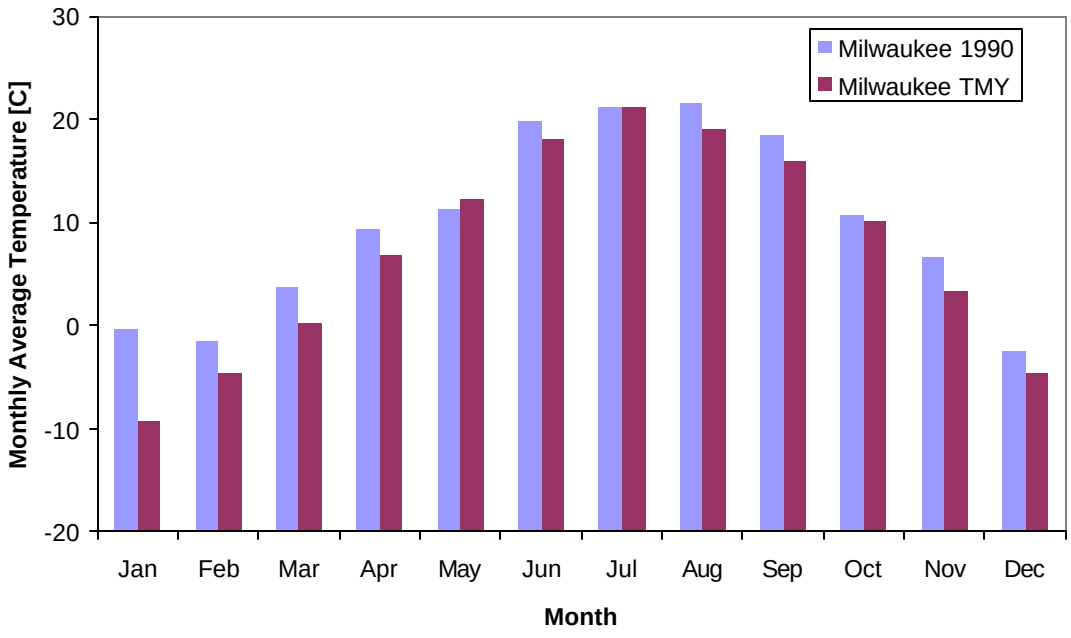

Figure 5.2-1: Monthly average temperatures: Milwaukee 1990 and TMY

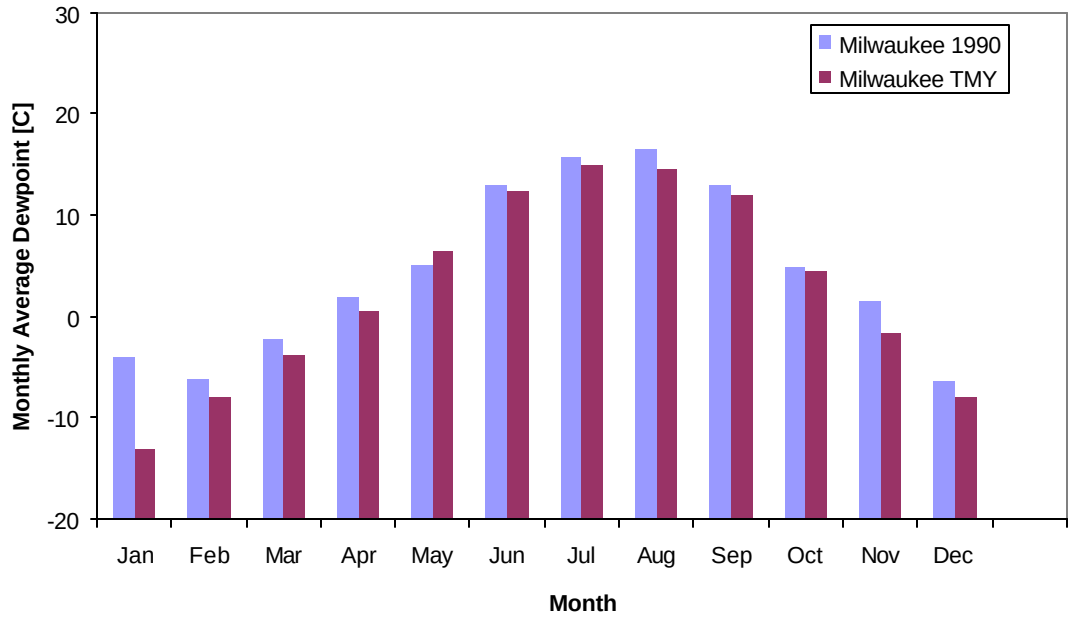

Figure 5.2-2: Monthly average dewpoints: Milwaukee 1990 and TMY

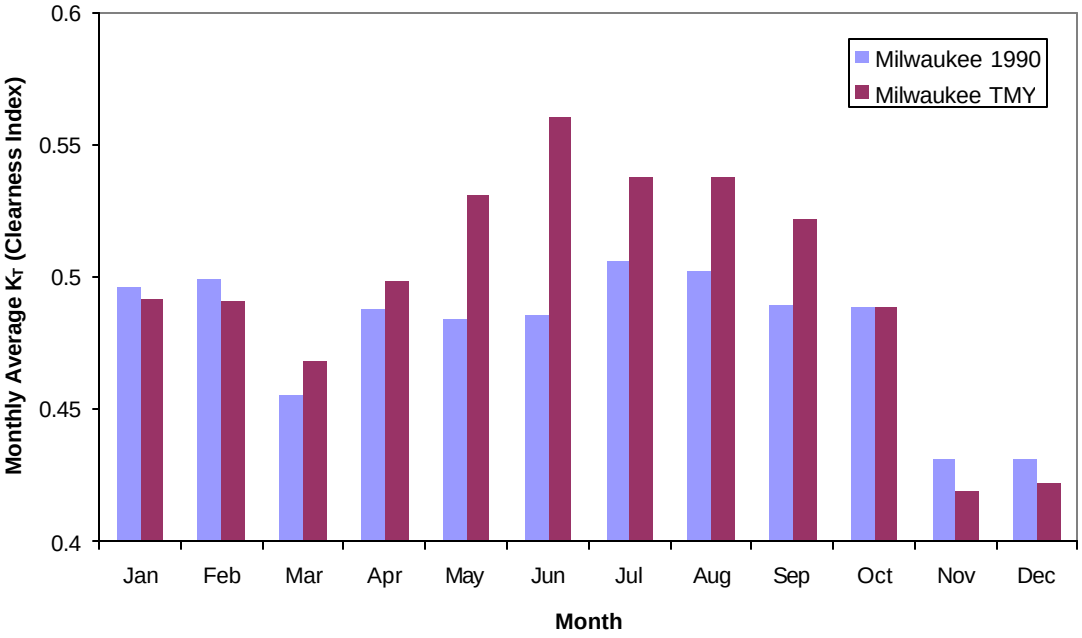

Figure 5.2-3: Monthly average K_T values Milwaukee 1990 and TMY (expanded scale)

From Figures 5.2-1 and 5.2-2 it is apparent that every month in 1990 except July and October was warmer than in a "typical year." The difference is usually on the order of 2 C. However, this trend is particularly noticeable in January when the 1990 data was an average of 9 C warmer than the TMY data. On the whole, 1990 was an exceptionally warm year in Milwaukee.

Figure 5.2-3 shows that 1990 was also not a typical year in terms of cloudiness. $\overline{K}_T$ values (monthly averages for K_T) for the two data sets were similar in November, December, January, and February. The 1990 $\overline{K}_T$ values were about 0.01 greater than the TMY values for these months, but these small differences are not significant. On the other hand, the spring and summer months of May, June, July, August, and September were considerably cloudier in the 1990 data than the TMY data set. This is particularly evident in June, when the 1990 $\overline{K}_T$ is more than 20% less than the TMY value.

The normalized fractional distributions for each day's value of $\overline{T}$, $\overline{T}_{dp}$, K_T are graphed in Figures 5.2-4, 5.2-5, and 5.2-6. The X-axis of these graphs indicates the fraction of days in the year with values of $\overline{T}$, $\overline{T}_{dp}$, or K_T equal to or less than the corresponding y-value. The graphs are essentially 365 values of $\overline{T}$, $\overline{T}_{dp}$, and K_T arranged in ascending order.

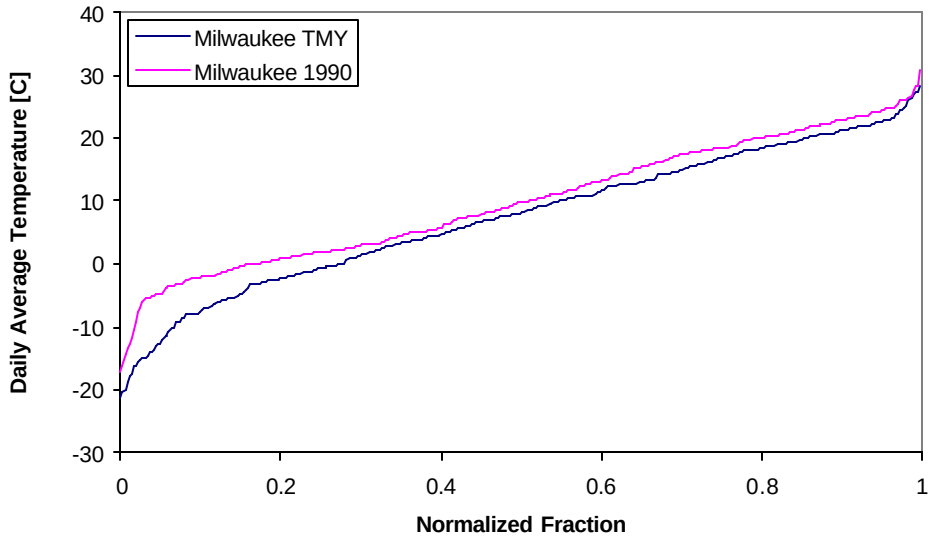

Figure 5.2-4: $\overline{T}$ distribution: Milwaukee 1990 and TMY

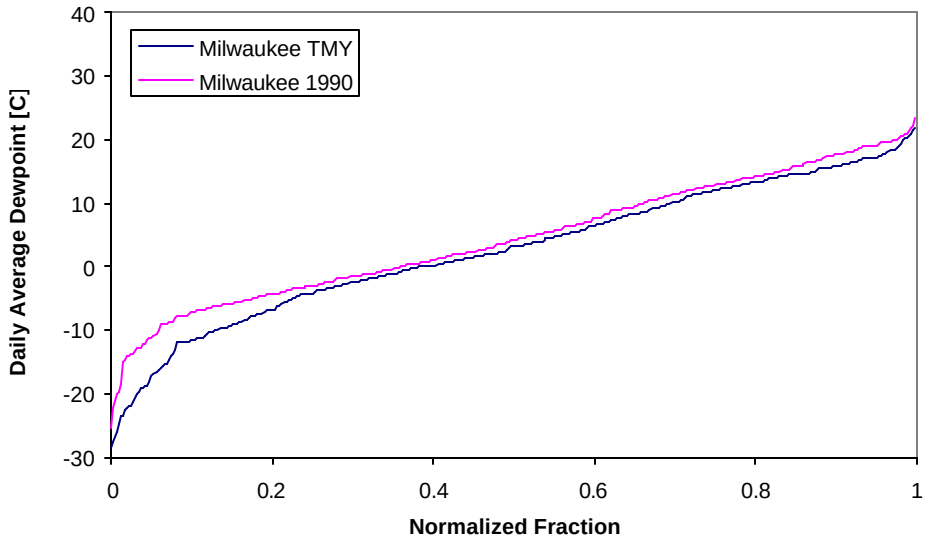

Figure 5.2-5: $\overline{T}_{dp}$ distribution: Milwaukee 1990 and TMY

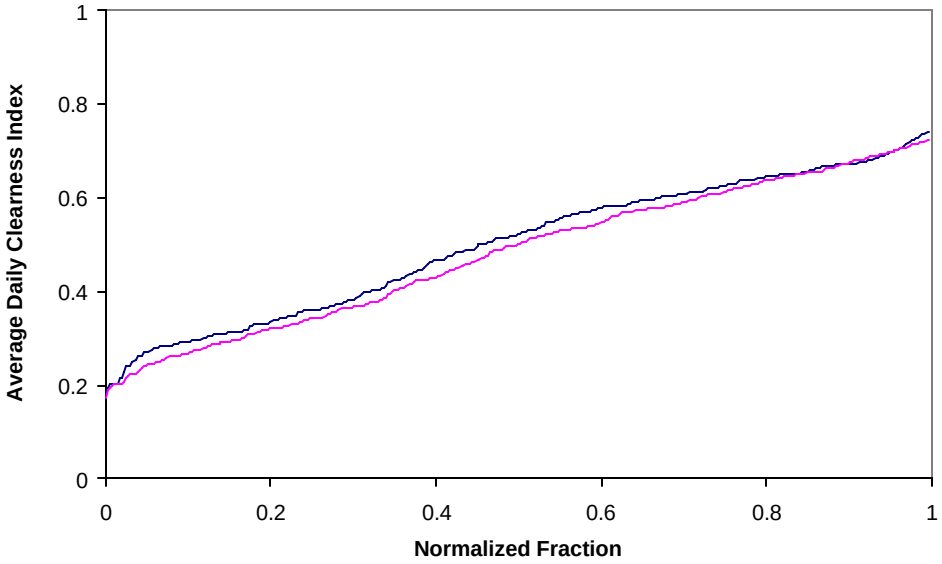

Figure 5.2-6: K_T distribution: Milwaukee 1990 and TMY

On the whole, a comparison with TMY suggests that 1990 was not a good year for PV. The main reason for this is a cloudy summer. Available solar energy is greatest during these months, so an unusually cloudy summer penalizes PV generation more than a cloudy winter. In addition, electrical demand reduction is most critical to both customers and utilities during the summer months. 1990 was also a warm year, imposing a further small penalty on PV performance. Since meteorological conditions in 1990 were poor, it safe to say that the Milwaukee simulations will provide conservative estimates of BIPV system performance.

5.3 Building Load Data

The building load data were obtained from the Commercial Cooling Load Library, a record of building loads for 45 commercial buildings in the Milwaukee area [the Fleming Group, 1994]. Cooling Load Library data sets are not downloadable. The data of interest were obtained from the Energy Center of Wisconsin on diskette. The Library includes loads from 1989, 1990, and 1991, although not all the buildings include complete records for all three

years. The identity of the individual buildings is not given in the report for the sake of anonymity; some of the records may reveal excessive energy consumption. However, each building is grouped into one of five major types: retail, office, grocery, restaurant, or health. The total floor area and number of floors is also provided for each building.

The electrical load data in the Library were obtained through direct monitoring. Each data point is the electrical energy consumption over a fifteen minute interval. As the name suggests, the Cooling Load Library also estimates the portion of the total electrical load that goes to satisfy space cooling needs at each quarter-hour interval. The modeling schemes employed in estimating the cooling loads are outside the scope of this work since the benefits of PV depend only on total load and not on how utility draw is allocated within a building.

Three building were studied in the Milwaukee simulations. The essential characteristics of these buildings are summarized in Table 5-3.1.

Table 5-3.1: Commercial Cooling Load Library buildings employed in Milwaukee simulations

Library Building Code	***Building Type***	***Total Floor Area [ft^2]***	***Floors***	***Average Load [kW]***	***Max Load [kW]***
13	Grocery	24300	1	246.9	413.6
46	Office	350000	20	1030.5	2268.0
54	Retail	12000	1	20.5	48.0

Plotting the loads as functions of time over the course of the year does not produce legible graphs because the load values change quickly. They usually reach local minima and maxima once each day. Instead of graphing with respect to time, the total electrical loads and cooling loads for each fifteen minute interval were plotted as fractional distributions in Figures 5.3-1, 5.3-2, and 5.3-3. The values for total load and cooling load at any given x-value *do not* correspond to the same times.

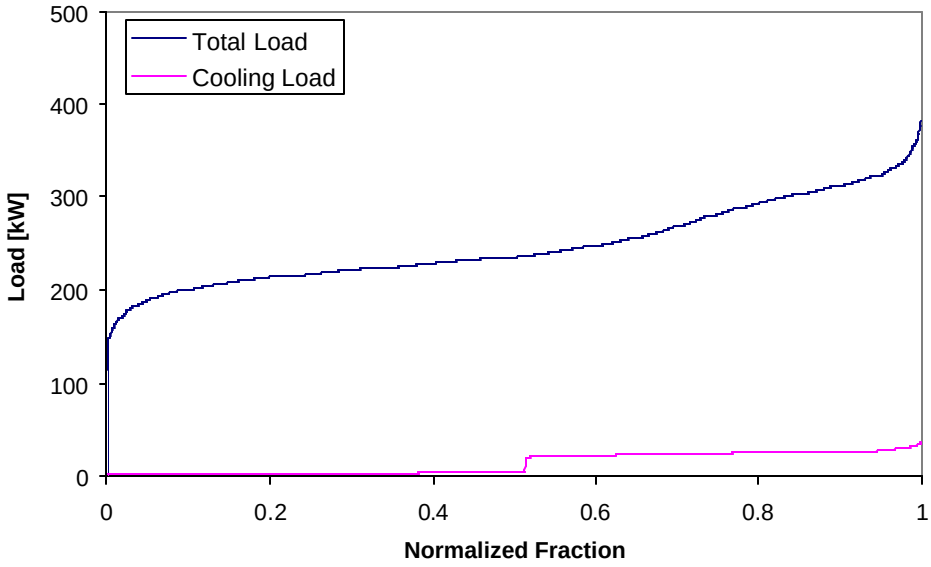

Figure 5.3-1: Load distribution for grocery (Building #13)

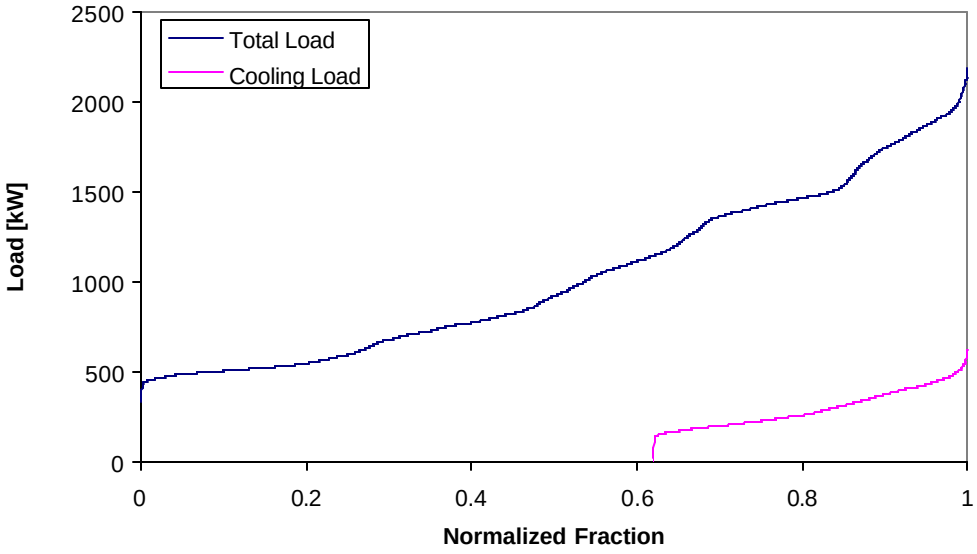

Figure 5.3-2: Load distribution for office highrise (Building #46)

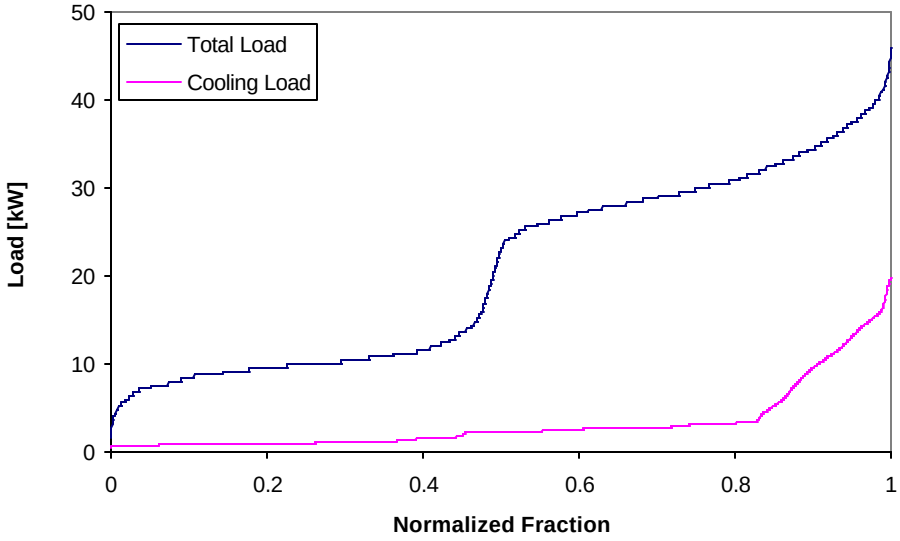

Figure 5.3-3: Load distribution for retailer (Building #54)

5.4 Utility Rate Schedules

A **rate schedule** is a list of prices a customer pays for electrical energy purchased from a utility at various times. It costs a utility more to distribute power to customers at peaking times when the total draw on the utility is high than at times when the load is small. At these times the utility is forced to run its smaller, more costly plants such as gas turbines that generally remain idle during times of average power draw. Worse yet, the utility may have to purchase electricity from a neighboring power company if it lacks the capacity to satisfy customers' power demands. Rate schedules reflect the cost of power generation. Utilities charge their customers more during peaking periods to encourage conservation at these times and to help recoup losses from costly generation and energy purchase.

Residential customers may pay a flat rate per unit kWh of electrical energy; this is the simplest possible rate schedule. Some utilities provide residential customers the option of

time-of-use rates in which power is cheaper at night and more expensive during the day. Commercial and industrial (C & I) customers generally consume more energy and are subject to more complex rate schedules. C & I schedules usually include time-dependent rates for energy consumption or **usage**. These rates may be subject to hourly and/or seasonal variation. In addition, C & I schedules usually include monthly **demand charges** on the largest instantaneous power consumption over the course of the month. Consider a factory that usually runs a steady load of 5 MW but briefly consumes 20 MW for a fifteen minute period. It will pay a demand charge for that month based on a 20 MW power consumption. This quick spike does not represent a significant energy consumption and therefore does not contribute much to the usage charge. However, if it were eliminated the demand portion of the factory's power bill would drop by 75%. For many C & I customers demand charges are about as large as usage charges, making demand reduction an important aspect of conservation. A second demand charge is also included in some C & I rate schedules. This is the **twelve-month rolling demand** or **ratchet charge**. The ratchet charge is based on the largest instantaneous power consumption over the last twelve months. In essence, a customer continues to pay for a single spike in power consumption for a year after it occurs.

The BIPV Simulation Program includes 24 residential, commercial, and industrial rate schedules. The five major Wisconsin utilities are represented: Madison Gas and Electric, Northern States Power Company, Wisconsin Power and Light, Wisconsin Public Service Corporation, and Wisconsin Electric. The rate schedules for all of the utilities except Wisconsin Electric were downloaded from company websites. The Wisconsin Electric schedules were obtained from a pamphlet mailed by marketing employee Ron Pugh [1998]. Two Wisconsin Electric commercial schedules were employed in the Milwaukee simulations. These rate schedules are summarized in Table 5.4.1.

Table 5.4-1: The two Wisconsin Electric rate schedules used in the Milwaukee simulations

Rate Schedule	***Large Secondary: Demand & Time-of-Use***	***Small Secondary: Demand & Time-of-Use***
Applicable Buildings	Grocery (#13) Office Highrise (#46)	Retail (#54)
On-Peak Usage Rate	$0.0375 per kWh	$0.0537 per kWh
Off-Peak Usage Rate	$0.0244 per kWh	$0.0537 per kWh
Monthly On-Peak Demand **** See Exception Below ****	$9.29 per kW	$4.50 per kW
Ratchet	$0.68 per kW	N/A

Wisconsin Electric's on-peak period is 9 am to 9 pm. Weekends and holidays are exempt from on-peak rates. There is no seasonal variation in usage or demand charges. There is one unusual feature in this rate schedule; the monthly demand rate may be reduced for months with few **on-peak hours of use.** This quantity (OPHU) is defined as the monthly on-peak energy use divided by the greatest on-peak demand.

$$OPHU \equiv \frac{Energy_{on-peak}}{Power_{\max,\, on-peak}} \qquad \text{Eq. 5-4.1}$$

If the OPHU total for the month is less than 100, the monthly demand rate for the large secondary schedule (grocery and office highrise) is adjusted according the formula

$$Rate_{Demand} = \$9.29 - [\$0.0563(100 - OPHU)] \qquad \text{Eq. 5-4.2}$$

For OPHU values less than 100 the monthly demand rate in the small secondary schedule (retail) becomes

$$Rate_{Demand} = \$4.50 - [\$0.0225(100 - OPHU)] \qquad \text{Eq. 5-4.3}$$

This scheme reduces the demand charges for customers who consume the majority of their energy during off-peak periods. If most energy consumption occurs at night, this will be reflected in low OPHU values. The monthly OPHU for the office highrise studied in this work never drops below 1000. However, the OPHU for the grocery and retail is less than 100 for some months of the year, resulting in small demand rate discounts.

5.5 Total Utility Load Data

The final data set employed in this work is total hourly loads, or **utility demand obligation**, for Wisconsin Electric in 1990 [Wisconsin Electric, 1998]. Ronald Pugh from Wisconsin Electric's marketing department supplied this information. The utility load data were not used directly in the Milwaukee simulations as they have no bearing on PV system performance or customer savings. However, this data set was combined with the energy generation results of the simulations to examine potential utility benefit from BIPV. This procedure is described in Chapter 7. Wisconsin Electric's demand obligation in 1990 varies from about 1700 MW to 4300 MW. Figure 5.5-1 shows the normalized fractional distribution of the utility load data:

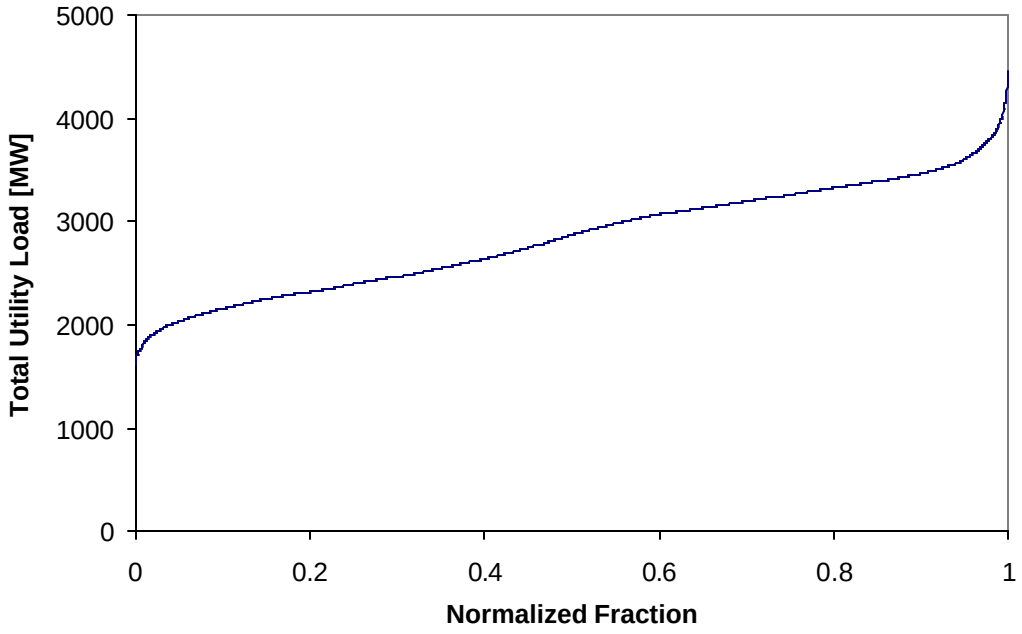

Figure 5.5-1: 1990 load distribution curve for Wisconsin Electric

The distinct "tail" on the upper end of the distribution shows that there are a few periods when Wisconsin Electric's load is exceptionally large. The utility looses money at these points and stands to benefit from PV or other parallel generation which could help to level the load.

The total utility demand obligation exhibits a noticeable seasonal and hourly variation. The load is greatest in summer and winter and smaller in spring and fall. This pattern is typical of utilities in continental climates with summer air conditioning loads and winter electric heating loads. Figure 5.5-2 shows the average obligation for each month.

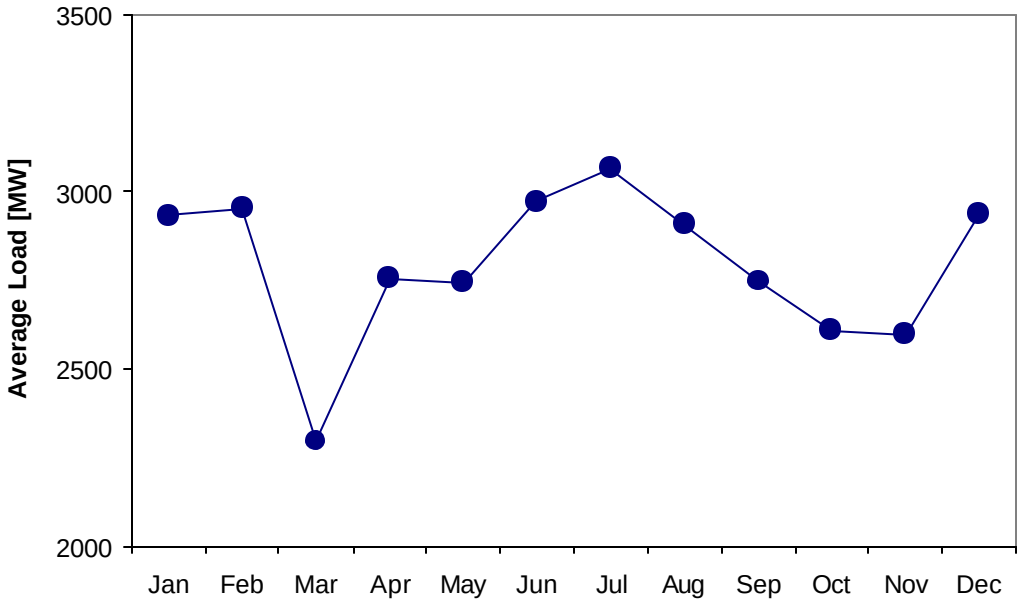

Figure 5.5-2: Wisconsin Electric's average monthly loads (expanded scale)

The hourly variations in the average load are greater than the seasonal variations. Loads are generally greatest from about 10:00 AM to 5:00 PM, falling off quickly after 9 PM. Wisconsin Electric's on-peak time for weekdays is from 9:00 AM to 9:00 PM, coinciding with the hours at which the average obligation is greatest. It is interesting to note the small dip in average load around 3:00 PM.

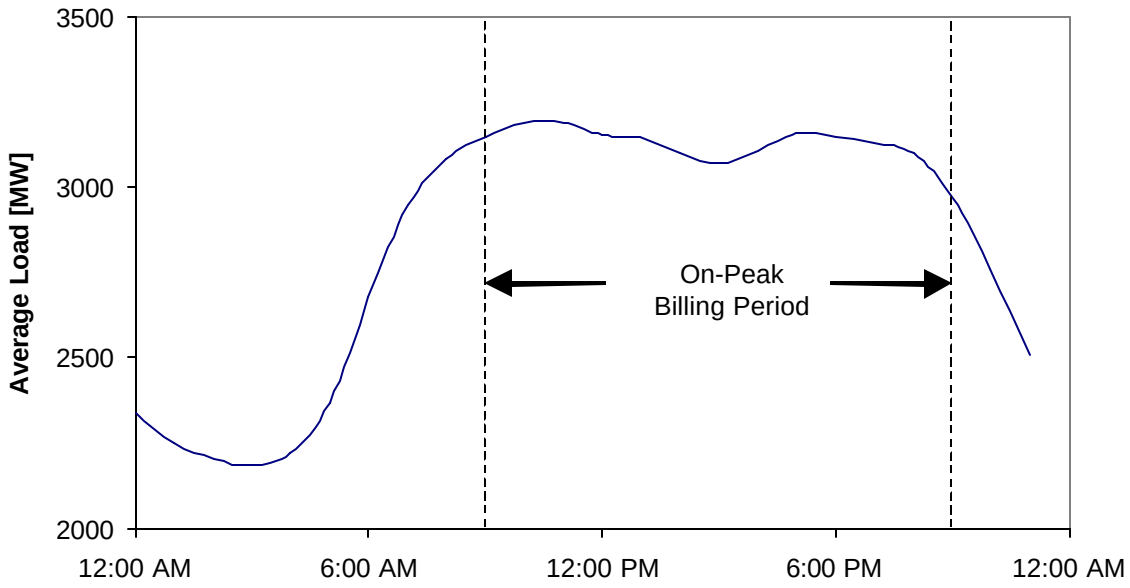

Figure 5.5-3: Wisconsin Electric's hourly average loads and on-peak billing period

5.6 Summary

Four data sets were employed in the 1990 Milwaukee simulations. The first set is weather data, including hourly values for solar radiation, ambient temperature, and humidity. The solar data were taken from the NREL website [NREL, 1992], while the temperatures and humidities were obtained from the Commercial Cooling Load Library [the Fleming Group, 1994]. These data were compared to NREL's TMY data which represent meteorological conditions in an average year. These comparisons show that 1990 was an unusually warm year in Milwaukee. In addition, the summer of 1990 was exceptionally cloudy. These are not good conditions for effective PV operation, so the Milwaukee simulations will produce conservative results in estimating the long-term feasibility of BIPV.

The second data set is 15-minute electrical loads for three commercial buildings in the Milwaukee area: a supermarket, an office highrise, and a retail store. These loads each

exhibit distinct daily and seasonal trends. The load data were obtained from the Commercial Cooling Load Library [the Fleming Group, 1994].

The third set of data is utility rate schedules from Wisconsin Electric, the Milwaukee utility. Two rate schedules were employed in the Milwaukee simulations. The grocery and office highrise are billed under the first schedule, "Large Secondary." The retailer is billed under the "Small Secondary" schedule. Both of these schedules include energy usage and monthly demand charges. Demand is weighed more heavily in the Large Secondary schedule, while the Small Secondary schedule places more weight on energy consumption.

The final data set is total hourly utility loads, given by Ron Pugh of Wisconsin Electric [1998]. The largest loads occur in the summer months when air conditioning demand is high. How closely solar generation coincides with large utility loads is important in assessing the value of BIPV to the utility, as discussed in Chapter 7.

CHAPTER 6

Simulation Results: Customer Benefits

The PHANTASM program was used to examine the potential physical and economic performance of BIPV arrays for three commercial buildings in the Milwaukee area. This chapter presents the results of these simulations and examines how these results depend on the electrical consumption patterns of the buildings. In this chapter all discussions on the potential benefits of PV are presented from the point of view of the building owner (electric customer). Chapter 7 uses the simulation results to investigate how large-scale BIPV implementation could impact the electric utility.

Each simulation examines the annual performance of a 20kW rooftop array placed atop a building. The simulations used historical weather data and building load data, both from 1990. In order to obtain meaningful results it is essential that the weather data and load data for a simulation cover the same time period. The rate schedules of Wisconsin Electric, the Milwaukee utility, were employed in determining monetary solar savings. Three buildings were studied: a supermarket, a twenty-story office highrise, and a mid-size retailer. In reality, these buildings are not actually outfitted with PV. The simulations are intended to calculate how much money the owners *would have saved* in 1990 if PV arrays had been mounted on their buildings.

The data sets employed in the BIPV simulations are discussed in detail in Chapter 5. These data include weather, building loads, utility rate schedules, and total utility demand obligation.

6.1 Simulated BIPV Systems

Physically, the three buildings examined in this study were quite different. The supermarket and retailer are both flat-roof buildings with a single story. From an engineering perspective, sloped rooftop arrays are the most practical BIPV arrangement for such buildings. The twenty-story office highrise, on the other hand, provides a much greater surface area that may be outfitted with PV. Commercial skyscrapers have been built implementing PV into the facade, rooftop, window sunshades, and even the windows themselves.

Identical PV systems were simulated on the three buildings. Using similar systems allows the study to focus on the issue of how PV generation coincides with electrical consumption without simultaneously considering differences between systems. A 20 kWp fixed rooftop array with a single orientation is simulated for each building. The system consists of 200 Siemens SR100 modules each rated at 100 Wp. Specification for the SR100 were obtained from an on-line manufacturer's catalog [Siemens, 1998]. The SR100 is a large single crystal module, representing the most widely used PV technology. Each module has an area of 0.89 m^2, so the entire array measures 178 m^2. PHANTASM does not account for shading losses when one row of modules in an array casts a shadow on another. However, the roof of each building is large enough that rows may be spaced widely to minimize shading losses. The smallest building, the retailer, has a total floor area of 1115 m^2 so the roof area is slightly greater. Thus, the kW array will require only about one sixth the roof area of this building. This fraction is smaller for the office highrise and the grocery.

The inverter for the PV system is taken to have a constant efficiency of 93%, a typical value. A large value (100000 W) is used for the inverter capacity. This eliminates the possibility of PV generation exceeding the inverter capacity. An undersized inverter should not pose a problem in a well-engineered BIPV system. The PV incidence angle modifier correlation described in Section 3.14 was employed in each simulation.

6.2 PV Array Orientation

One advantage to rooftop PV arrays is that their orientation need not be dictated by the exposure of other surfaces on the building. The orientation of PVs built into the façade of a building, for instance, clearly cannot differ from that of the façade itself. One question this work addresses is how a rooftop array should be oriented to optimize energy production and monetary savings for each building.

Consider a hypothetical location where average normal insolation does not change from morning to afternoon or from summer to winter. In this case the annual energy output of the PV array will be optimized by using a south-facing orientation (in the northern hemisphere) sloped at the latitude of the location. However, in the Midwest and many other regions, winter is cloudier than summer. This suggests that annual energy production can be maximized by using an array sloped at an angle less than the latitude. Such an orientation will reduce the average angle of solar incidence during the summer when the sun is high in the sky and more radiation is available. Moreover, the average insolation in some climates is not symmetric about noon. In most locations along the US Pacific coast, for instance, early morning is often cloudier than mid afternoon. It would be advantageous to face PVs west of due south to maximize energy production in such a climate.

If a building's rate schedule does not include demand charges or time-dependent usage rates, the optimal array orientation for energy production will also maximize solar savings. This orientation is chosen according to location and climate as discussed above. However, if electric rates are higher in the afternoon than the in morning, it may be beneficial to increase PV production during these on-peak periods by facing the array a few degrees to the west. Likewise, demand charges can be reduced by orienting the PV array to maximize output when the electrical load is large. The issues of climate and load involved in optimizing PV orientation are complex and often contradictory. It is difficult to produce estimates more precise than the qualitative rules of thumb discussed here without resorting to either simulation or experiment.

Nine array slopes ranging from 23 degrees to 63 degrees were examined for each building. In Milwaukee these values correspond to 20 degrees less than latitude and 20 degrees greater than latitude respectively. In addition, five azimuth angles were tested, ranging from 0 degrees (due south) to 40 degrees west of south. Each combination of slope and azimuth was examined, requiring 45 simulations per building. 40 southeast-facing additional orientations were also examined for the grocery, as discussed in Section 6.4. Each year-long simulation for a given building and array orientation took slightly over a minute on a 450 MHz Pentium II computer. Section 6.3 addresses the relationship between annual energy generation and array orientation; this result is independent of the buildings' loads. Sections 6.4, 6.5, and 6.6 discuss the optimization of PV orientation to maximize monetary savings for each building. The monthly and hourly average load patterns are plotted for each building along with the top 15-minute loads. This information helps to explain why a particular orientation is best for each building.

6.3 Annual PV Energy Generation

The annual energy production for the various PV orientations was the same for each building. Energy production is dependent only on PV system parameters and on weather; it is not a function of building load. Figure 6.3-1 illustrates the annual energy generation for each array orientation.

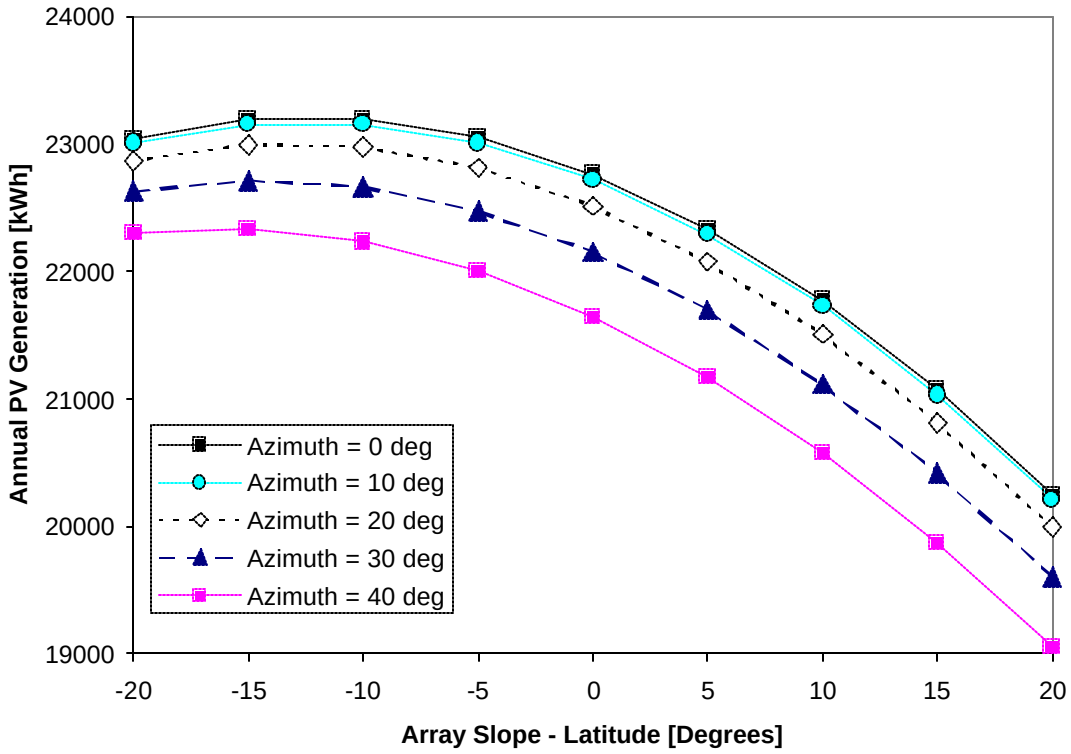

Figure 6.3-1: PV orientation and total annual energy generation. Scale is expanded on y-axis.

Energy output is maximized with a south-facing array sloped at ten degrees less than latitude. The annual PV generation in this case is 23197 kWh. The output of an array oriented 10 degrees west of south is nearly identical to the south-facing case. On the whole, the energy production is rather insensitive to orientation over the range examined. The annual output changes by about 1000 kWh from a surface azimuth of 0 degrees to 40 degrees. Energy production falls by about 2500 kWh when a slope equal to latitude plus 20 degrees is used rather than the optimal value of latitude minus 10 degrees. Optimum energy production at a slope less than latitude is consistent with the fact that in Wisconsin there is generally more solar energy available in summer than in winter.

Wisconsin Electric's on-peak period is 9:00 AM to 9:00 PM on working days, and demand charges are assessed only during this period. All three buildings examined in the simulations are subject to demand charges. The energy usage rate in the "Large Secondary" schedule

goes up during the on-peak period, but usage rates are constant under the "Small Secondary" schedule. The grocery and the office highrise are billed under the Large Secondary schedule, while the retailer is billed under Small Secondary. Table 5.4-1 summarizes these two rate schedules.

In general, energy generated during the on-peak period is more valuable to both the electric customer and the utility than off-peak energy. Figure 6.3-2 shows annual on-peak energy generation for each orientation.

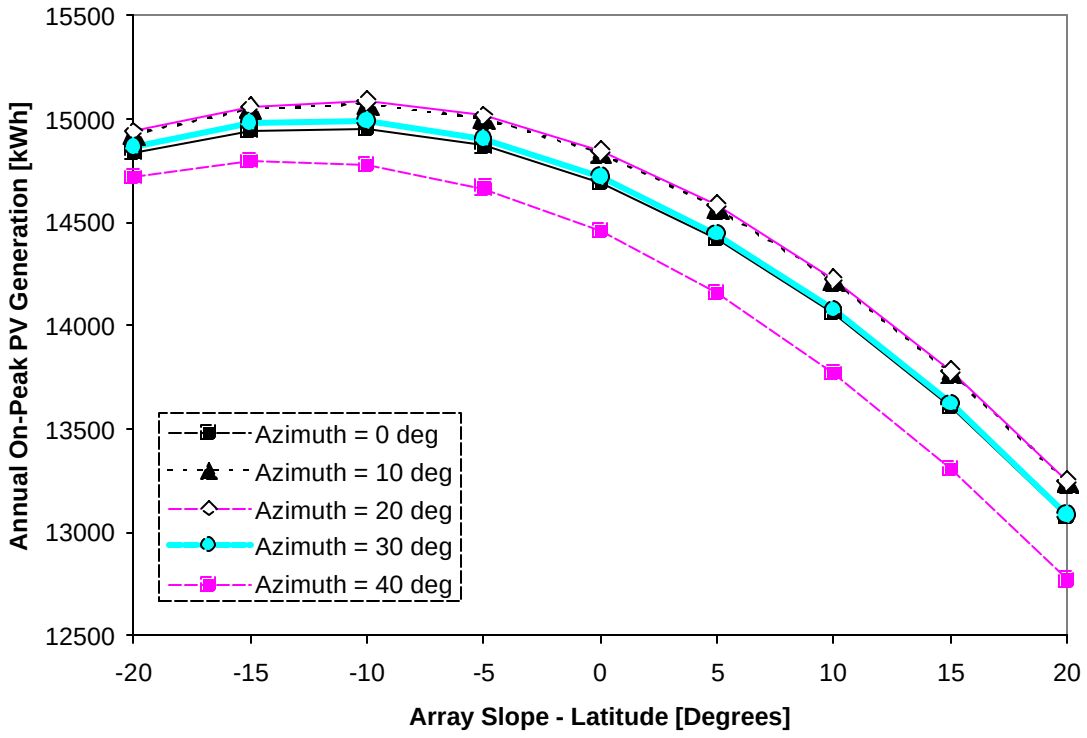

Figure 6.3-2: PV orientation and annual on-peak energy generation. Scale is expanded on y-axis.

Unlike total energy, on-peak energy production is maximized by facing the PV array west of due south. The on-peak optimum is a slope of 10 degree less than latitude and an azimuth of 30 degrees. Over the course of the year this orientation produces 15088 on-peak kWh.

Morning hours prior to 9:00 AM do not fall in the on-peak period. Thus, on-peak energy is maximized by orienting the array to produce more output during the afternoon when the sun is in the western portion of the sky.

6.4 Simulation Results for Grocery

The first building case study is a single-story grocery store with a floor area of 24300 ft^2. The grocery is billed under Wisconsin Electric's "Large Secondary" schedule. Figure 5.4-1 illustrates the annual fractional load distribution for the grocery. Cooling is a relatively small portion of the total electrical load for this building. The cooling load does not include product refrigeration, the largest source of energy consumption in supermarkets [Mitchell, 1998]. An unusual feature of the load pattern for this building is that average loads are significantly greater during the winter months than during the summer. This pattern is indicative of electric heating. Figure 6.4-1 shows the monthly average loads for the grocery.

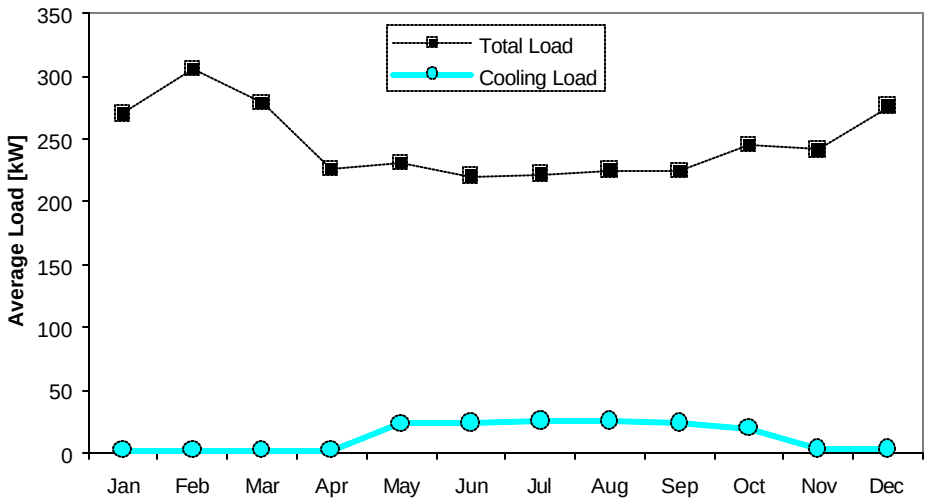

Figure 6.4-1: Monthly average loads for grocery. Greater loads in winter than summer suggest that the building is electrically heated.

Figure 6.4-2 shows the hourly loads averaged over the year for this building. Over the course of the day the average load is quite level, varying by only about 10% from day to night. Even though the store probably closes in the evening, the product refrigeration must run continually.

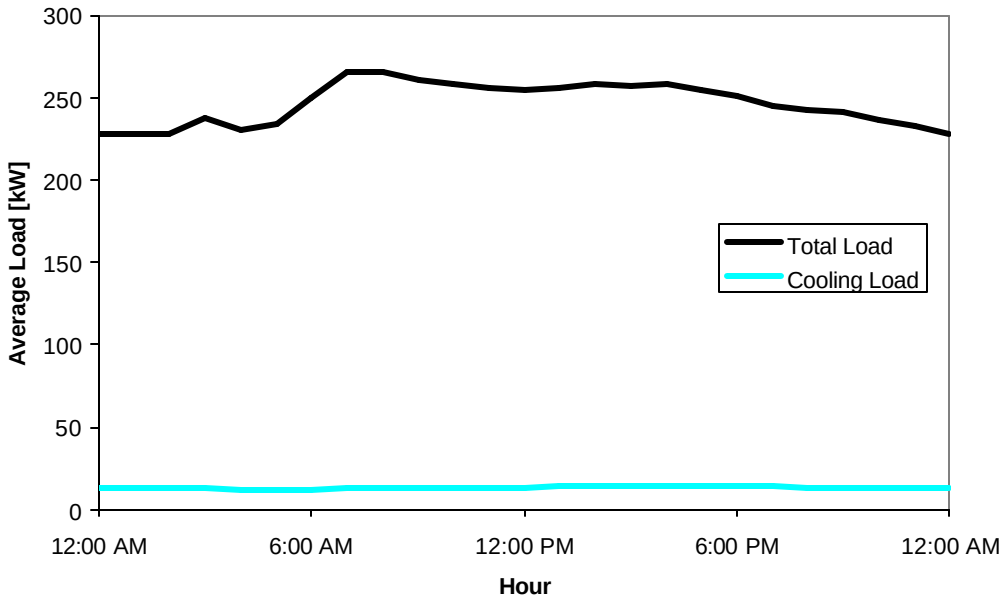

Figure 6.4-2: Hourly average loads for grocery over entire year. The load shows little change from day to night.

The average hourly loads for the cooling season (June, July, August, and September) are plotted in Figure 6.4-3. During the cooling season, total loads are about 25 kW less than the yearly averages in Figure 6.4-2 since heating is unnecessary. The shape of the hourly average load curve for the cooling season is almost identical to that for the entire year. On average, cooling loads are about 10 kW higher during these four months than over the whole year. Cooling loads show no significant hourly variation.

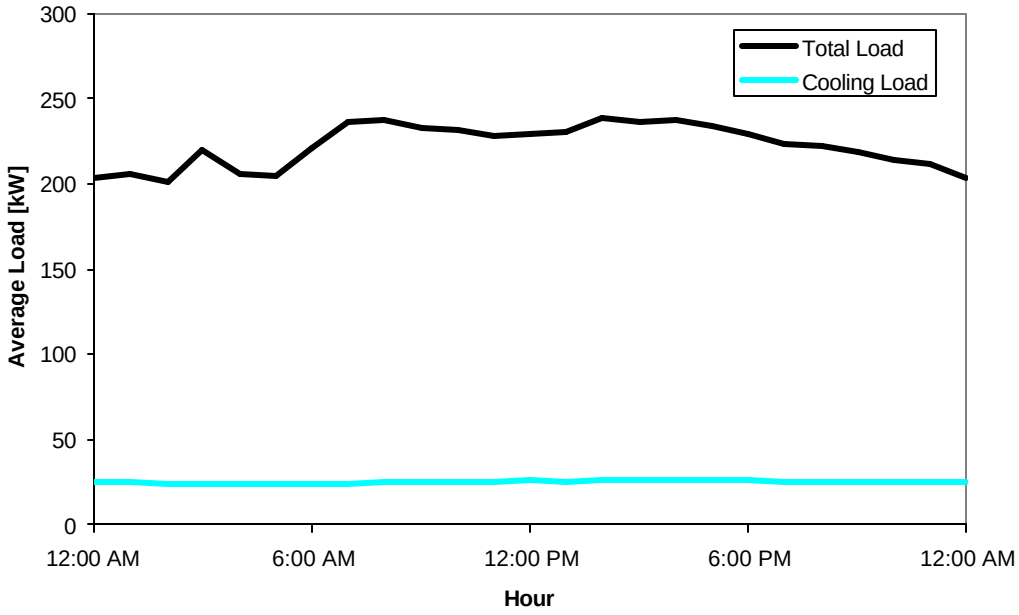

Figure 6.4-3: Hourly average loads for grocery during the cooling season. Total loads are slightly less than the averages for the year.

PHANTASM was run for 45 array orientations using the 15-minute load data for the grocery in conjunction with Wisconsin Electric's "Large Secondary" rate schedule. Figure 6.4-4 illustrates the annual monetary savings for each orientation.

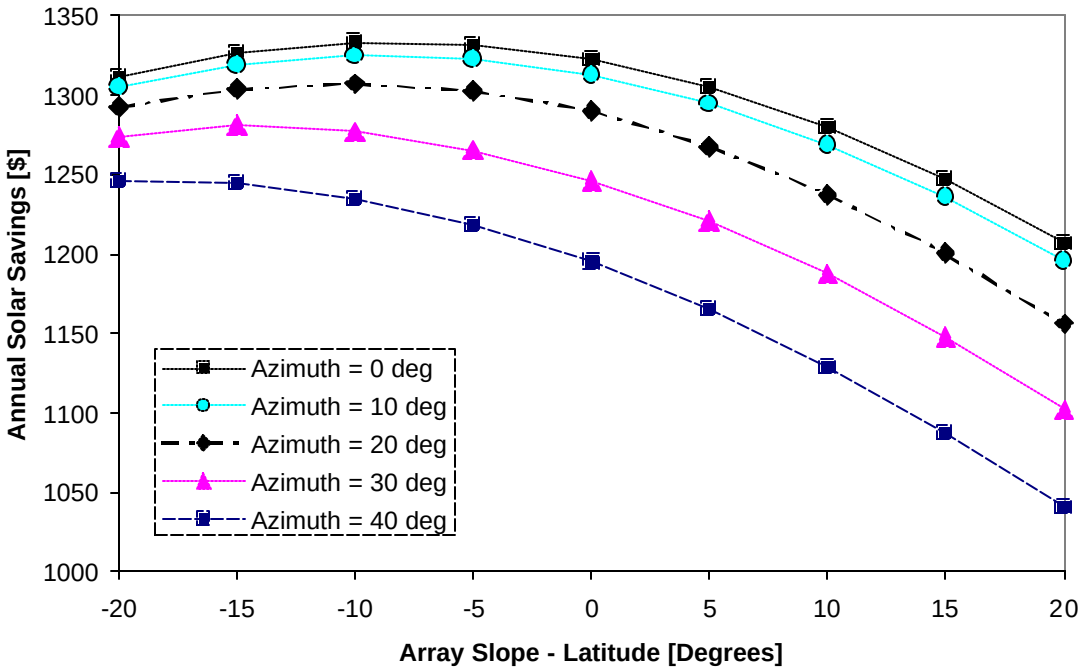

Figure 6.4-4: Annual monetary savings for arrays on grocery facing south and southwest

The south-facing array with a slope of 5 degrees less than latitude produces the most savings: $1345. Of this total, $762 is in usage charges and $583 is in demand charges. Figure 6.4-4 shows that facing the array to the west reduces savings. Plotting the top loads over the course of the year provides some insight into why this is the case. Figure 6.4-5 shows the top 15-minute loads in chronological order; values for these points are on the left y-axis scale. The right y-axis scale gives the direct normal radiation at each of these points, providing an estimate of available solar energy. The time of day for each point is shown on the x-axis.

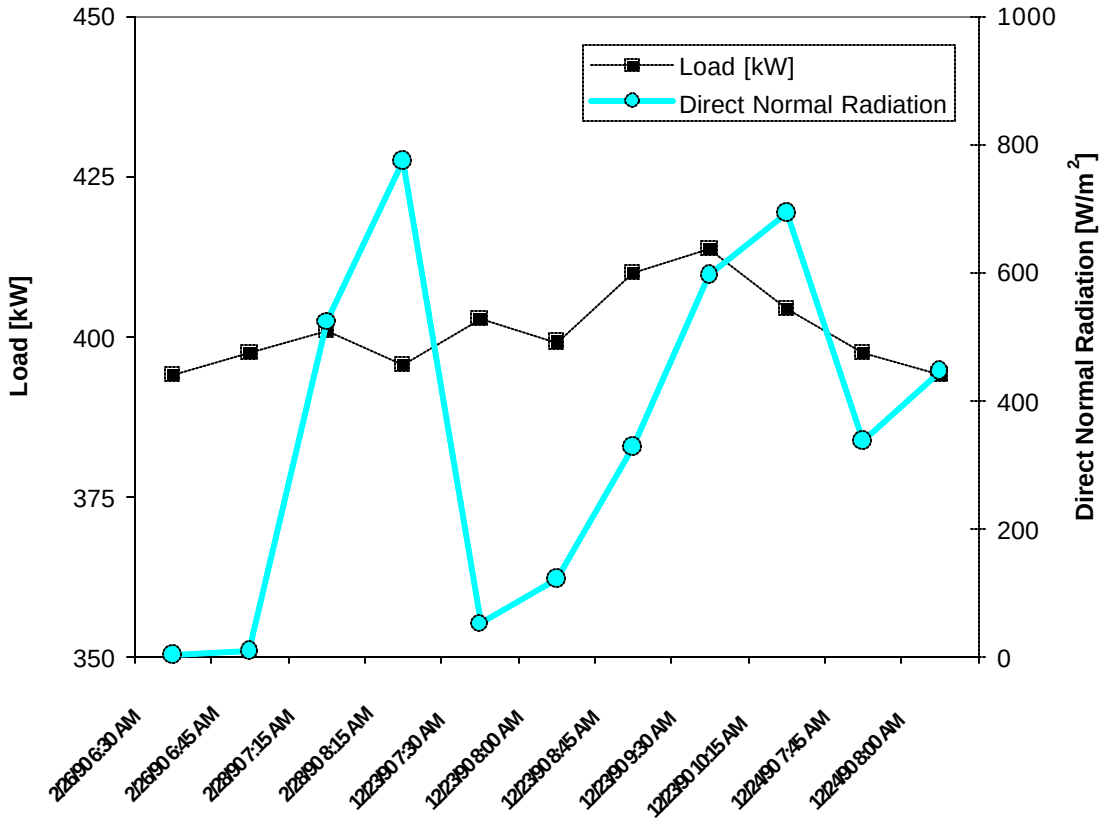

Figure 6.4-5: Top 15-minute loads for grocery, shown with hour of occurrence and direct normal insolation. Scale is expanded on left-hand y-axis.

Surprisingly, every one of these loads occurs during an off-peak period. Most of the loads happen before the on-peak period begins at 9:00 AM, and those that occur later fall on the weekend. All of these top loads occur on cold, clear winter mornings in February and December. This lends further support to the hypothesis that the grocery employs electric heating. Half of the loads occur when the direct normal radiation is greater than 400 W/m^2, offering the possibility for PV load reduction. Moreover, low ambient temperatures enhance photovoltaic efficiency at these times. However, demand reduction provides no economic benefit for the building owner at the times shown in Figure 6.4-5 since they do not fall in the

on-peak period. Figure 6.4-6 graphs the top *on-peak* loads for the grocery. Reducing these loads through parallel generation offers the possibility for demand charge savings.

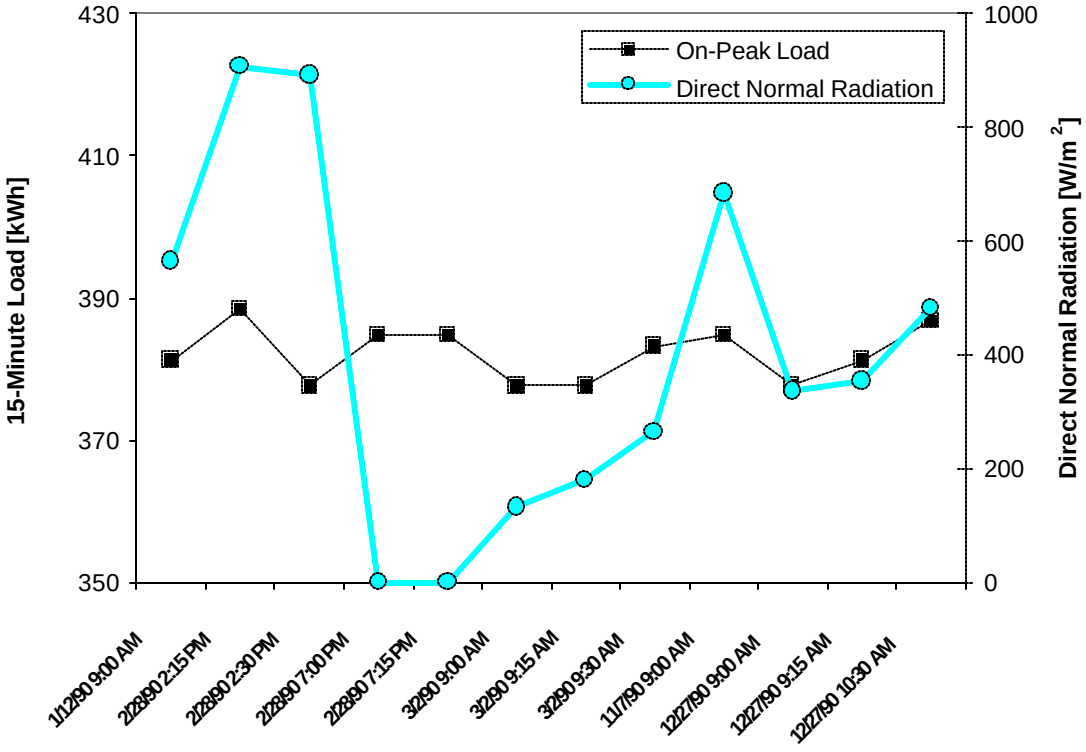

Figure 6.4-6: Top 15-minute on-peak loads for grocery, shown with hour of occurrence and direct normal insolation. Scale is expanded on left-hand y-axis.

Most of these loads occur in the morning shortly after the on-peak period begins at 9:00 AM, and all the loads occur during cold months in winter or late autumn. Two of the loads occur after dusk and cannot be reduced by PV parallel generation. Since many of the top loads occur before noon, it is possible that facing the arrays to the southeast may be beneficial. The monetary savings for 40 orientations with azimuths ranging from 10 to 40 degrees east of south are shown in Figure 6.4-7.

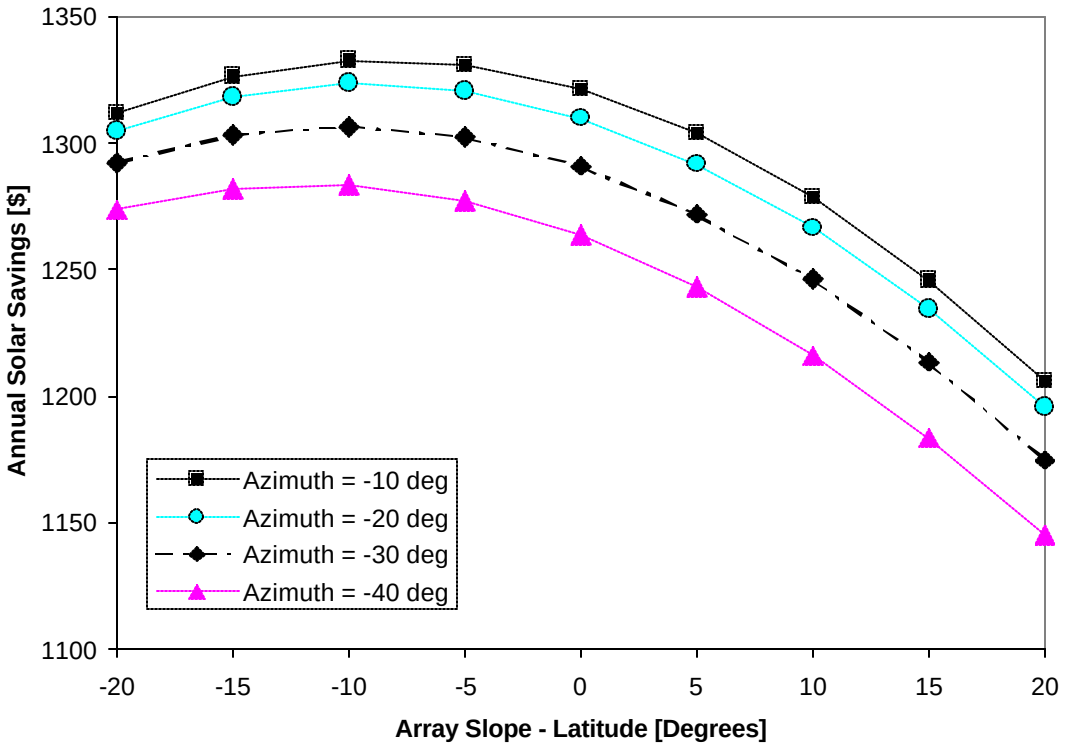

Figure 6.4-7: Annual monetary savings for arrays on grocery facing southeast

The best southeast orientation is 10 degrees east of south with a slope of 33 degrees. This setup produces an annual solar savings of $1346, one dollar more than an array facing due south with the same slope. An array facing a few degrees to the east offers slight improvement over one facing due south.

This result is rather surprising; it seems intuitive that facing the array to the southeast should be even more beneficial when the largest loads occur in the morning. However, the opportunity for demand reduction in any given month depends on how closely PV generation coincides with the *largest loads for that month.* Even if the top loads for a particular month are not the largest of the year, demand costs can be reduced if PV works well when those loads occur. This raises the question of summer demand reduction for the grocery even though loads are generally lower during this season. Figure 6.4-8 illustrates the grocery's

monthly demand savings for an optimal array (south-facing, sloped 10 degrees less than latitude).

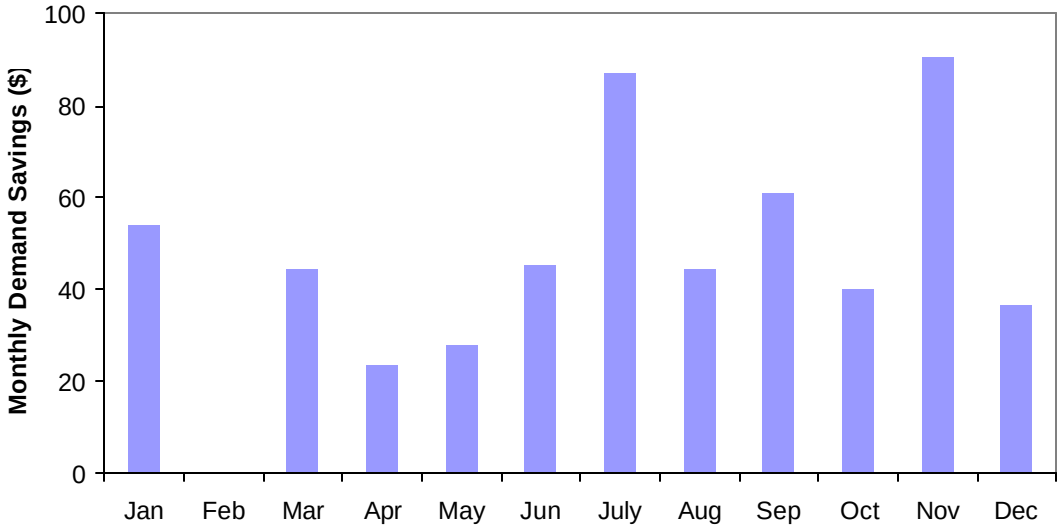

Figure 6.4-8: Monthly PV demand charge reduction for grocery. Significant demand reductions occur during summer months even though largest loads are in winter.

Demand charge reduction is significant throughout the year, not just during the winter months when loads are at their greatest. The largest summer loads usually occur in the afternoon. This means that orienting the PV to the east to maximize performance on winter mornings when the greatest loads of the year occur will result in a penalty during the summer months. Figure 6.4-8 helps to explain why orienting the array to the southeast is only very slightly better than facing it due south.

6.5 Simulation Results for Office Highrise

The twenty-story office highrise is a very large building with a total floor area of 350000 ft^2. Like the grocery, the office highrise follows Wisconsin Electric's "Large Secondary" rate schedule. The annual fractional load distribution for this building is shown in Figure 5.3-2. In general, the electric load of the office is more variable than that of the grocery. The

maximum load for the office is 2268.0 kW, while the annual average load is less than half this value, 1030.5 kW. The monthly variation of average load is shown in Figure 6.5-1.

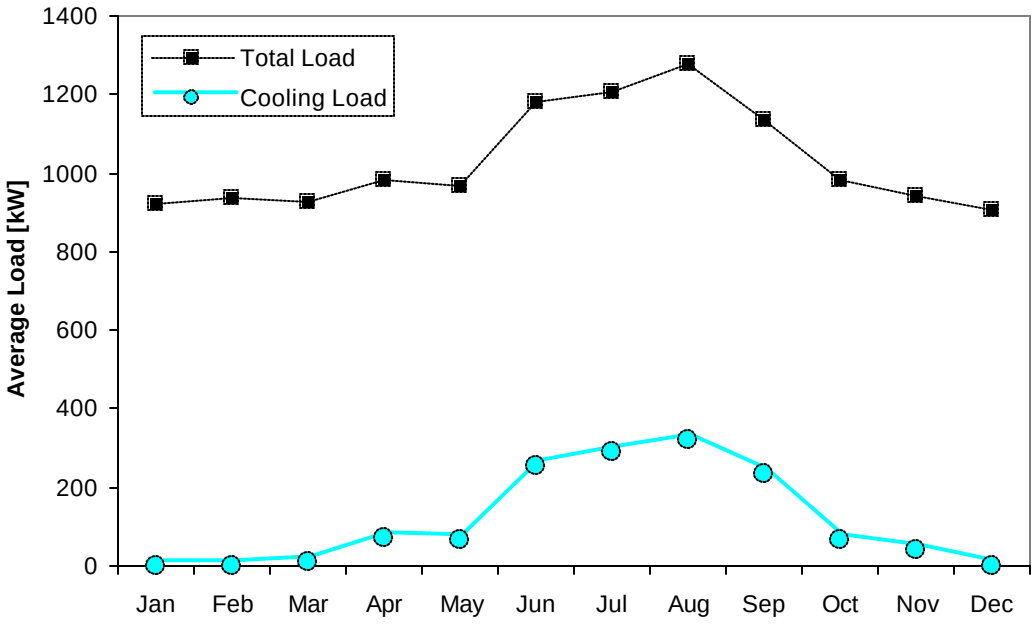

Figure 6.5-1: Monthly average loads for office highrise

The average load is about 25% greater in summer than in winter. The monthly trend for total load and cooling load is almost identical, indicating that the seasonal variation in the office is due almost exclusively to air conditioning. Low winter loads suggest that the building is heated with gas. Figure 6.5-2 shows the hourly load distribution for the office highrise with loads averaged over the entire year. The hourly averages for the cooling season of June, July, September, and August are given in Figure 6.5-3. Qualitatively, these graphs are very similar.

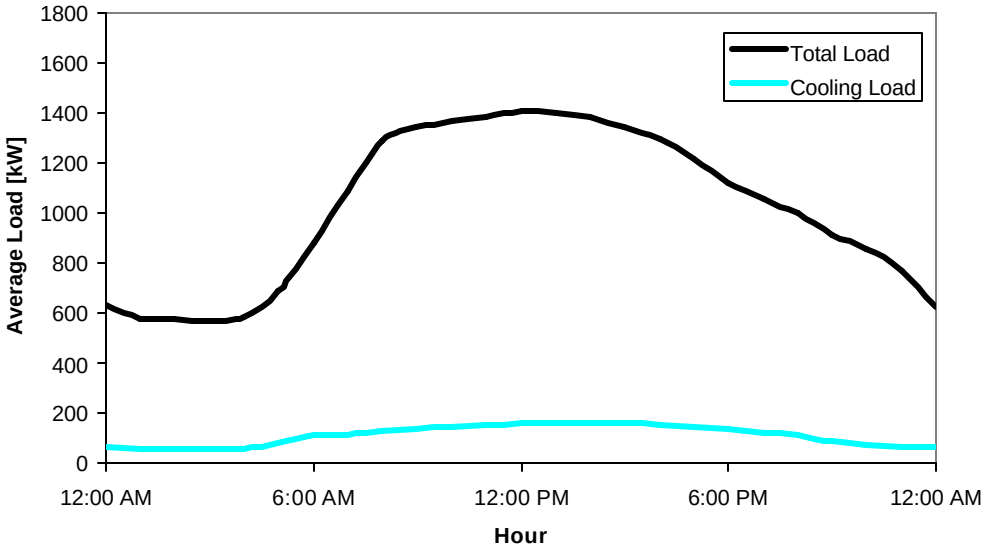

Figure 6.5-2: Average hourly loads for office highrise over entire year. Load appears to be closely linked to building occupancy.

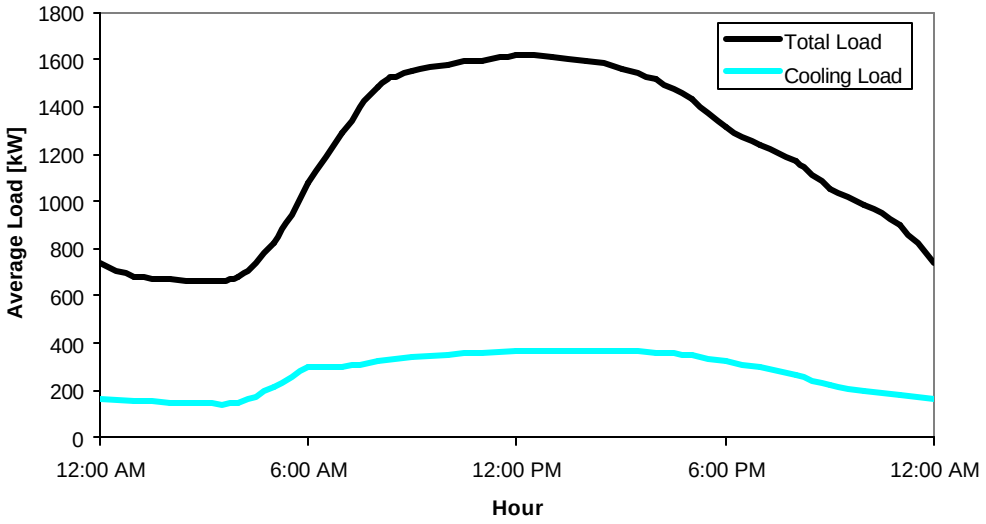

Figure 6.5-3: Average hourly loads for office highrise during cooling season. With the exception of greater cooling demand, the load pattern is almost identical to the annual average.

Figures 6.5-2 and 6.5-3 show that unlike the grocery, the average load of the office highrise exhibits a large hourly variation. The load appears to be tied closely to building occupancy.

It reaches a minimum value around 3 AM and peaks at noon. Since the largest average monthly loads occur in August and the average hourly loads are greatest around noon, it is likely that hot summer days account for biggest single loads. The hourly average loads for the cooling season and the entire year exhibit very similar trends. Both the total load and cooling load are about 120 kW greater in Figure 6.5-3 than in Figure 6.5-2.

The annual monetary savings for 45 array orientations are shown in Figure 6.5-4.

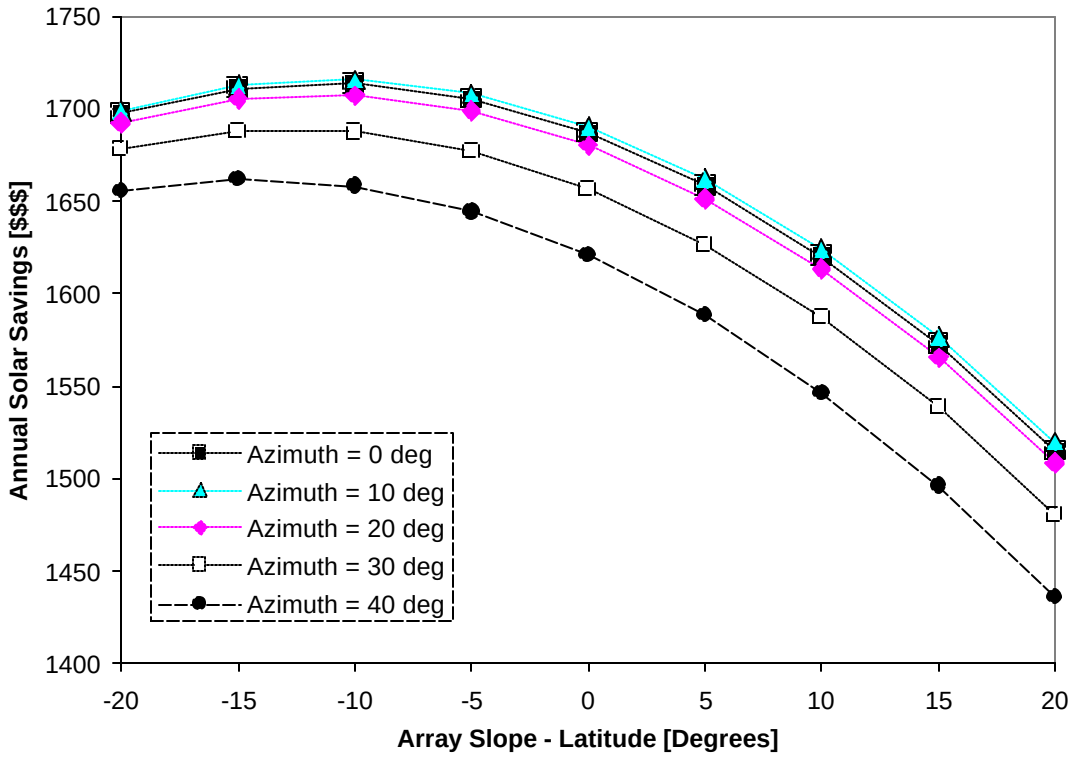

Figure 6.5-4: Annual monetary savings for arrays on office highrise facing south and southwest

The optimal orientation is ten degrees west of south sloped at ten degrees less than latitude. This arrangement produces $1715 in annual solar savings. $762 of this is in usage charges and $963 is in demand. The optimal usage savings is identical to that in the grocery. However, PV saves $369 more in demand charges for the office building than for the grocery. This indicates that the large loads in the office coincide more closely with clear

daytime hours during the utility on-peak period. Since the optimal orientation is west of south, load reduction appears to be more critical in the afternoon than in the morning. This evident from Figure 6.5-5, which gives the top loads along with their time of occurrence and direct normal radiation.

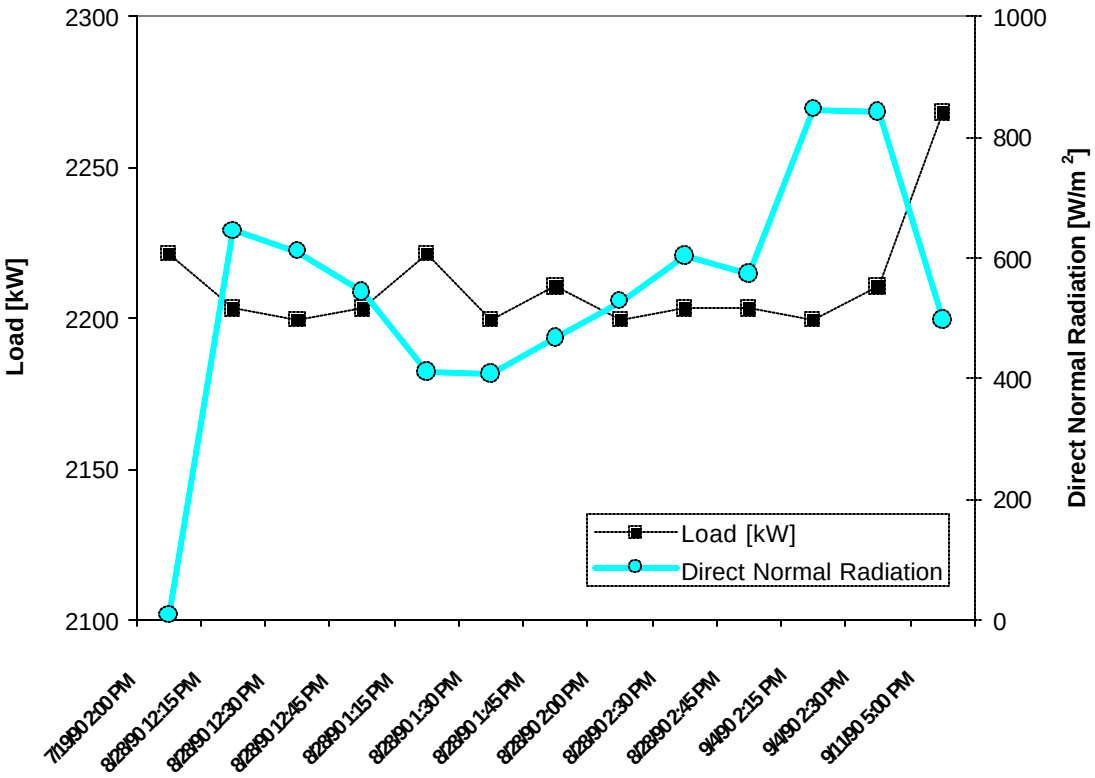

Figure 6.5-5: Top loads for office highrise shown with time of occurrence and direct normal solar radiation. All of the loads occur during the utility's on-peak period.

All of the top loads occur during warm periods in July, August, or September. Unlike the grocery loads, every one of the top loads for the office highrise occurs during Wisconsin Electric's on-peak period. Nine of the thirteen loads occur on a single hot day, August 28. Each of these points except the first one on July 19 coincide with periods of at least moderate sunshine, providing an excellent opportunity for PV demand reduction. The weather data

indicates minimal solar radiation and high humidity from about 1:00 PM to 3:30 PM on July 19, suggesting an afternoon thunderstorm.

Figure 6.5-5 indicates that the largest loads occur during the summer. This does not rule out the possibility of demand reduction in the winter, however. The grocery experienced significant PV demand charge reduction throughout the year, as shown in Figure 6.4-8. Figure 6.5-6 gives the monthly demand charge reduction for the office using the optimal PV orientation of 10 degrees west of south with slope of 10 degrees less than latitude.

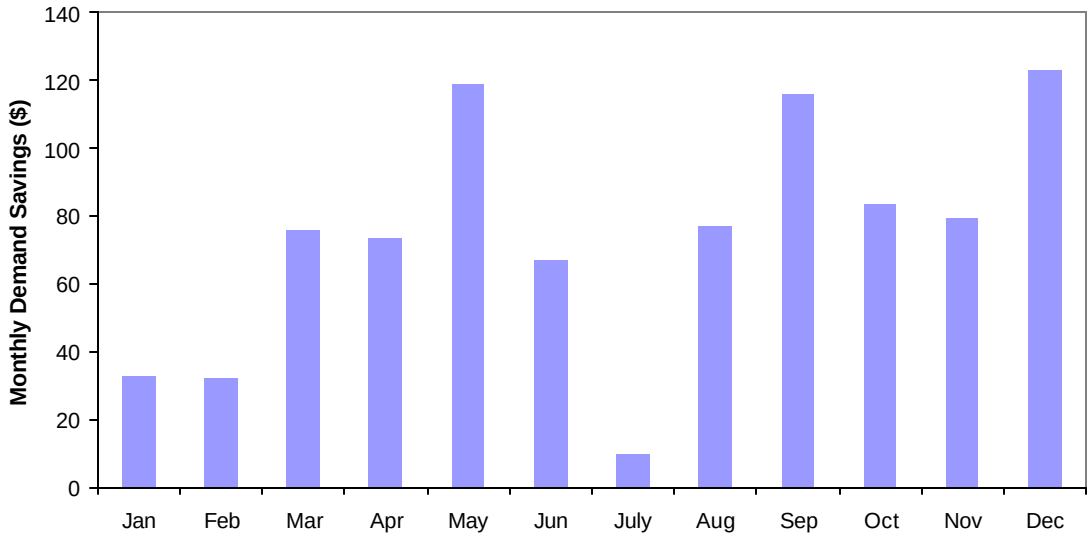

Figure 6.5-6: Monthly PV demand charge reductions for the office highrise. Demand savings are significant in spring and autumn even though all the largest loads occur in summer.

As with the grocery, demand reduction is an important consideration throughout the year. There is very little demand reduction in July despite high average loads during this month. Figure 6.5-6 shows that the greatest load for this month occurs during an unusually cloudy daytime period, allowing little opportunity for peak shaving. The greatest monthly demand savings occur in December, even though Figure 6.5-1 indicates relatively low average loads for the month.

6.6 Simulation Results for Retailer

The final building examined in the Milwaukee simulations is a single story retailer with a floor area of 12000 ft^2. Unlike the office and grocery, the retailer is billed under Wisconsin Electric's "Small Secondary" rate schedule. Compared to Large Secondary, the Small Secondary schedule bills energy usage more heavily and demand more lightly. Figure 5.3-3 illustrates the annual fractional load distribution of the retailer. Its loads are much smaller than either the grocery or the office highrise, so the energy production from a 20 kWp PV array will account for a more significant fraction of the total load. The average monthly loads for the retailer are shown in Figure 6.6-1.

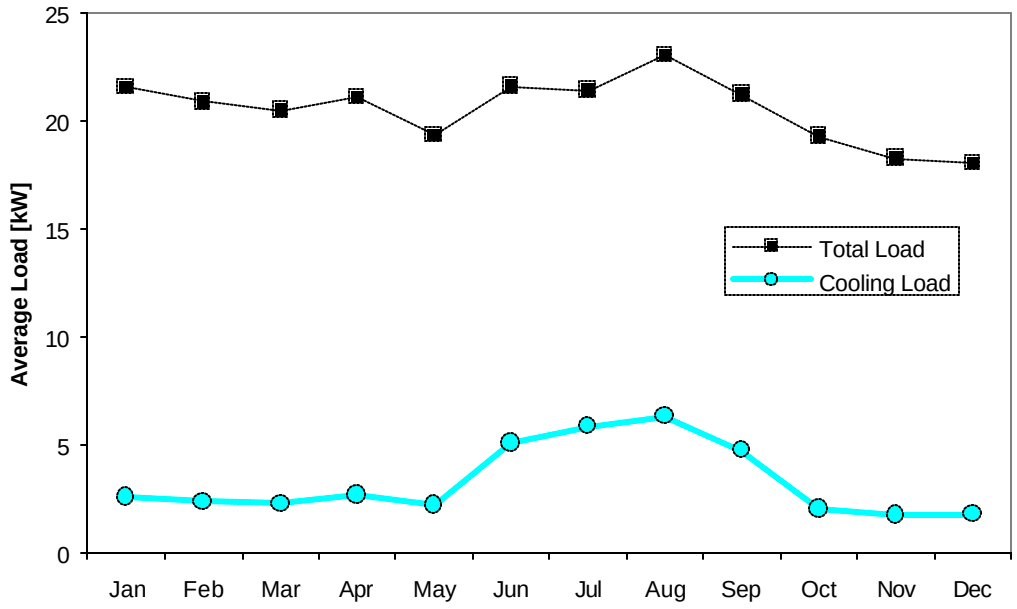

Figure 6.6-1: Monthly average loads for retailer. Like the office highrise, loads are greatest during the summer months.

This building's average load is greatest in summer, although the seasonal variation in total load is fairly small. The variation in average hourly load is much more significant. Figure

6.6-2 gives the mean hourly load averaged over the entire year. The average hourly load pattern for only the four-month cooling season is shown in Figure 6.6-3.

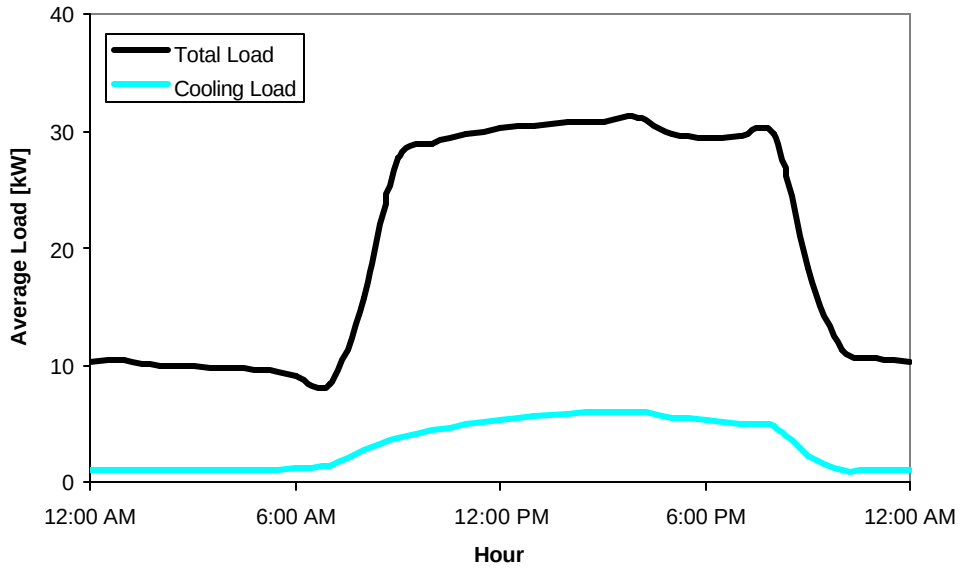

Figure 6.6-2: Hourly loads for retailer averaged over entire year. Mean loads vary by a factor of three from day to night.

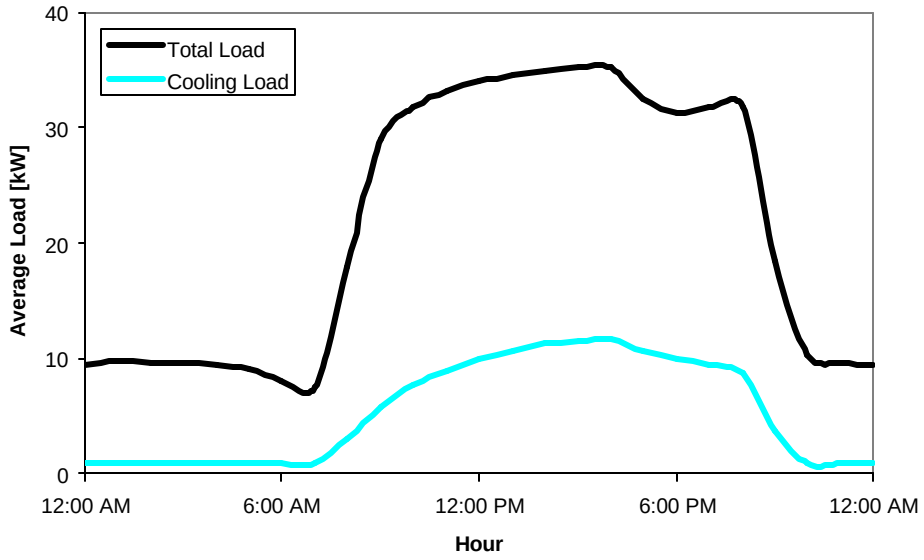

Figure 6.6-3: Hourly loads for retailer averaged over June, July, August and September. The load pattern in similar to the yearly average except that cooling loads are roughly twice as large.

There is a very distinct variation in the building's average load over the course of the day. Nighttime loads, from about 10:30 PM to 7:00 AM, average about 10 kW. From 9:00 AM to 9:00 PM the average load is roughly 30 kW. This cycle clearly corresponds to the store's business hours. Unlike the average hourly loads for the office highrise (Figure 6.5-2), the retailer's load falls off quickly at night over the course of about an hour. Presumably all employees and customers leave when the store closes while some people continue to work into the night at the office.

The monetary savings for 45 array orientations facing south and southwest are illustrated in Figure 6.6-4.

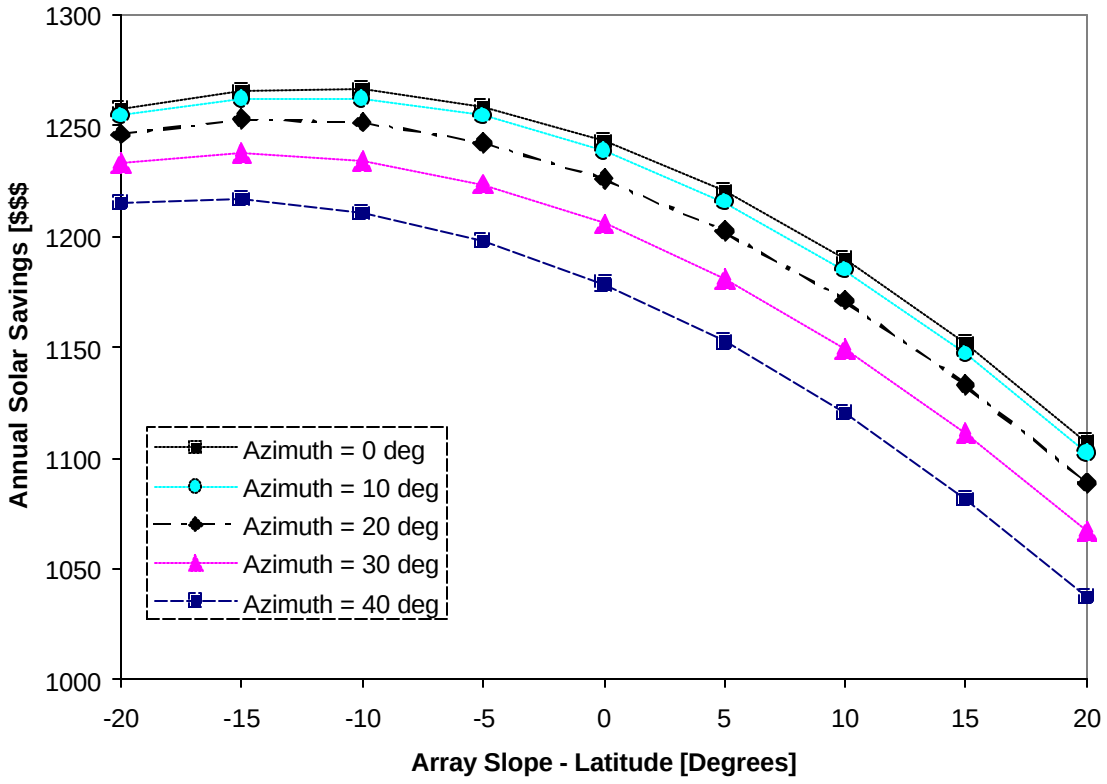

Figure 6.6-4: Annual monetary savings for arrays on retailer facing south and southwest

A south-facing array with a slope of ten degrees less than latitude produces the greatest savings. This is the same orientation that maximizes total energy generation, as shown in Figure 6.3-1. Using this orientation saves $1250 over the course of the year. Only $5 of this total comes from demand shaving. The usage savings are almost $500 greater than for either the grocery or the office. This is not because the PV array generates significantly more energy on the retailer than on the other two buildings. However, usage rates are higher under the Small Secondary schedule than under the Large Secondary schedule, making PV-generated kWh more valuable. Figure 6.6-5 highlights the top 15-minute loads for the retailer. Separate symbols distinguish those loads occurring at on-peak and off-peak periods.

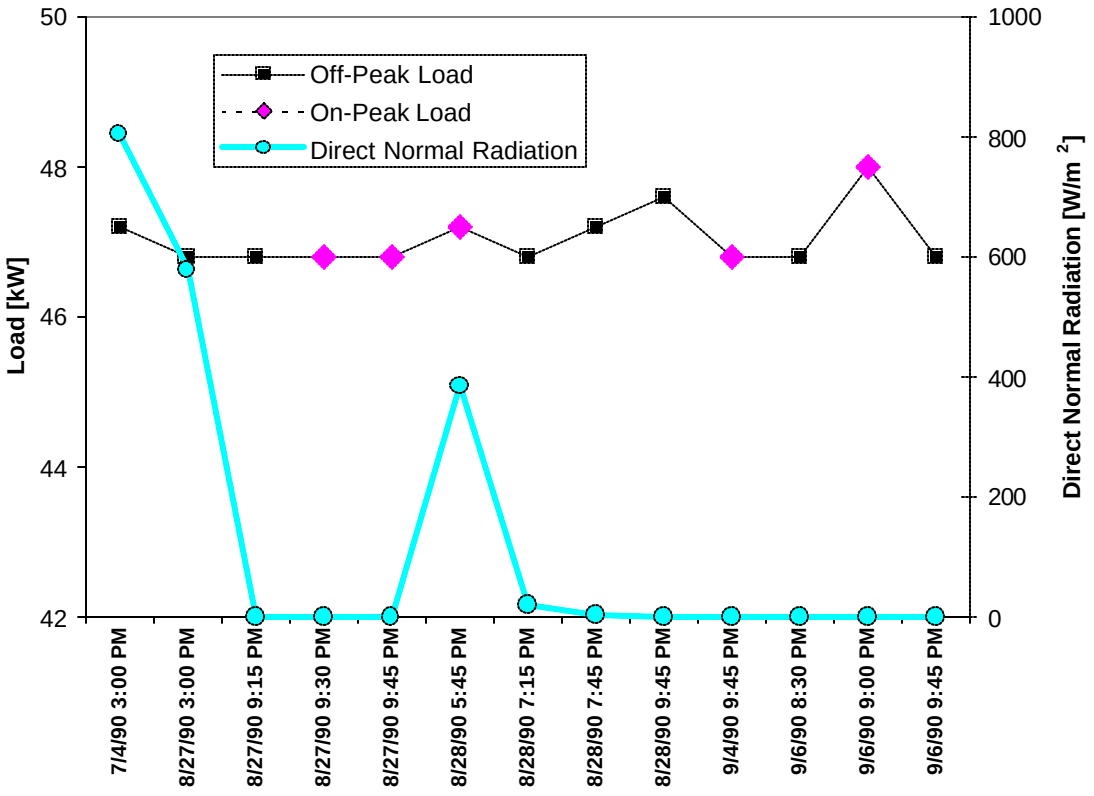

Figure 6.6-5: Top loads for retailer shown with hour of occurrence and direct normal solar radiation. Scale is expanded along the left y-axis.

Of these top loads, only three occur during sunny periods. Eight actually occur after sunset. Most importantly, only one of the on-peak loads in Figure 6.6-5 occurs before dusk (4:45 on August 28). Figure 6.6-6 shows only the top on-peak loads, along with direct normal insolation.

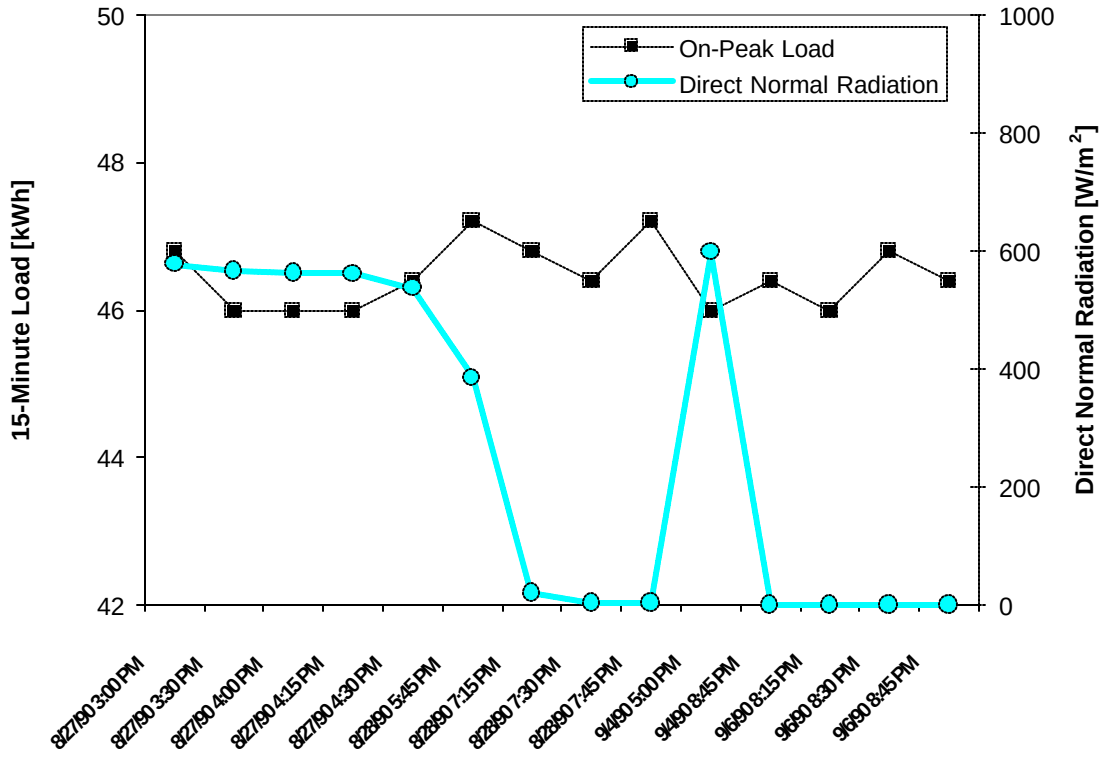

Figure 6.6-6: Top on-peak loads for retailer shown with hour of occurrence and direct normal solar radiation. Scale is expanded along the left y-axis.

Five of these loads occur during reasonable sunny periods and are subject to PV load shaving. However, the building owner sees essentially no reduction in demand charge. The reason is that other large loads occur at night during the same month, and these cannot be reduced by PV. The demand charge is based on the largest single monthly load. This means that a customer can only save significantly on the monthly bill if *every* large load in that month can be reduced. It is clear that this building's loads are very poorly matched to photovoltaic parallel generation.

The retailer's loads are much smaller than those for the grocery or office highrise, so a 20 kW PV system generates proportionately more energy than for the other buildings. At some times photovoltaic generation actually exceeds the load, allowing the retailer to sell power

back to the utility. Net-metering laws require the utility to purchase a customer's excess parallel generation at the customer's usage rate for that time. Figure 6.6-7 shows the total energy sold for each month.

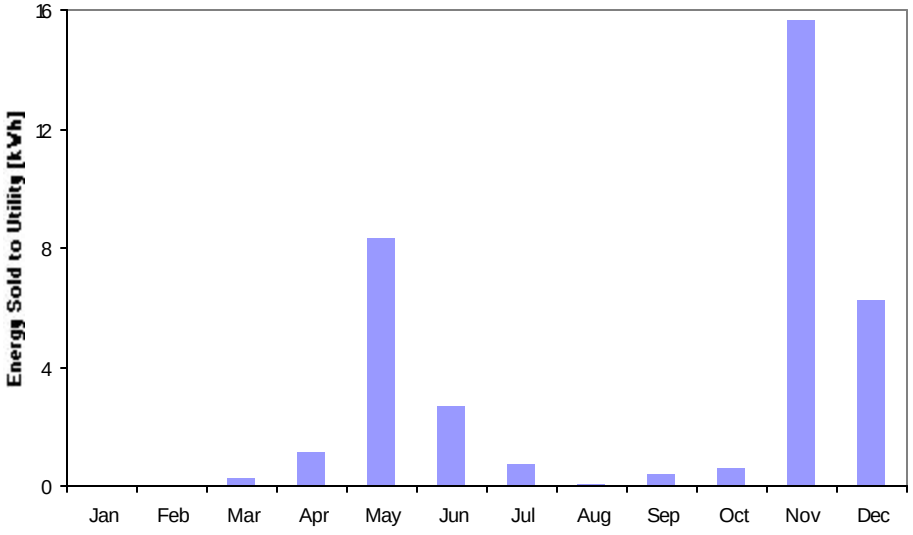

Figure 6.6-7: Monthly values for excess PV generation sold back to the utility.

Most of the excess energy is produced during May, November, and December. In May, the excess generation occurs on several clear mornings before the store opens for business. The energy sold in November is mainly the result of a very clear Veteran's Day during which the store is closed and loads are low. Likewise, the business closes on Christmas, accounting for excess energy in December. The energy sold back to the utility over the course of the year is not economically significant, totaling only 36 kWh. However, examining when excess generation occurs may be important for grid-tied buildings with very large PV capacity.

6.7 Conclusions and Summary

This chapter discusses the results obtained from running PHANTASM for three commercial buildings in the Milwaukee area. Annual monetary savings were calculated for 20 kW

rooftop crystalline PV arrays. The array orientation was optimized for each building. Table 6.7-1 summarizes the simulation results.

Table 6.7-1: Orientation, annual energy generation, and monetary savings for optimized PV arrays

Building	***Slope – Latitude***	***Azimuth***	***Energy Generation***	***Usage Savings***	***Demand Savings***	***Total Savings***
Grocery	-10	-10	23197 kWh	$757	$589	**$1346**
Office Highrise	-10	+10	23154 kWh	$762	$953	**$1715**
Retailer	-10	0	23197 kWh	$1245	$5	**$1250**

The energy generated by the optimized PV systems does not vary much between buildings. There are significant differences in total savings between the buildings, however. These discrepancies occur for two reasons. The first is that the buildings do not all follow the same rate schedule. The retailer is billed under the Small Secondary schedule, while the grocery and office highrise are billed under the Large Secondary schedule. Small Secondary has greater usage rates; this is why the retailer saves so much more in usage charges than the other two buildings despite generating only slightly more energy.

The second reason for the differences in savings is how closely each building's greatest on-peak loads coincide with periods in which solar energy is readily available. The largest loads for both the grocery and the office occur predominantly during daylight hours. In general, the grocery's largest loads occur during cold winter mornings because of electric heating. These clear, cold periods are ideal times for PV. However, many of these top loads occur before utility on-peak period begins at 9:00 AM. Peak shaving is irrelevant to the building owner before this time since demand charges are not assessed. The greatest loads for this building coincide well with solar availability but not always with the rate schedule. The grocery sees significant demand reduction in summer as well as winter, even though loads are not as large during these months.

The office building probably employs gas heating, so its greatest electrical consumption occurs during hot summer afternoons when cooling loads are high. These periods are often sunny and occur during on-peak hours, allowing PV generation to reduce demand charges significantly. Demand savings exceed usage savings for this building. Of the three buildings examined in this work, BIPV is most beneficial to the office highrise.

The small retail store sees the least benefit from BIPV. It saves more in usage charges than the office and the grocery because it is billed under a different schedule. However, its demand savings are negligible. The reason for this problem is simple: this building consumes the most electricity after sunset when solar energy is unavailable. It represents an extreme mismatch of load and solar availability.

The demand shaving benefits of BIPV are summarized in Table 6.7-2.

Table 6.7-2: Time of peak loads and potential for PV demand reduction in each building

Building	***Time of Greatest Building Loads***	***PV Demand Reduction Potential***
Grocery	Cold clear winter mornings	**Moderate**: PV performs well but top loads often occur before demand charge assessment begins at 9:00 AM.
Office	Hot summer afternoons	**Good**: Top loads occur during utility's on-peak hours and often coincide with high insolation.
Retailer	Evenings after dusk	**Minimal**: There is usually no sun when loads are greatest.

CHAPTER 7

Milwaukee Simulation Results: Utility Benefits

Chapter 6 evaluates the potential benefits of BIPV for three commercial electric customers in Milwaukee. PHANTASM determines solar savings based on historical building load data and utility rate schedules. The monetary solar savings are dependent on both total energy production and how closely the times of PV generation coincide with large building loads. This chapter discusses the benefits of large-scale BIPV implementation from the perspective of the utility.

The utility's cost for generating a kWh of electricity is not constant. Most utilities own a number of plants with different operating costs. At times when the utility's total demand obligation is moderate, only large plants with low operating costs are run. The generation cost per kWh at these times is quite low, and parallel generation from PV or other sources is not particularly valuable to the utility. When demand obligation is very large, the utility must run its most expensive plants, generally gas turbines. It may also be forced to purchase power from a neighboring utility if demand exceeds generating capacity. At these times the utility's cost for each kWh may exceed the selling price, so the utility stands to benefit from customer parallel generation to reduce demand obligation. From a commercial customer's perspective, the potential benefits of BIPV depend largely on PV performance at times when building loads are large. Similarly, the value of BIPV implementation for the utility is dependent on how closely PV generation coincides with times when customers consume the most energy.

7.1 Total Energy and On-Peak Optimization

Figure 6.3-1 gives the total annual energy production of a 20 kW PV array as a function of orientation. The optimal orientation to maximize energy production for 1990 in

Milwaukee was found to be a south-facing array sloped at ten degrees less than the latitude. Figure 6.3-2 shows how orientation effects total energy production during on-peak hours only. Wisconsin Electric's on peak period is from 9 AM to 9 PM on working days. Solar energy prior to 9 AM cannot contribute to on-peak generation, so the "on-peak optimization" is west of south to take advantage of afternoon sun. An array facing 20 degrees west of south sloped at 10 degrees less than latitude maximizes on-peak generation. In general, the utility stands to benefit the most from parallel generation during the on-peak hours. The discussions in this chapter will refer to PV arrays optimized for "total energy generation" and "on-peak generation."

7.2 BIPV and Average Hourly and Monthly Loads

Wisconsin Electric's average loads are greater in summer than in winter. The winter loads, in turn, are larger than those in spring and fall. In the Midwestern climate PV is most effective during the summer, so average PV production coincides fairly well with utility loads on a seasonal basis. Figure 7.2-1 shows the monthly average utility load and generation of a 20 kWp PV system optimized for on-peak energy production. The values for PV generation are much less than the 20 kWp rated capacity because all hours including nighttime are included in the monthly average calculation.

On average, PV generation also coincides with utility load on a daily basis. Utility loads are usually greater during the day than in the evening, and of course PVs function only during the daytime. The daily variations in average utility load are much larger than the monthly variations. Figure 7.2-2 shows the average utility load and PV generation over the course of the day.

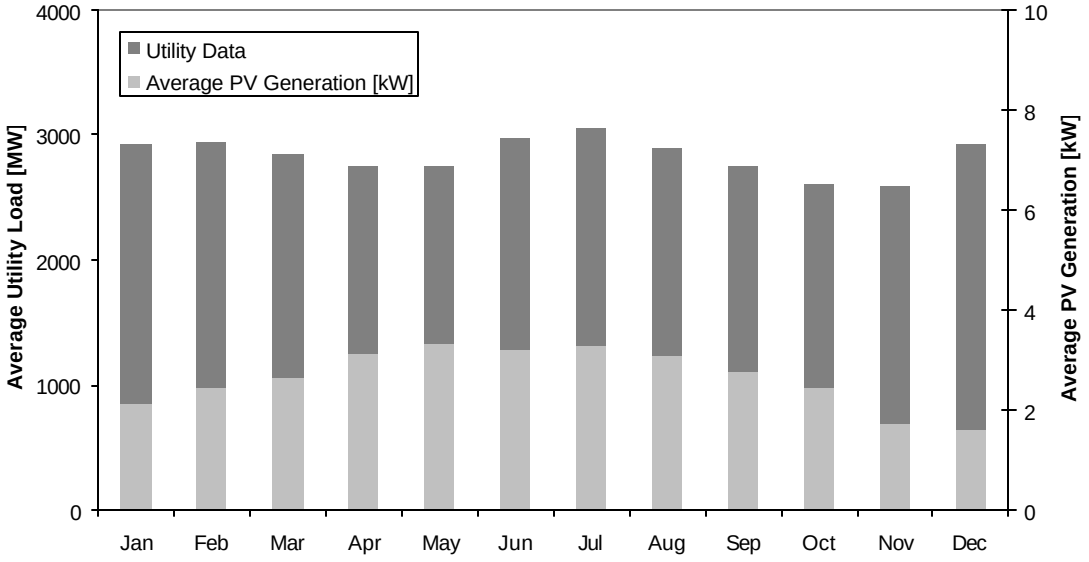

Figure 7.2-1: Monthly average utility load and generation from a 20 kWp PV array.

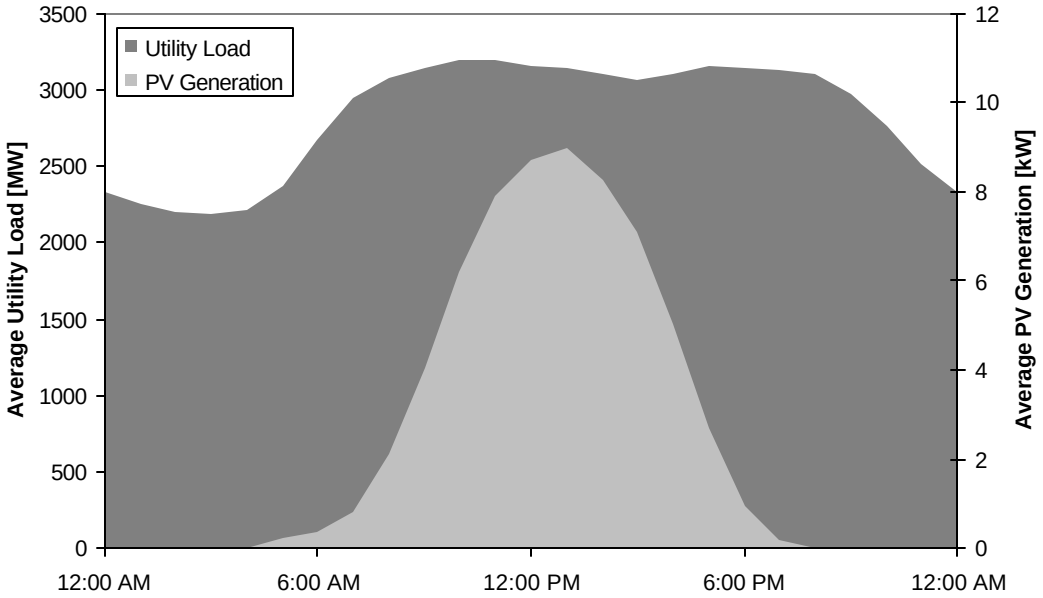

Figure 7.3-2: Average utility load and PV generation over the course of the day. PV system is 20 kWp optimized for on-peak generation

7.3 BIPV and Load Distribution Curves

A utility load distribution curve is essentially a graph of the utility's total demand obligation over the course of the year ordered from smallest to largest load. Wisconsin Electric's load distribution curve for 1990 is shown in Figure 5.5-1. There is a steep "tail" of unusually large loads on the far right side of the distribution. These are hot periods in summer when exceptionally heavy cooling loads strain the utility's capacity. It is at these times that PV or other parallel generation schemes have the most potential to benefit the utility. A qualitative method the estimate the impact of BIPV implementation is to examine how PV changes the load distribution curve. Figure 7.2-1 shows how the load distribution changes when 500 MWp and 1000 MWp installed PV are added to the grid. It is important to note that two points falling at the same y-value *do not* occur at the same time. Each of the three load curves is ordered individually from smallest to largest without regard to time of occurrence. The utility load data were supplied in hour-long increments, while the Milwaukee simulations were run using a timestep of fifteen minutes. Thus, the four PV generation results for each hour were averaged to determine how PV effects the utility load for that hour.

PV impacts the upper half of the load distribution curve more substantially than the lower half. This is because the lower loads more often occur at night when PV offers no benefit. A key issue is the influence of PV at the upper end of the distribution curve. Figures 7.3-2 and 7.3-3 show the top 10% and 1% of the distribution curve. Figure 7.3-3 also contrasts PVs optimized for total energy generation (TE) and on-peak energy generation (OP).

Most of the top 10% of the load distribution curve is reduced by about 150 MW when 1000 MWp PV is installed. Figure 7.3-3 shows that the reduction is slightly larger in the lower range of the top 1%, about 200 MW. However, at the most extreme loads the influence of PV falls off substantially. The very top of the distribution curve is reduced by only about 120 MW for 1000 MWp PV capacity. Figure 7.3-3 also shows that the on-peak optimization changes the upper range of the distribution curve more favorably than

PVs optimized for total energy production. This is because the largest loads almost always fall during the on-peak period.

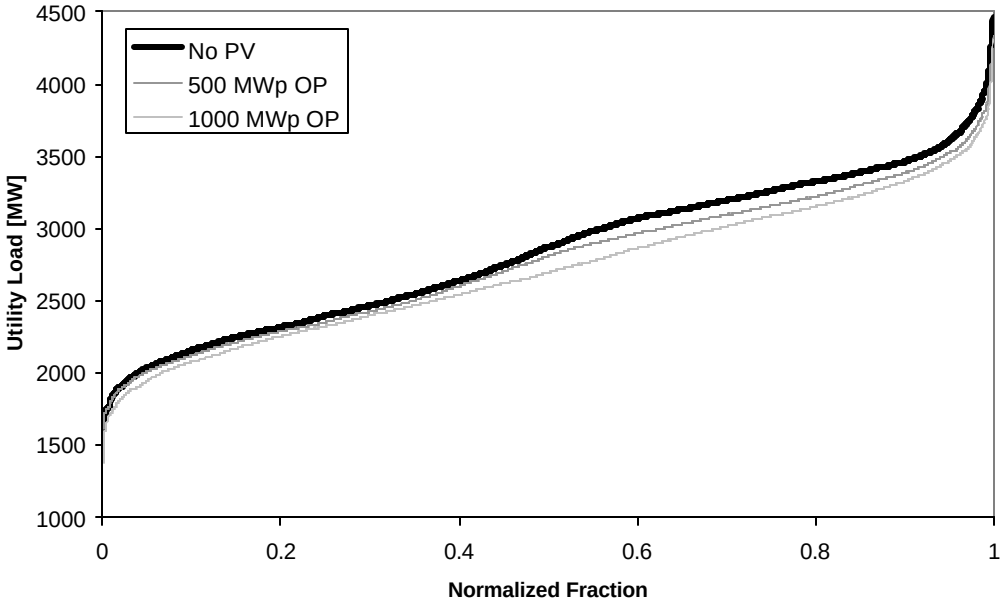

Figure 7.3-1: Annual load distribution curve with 500 MWp and 1000 MWp of installed BIPV capacity. The PV is optimized for on-peak (OP) energy production.

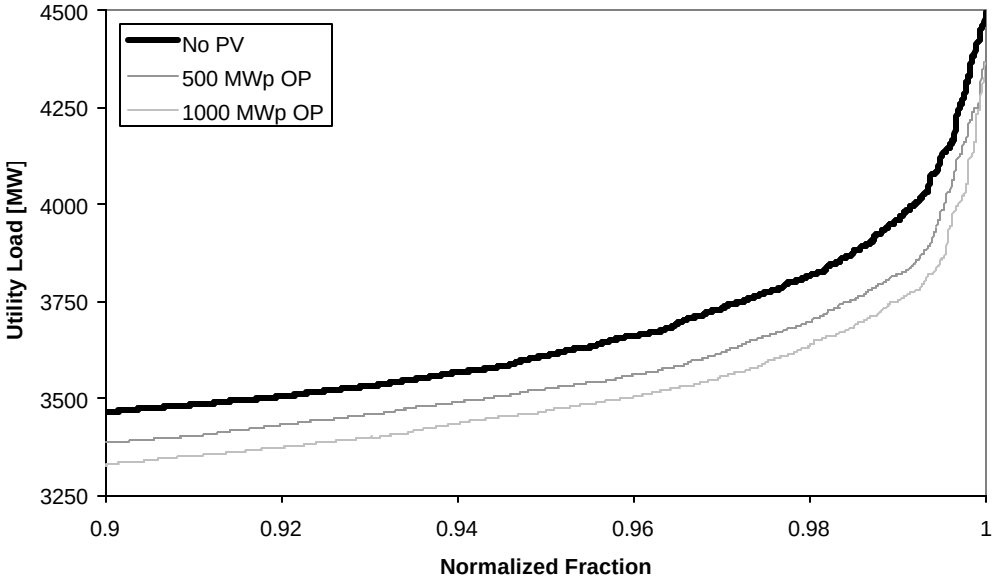

Figure 7.3-2: Top 10% of the utility load distribution curve with 500 MWp and 100 MWp installed BIPV capacity. The PV arrays are optimized for on-peak generation.

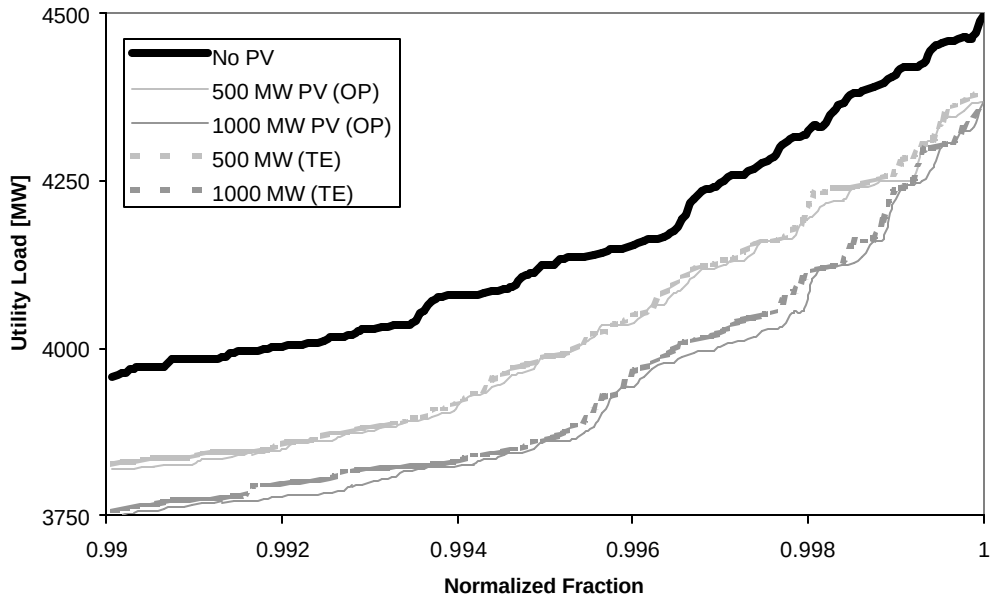

Figure 7.3-3: Top 1% of the utility load distribution curve with 500 MWp and 1000 MWp installed BIPV capacity optimized for on-peak (OP) and total energy production (TE).

7.4 Marginal Plant Energy Cost Analysis

When grid-tied BIPV systems produce energy, some of the utility's load is displaced. This means that the utility may reduce its generation by running a plant at less than full capacity or perhaps shutting off one or more plants. For the most part, a utility will use its most inexpensive available plants to fulfill its load in order to minimize cost. Combustion turbines, for instance, are usually the last plants to be turned on when the load becomes large and the first to be deactivated when the load falls off. The most costly plant in the generating mix at any given time is known as the "marginal plant." The operating cost of this plant is what determines the value of PV-generated kWh at that time.

Two pieces of information are necessary to determine the marginal plant. The first is the total utility load. The second is a list of plants in the utility, along with their capacities and operating costs. EUSESIA (Electric Utility Solar Energy System Impact Analysis), a TRNSYS program developed by Trzesnieski, evaluates the value of thermal or photovoltaic solar systems to a utility through a marginal plant analysis [1995]. The EUSESIA package includes the complete 1991 generation mix for six Wisconsin utilities including Wisconsin Electric. Although this work relies on 1990 load data, Wisconsin Electric's plant mix should not have changed significantly over the course of one year. The list of Wisconsin Electric's plants is given in Appendix E.

EUSESIA employs statistical methods to account for the possibility of plant outages that temporarily reduce the utility's generation capacity. The outages are divided into two types. "Forced outages" are unexpected breakdowns that occur randomly. The EUSESIA utility plant data includes the fraction of time during which each plant is down due to forced outages. "Scheduled outages" are regular intervals during which some plants are deactivated or run only at partial capacity for maintenance purposes. For Wisconsin Electric, all scheduled outages occur between March 1 and May 1 or September 20 and November 20.

EUSESIA also accounts for energy losses in transmission and distribution. BIPV parallel generation is consumed on-site and is not subject to such losses. Thus, the amount by which the utility generation is reduced by grid-tied BIPV systems is somewhat greater than the energy produced by the PV systems themselves. By totaling the marginal cost of parallel generation at each hour and dividing out transmission and distribution losses, EUSESIA calculates the utility's monetary savings in energy production over the course of a year. This is summarized in the following equation:

$$Savings_{Energy} = \frac{\sum_{j=1}^{8760} Q_{PV,j} Cost_j}{(1 - Loss_{trans})(1 - Loss_{dist})} \qquad \text{Eq. 7.4-1}$$

$Q_{PV,j}$ and $Cost_j$ are the values for PV generation and marginal energy cost at each hour. $Loss_{trans}$ and $Loss_{dist}$ are the fractions of centrally generated energy lost in transmission and distribution respectively. For this work $Loss_{trans}$ was assumed to be 2% and $Loss_{dist}$ to be 3%.

The annual utility energy savings for single 20 kWp systems optimized for total and on-peak energy production are shown in Table 7.4-1.

Table 7.4-1: Utility savings and annual energy production of 20 kWp BIPV systems

BIPV System Optimization	***Utility Energy Savings (Generation Level)***	***Utility Monetary Savings***	***Value of PV Generation***
On-Peak	24168 kWh	$476	$0.0197 / kWh
Total Energy	24402 kWh	$482	$0.0198 / kWh

The average value of photovoltaic electricity is just under $0.02 per kWh based on the cost of the conventional generation it replaces. This is considerably more valuable than

Wisconsin Electric's nuclear and cheaper coal generation ($0.0048 and roughly $0.01 per kWh respectively). On the other hand, the gas turbines operate at $0.06 per kWh.

7.5 Utility Demand Reduction

A second factor in assessing the value of grid-tied BIPV for a utility is how well BIPV systems offset the need for the utility to install additional conventional capacity. The total capacity that a utility must install is essentially dictated by the greatest loads it may expect. For this reason, the demand reduction potential of BIPV systems is closely tied to their performance at times when utility loads are greatest. Figure 7.3-3 shows how 500 MW and 1000 MW ensembles of BIPV systems would effect the top 1% of the utility distribution curve. Another way to visualize PV performance at high utility loads is show how PV installation will reduce each load at a given time. Figure 7.4-1 illustrates how each of the top 50 hourly utility loads is reduced by 500 MWp of installed PV capacity, optimized for on-peak production. Most of the top loads occurring before 4 PM are reduced by at least 200 MW. Not surprisingly, the PV performance at top loads drops off quickly in late afternoon.

EUSESIA uses solar performance at the largest utility loads to estimate how much new utility generating capacity is offset by installing solar systems. The number of peak hourly loads employed in this analysis, *N*, is a variable that may be set by the user. The demand reduction for a BIPV system is its average generation for the top *N* loads with transmission and distribution losses divided out:

$$Dem_{reduction} = \frac{\frac{1}{N}\sum_{j=1}^{N} Q_{PV,j}}{(1 - Loss_{trans})(1 - Loss_{dist})} \qquad \text{Eq. 7.5-1}$$

The demand reduction clearly depends on the somewhat arbitrary choice of a value for *N*. In this analysis, however, the result varies by only about 20% for values of *N* ranging from 10 to 50.

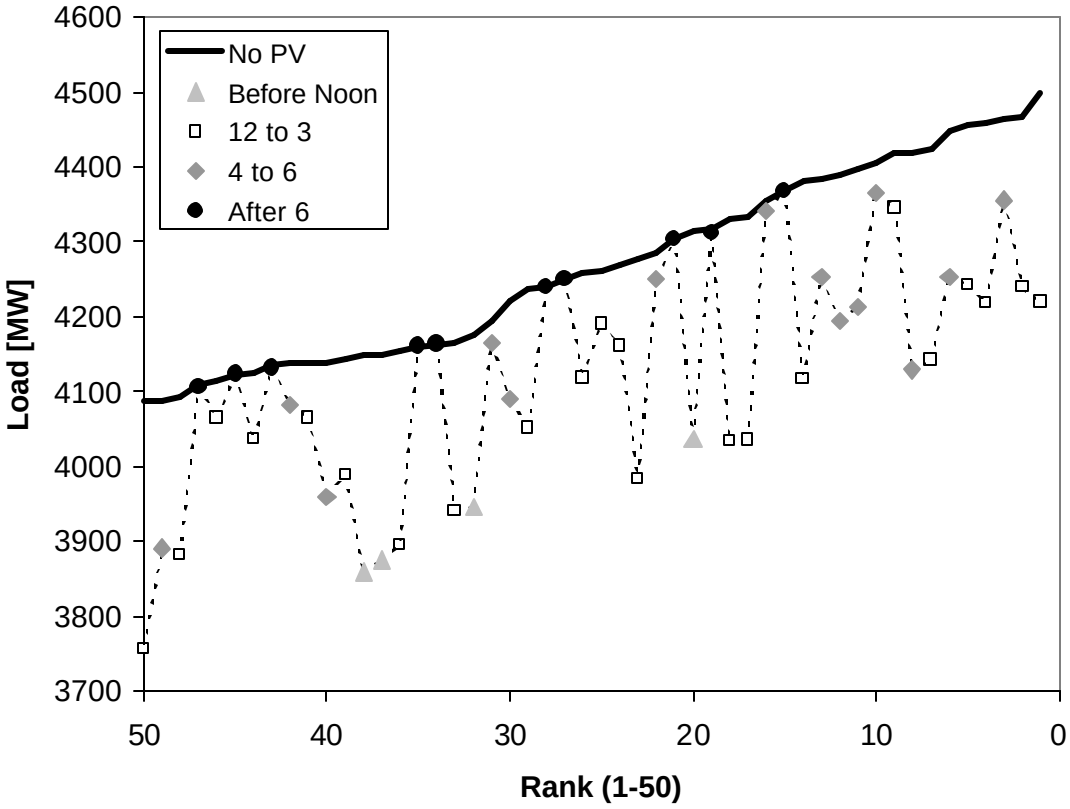

Figure 7.5-1: Reduction of the top 50 utility loads for 500 MWp installed BIPV. Separate symbols distinguish the hour of occurrence for each load. PV provides little load shaving benefit for loads occuring after 6 PM.

Figure 7.5-2 shows the demand reduction estimates using five values of *N* for 20 kWp systems optimized for on-peak and total energy production. These estimates suggest that 20 kWp installed PV capacity corresponds to roughly 8 kW of new gas turbine capacity for meeting top loads. On-peak optimization provides about 5% more utility demand reduction for each value of *N* except 20. The reason is that most of the solar energy available for loads ranking 10 to 20 occurs in the morning or early afternoon, as shown in

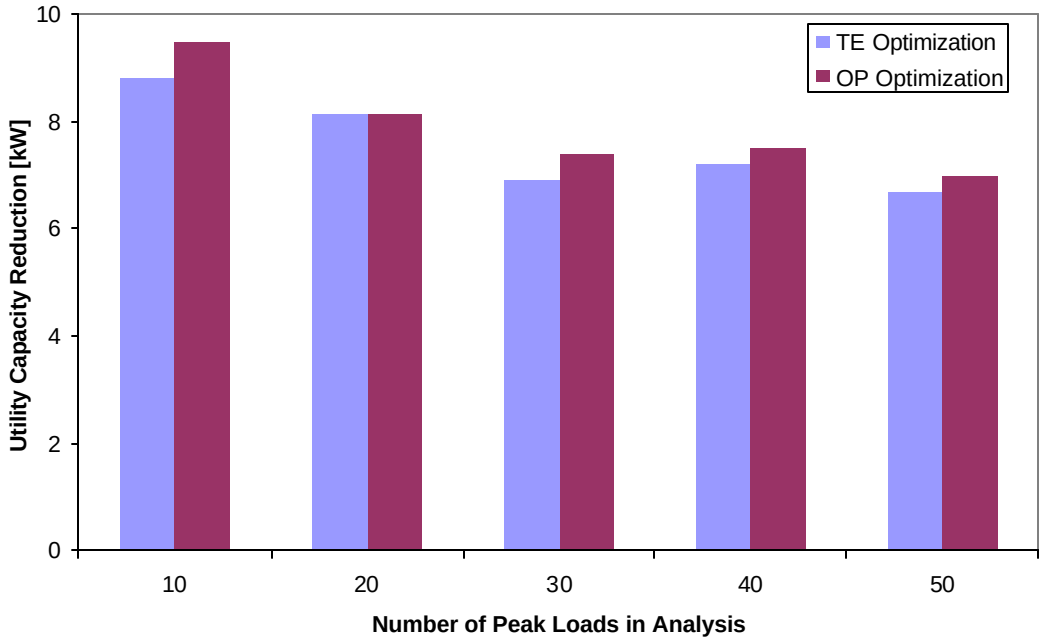

Figure 7.5-2: Utility capacity reduction for installation of 20 kWp systems optimized the total energy and on-peak generation.

Figure 7.5-1. In general, the demand reduction estimate goes down with larger *N* values. However, *N* = 40 produces slightly more optimistic results than *N* = 30. Figure 7.5-1 shows that PV performs unusually well for loads ranking in the 30s, so including these loads in the analysis enhances the demand reduction estimate.

EUSESIA calculates the monetary value of solar demand reduction by multiplying the results shown in Figure 7.5-2 by set costs for new generation, transmission, and distribution capacity. Gas turbine peaking plants are estimated to cost $325 per kW. In addition, new infrastructure requirements for transmission and distribution are each estimated to cost $100 per kW. Table 7.5-2 shows the results for the monetary demand reduction value of a 20 kWp PV system for values of *N* ranging from 10 to 50. These results show that 20 kWp BIPV system will replace roughly $4000 worth of conventional peaking plant capacity.

Table 7.5-1: Estimate of the monetary value of utility demand reduction for a 20 kW BIPV system.

N: # of Peak Loads Used in Demand Calculation	***Total Energy Optimization***	***On-peak Optimization***
10	$4345	$4669
20	$4017	$4016
30	$3407	$3646
40	$3546	$3712
50	$3293	$3451

7.6 Summary

This chapter examines the potential benefits of BIPV parallel generation from the perspective of the electric utility. Hourly 1990 load data for Wisconsin Electric, the Milwaukee utility, were employed in these analyses. On an hourly and monthly basis, PV generation coincides fairly well with average utility loads. Loads are generally largest during the daytime hours when PV is effective. Likewise, the utility experiences its greatest average loads during the summer months when PV systems produce the most energy.

EUSESIA, a TRNSYS package developed by Trzesniewski [1995], was used to calculate the value of photovoltaic energy and demand reduction for the utility. EUSESIA employs a "marginal plant" model to determine the average value of a kWh of PV generation. This model accounts for which plants the utility is running at a given time and assesses the value of PV generation at that time based on the operating cost of the most expensive operating plant. The average value to the utility of photovoltaic

electricity was found to be just under $0.02 per kWh. In addition, EUSESIA was used to estimate the value of the gas turbines peaking capacity and associated transmission and distribution infrastructure which could be replaced by a single 20 kWp BIPV system. 20 kWp PV capacity is equivalent to about 8 kW of gas turbine capacity, valued at roughly $4000.

These estimates for the value of PV to the utility are based on simulations from a single year; using some other year would produce different results. As discussed in Chapter 5, the weather in 1990 was unusually poor from the perspective of available solar energy. Combining the results of similar simulations for ten or twenty years would probably produce more realistic estimates. On average, PV might be (very roughly) 10% more productive than during 1990. Running more simulations would of course require more weather and utility load data. In addition, the plant list employed in the marginal plant analysis may not remain constant over this time span if new plants are built or old ones are decommissioned.

EUSESIA does not account for the possibility of total loads exceeding generating capacity, a very bad situation for the utility. Such a problem would be most likely to arise if a significant portion of the generating capacity suffered a forced outage during a peaking period. This situation will produce a brownout if the utility in question is unable to purchase excess power from a neighboring utility. PV is probably a more reliable power source than generation technologies that rely on mechanical energy conversion, making unexpected outages less likely. Moreover, the distributed nature of BIPV generation could help it to prevent brownouts. A large central plant could fail unexpectedly at any time, but there is very little chance of many small BIPV systems failing simultaneously and producing a large drop in total generating capacity. This analysis does not quantify the value of avoiding brownouts or wheeling for an individual utility.

CHAPTER 8

Conclusions and Recommendations

8.1 Project Summary

The goals of this project were twofold. The first objective was to develop a stand-alone TRNSYS software package for simulating the electrical and economic performance of building-integrated photovoltaic systems. This package, PHANTASM, relies on the TRNSED menu-based user interface. PHANTASM allows a user to define a grid-tied photovoltaic system in any location and examine its potential to reduce a building's electric bill. The program uses hourly weather data, building load data, and a real utility rate schedule. Both usage and demand charges are accounted for in assessing the economic impact of the BIPV system. The software employs a new five-parameter TRNSYS photovoltaic model that can simulate amorphous as well as crystalline PV modules. The five-parameter model is described in Chapter 3, while the other aspects of the PHANTASM program are discussed in Chapter 4.

The second goal of this work was to use PHANTASM to study the potential for the large-scale implementation of grid-tied BIPV systems in Wisconsin. Simulations were carried out for three commercial buildings in the Milwaukee area using electrical load data and weather from 1990. Rate schedules from Wisconsin Electric were employed to calculate solar savings for each building. The methods and results of these calculations are addressed in Chapter 6. In addition, the impact of BIPV on the electric utility was studied using EUSESIA, a TRNSYS program developed by Trzesnieski. 1990 total load data for Wisconsin Electric were employed in this analysis. EUSESIA uses a utility marginal plant model to determine the value of solar parallel generation at each time throughout the year. The program also examines photovoltaic performance during times

when utility loads are greatest to estimate the value of the conventional generating capacity that may be replaced by a BIPV system.

8.2 Conclusions

This study examines the performance of a 20 kWp rooftop BIPV array from the perspective of the electric customer and the utility. The present cost of such an array is roughly $80000. Three commercial buildings were examined: a grocery, an office highrise, and a retail store. Since commercial rate schedules generally include demand charges that penalize the customer for large instantaneous loads, the solar savings from BIPV depend largely on how well PV performance coincides with the greatest building loads. It was found that the greatest loads in the grocery occurred during winter mornings. These periods were often clear, providing moderate PV generation with an annual solar savings of $1346. The greatest loads for the office highrise occur on hot sunny afternoons, coinciding more closely with photovoltaic generation. Solar savings for the office was $1715. The retailer saved only $1250 because most of its greatest loads occur at night when the PV system is not operating.

A 20 kWp oriented to maximize energy production during the on-peak period produces 24168 kWh over the course of the year. A marginal plant analysis assesses the value of this energy for the utility is $476 or $0.0197 per kWh. Based on PV performance during the top 10 to 50 hourly utility loads during the year, the 20 kWp system has the same potential for meeting peaking demands as about 8 kW of gas turbine capacity. The value of this generation capacity and the associated transmission and distribution equipment is approximately $4000.

These results suggest that, in purely economic terms, grid-tied photovoltaic systems do not promise to be profitable investments at this time. However, photovoltaics have proven to be economical energy solutions in areas without electrical infrastructure, and there are several reasons to believe this study has produced conservative results. Perhaps

the most important is that electric rates in Wisconsin are among the lowest in the nation. Power is roughly twice as expensive on the Eastern seaboard and even more costly in Europe, so the value of photovoltaic generation in these area is proportionately greater.

Chapter 5 shows that weather conditions in 1990 were unusually poor for PV, mainly because of a cloudy summer. Rerunning the simulations in a more typical year would probably produce more optimistic results. Moreover, the climate in the Upper Midwest is not ideal for PVs. Most areas in the Western US are considerably sunnier, especially during winter.

Standard crystalline PV modules currently cost about $4 to $5 per peak watt. Amorphous modules are cheaper although a bit less efficient. However, both the cost and efficiency of PVs employing thin-film technology is improving rapidly. The production of PV capacity is growing by 20% annually, a trend that suggests economies of scale stand to further reduce PV costs.

8.3 Recommendations

PHANTASM is a useful tool for building designers interested in estimating the economic performance of a BIPV system. A number of simulation packages are available to predict the physical performance of photovoltaic systems. However, other solar simulation programs do not estimate the impact of demand savings by accounting for fluctuations in electrical consumption.

It would be useful to run further BIPV simulations in areas with more favorable climates and/or higher utility rates. These are the areas most likely to see large-scale market penetration of grid-tied PV systems in the near future. Furthermore, simulations involving amorphous technology would provide a useful comparison in determining whether crystalline or amorphous modules are most appropriate for a large-scale utility program.

Trzesnieski [1995] has pointed out that the EUSESIA program could readily be expanded to examine the utility impact of wind turbine systems. Modifying PHANTASM to include wind systems would be more complicated. However, the Rate Calendar and Utility Rate Schedule TRNSYS components are compatible with any sort of grid-tied parallel generation. A program including wind data and wind turbine model components could be developed to examine how the availability of wind energy coincides with building loads.

Finally, the scope of this study could be expanded to examine the environmental ramifications of renewable energy systems. One very important advantage of photovoltaic generation is that, from an environmental standpoint, it is completely benign. PV manufacture is an energy-intensive process, although the energy-payback time for emerging thin-film technologies is on the order of one year. Moreover, utility deregulation and stricter emissions standards are likely to lead to increased trading of emissions credits among utilities. PV implementation is an effective way to reduce emissions, and EUSESIA's marginal plant model provides a straightforward method to quantify these reductions for various utilities.

Bibliography

Beckman, William A. Personal communication: September, 1998.

Carlin, John; Fred Mayes, and Louise Guey-Lee. "Renewable Data Overview." *Renewable Energy Annual 1996*. Energy Information Administration: April 1997. http://www.eia.doe.gov/cneaf/solar.renewables/renewable.energy.annual/chap01.html

Cragan, Keary Elizabeth. *Impact on a Utility of an Ensemble of Solar Domestic Hot Water Systems.* M. S. Thesis – Solar Energy Laboratory, University of Wisconsin, Madison: 1994.

Duffie, John A. and William A. Beckman. *Solar Engineering of Thermal Processes*. New York: John Wiley & Sons, Inc., 1991.

Eckstein, Jurgen Helmut. *Detailed Modeling of Photovoltaic Components.* M. S. Thesis – Solar Energy Laboratory, University of Wisconsin, Madison: 1990.

Elliot, D. L. et al. *Wind Energy Resource Atlas of the United States*. National Renewable Energy Laboratory: October, 1986. http://rredc.nrel.gov/wind/pubs/atlas/

The Fleming Group. *Creating a Commercial Cooling Load Library*. Wisconsin Center for Demand-Side Research: 1994.

Fry, Bryan. *PHANTASM User's Manual.* Solar Energy Laboratory, University of Wisconsin: 1999.

Holihan, Peter. "Solar Industry Profile." *Renewable Energy Annual 1996.* Energy Information Administration: April 1997. http://www.eia.doe.gov/cneaf/solar.renewables/renewable.energy.annual/chap06.html

Holihan, Peter. "The Role of Electric Utilities in the Photovoltaic Industry." *Renewable Energy Annual 1996*. Energy Information Administration: April 1997. http://www.eia.doe.gov/cneaf/solar.renewables/renewable.energy.annual/chap07.html

Kato, Kazuhiko, Akinobu Murata, and Koichi Sakuta. "Energy Pay-back Time and Life-Cycle CO_2 Emission of residential PV Power System with Silicon PV Module." *Progress in Photovoltaics: Research and Applications* **6**: 105-115 (1998).

King, David L., Jay A. Kratochvil, and William E. Boyson. "Measuring the Solar Spectral and Angle-of-Incidence Effects on Photovoltaic Modules and Irradiance Sensors." *Proceedings of the 1994 IEEE Photovoltaics Specialists Conference*. Sept 30-Oct 3, 1997. pp. 1113-1116.

Klein, S. A. and Beckman, W. A. *PV F-Chart User's Manual, Macintosh Version 2.0*. Madison, Wisconsin: F-Chart Software, 1992.

Klein, S. A. et al. *TRNSYS: A Transient System Simulation Program, Version 14.2*. Solar Energy Laboratory, University of Wisconsin, Madison: July, 1996.

Klein, S. A. et al. *Using TRNSHELL and TRNSED: The TRNSYS Environment Programs, Version 2.0*. Solar Energy Laboratory – University of Wisconsin, Madison: October 1997.

Krom, Larry S. Wisconsin PV 1996. Wisconsin Energy Bureau: 1997.

Liu, B. Y. H. and R. C. Jordan. "The Interrelationship and Characterisitc Distribution of Direct, Diffuse, and Total Solar Radiation." *Solar Energy*, Vol. IV, July 1960, pp. 1-19.

Menicucci, F. F., and J. P. Fernandez. *User's Manual for PVFORM: A Photovoltaic System Simulation Program for Stand-Alone and Grid-Interactive Applications*. Sandia National Laboratories, July 1994.

Mitchell, John W. Personal communication: August, 1998.

Montes, Marcos J. "The American Secular Holiday Calendar." http://www.smart.net/~mmontes/ushols.html. July, 1998.

National Renewable Energy Laboratory. *User's Manual: National Solar Radiation Database -- 1961-1990*. September, 1992. http://rredc.nrel.gov/solar/pubs/NSRDB/

Omnion Power Engineering Corporation. 2010 Energy Drive. East Troy, WI 53120.

Osborn, D. E. and D.E. Collier, "Utility Grid-Connected Photovoltaic Distributed Power Systems," presented to the American Solar Energy Society (ASES) 1996 Conference (Asheville, NC, April 1996).

Perez, R. et al. "The Development and Verification of the Perez Diffuse Radiation Model," Sandia Report SAND88-7030. (Sandia National Laboratories, Albuquerque, NM 87185.) October, 1988.

Rabehl, Roger. *Parameter Estimation and the Use of Catalog Data with TRNSYS.* M. S. Thesis – Solar Energy Laboratory, University of Wisconsin, Madison: 1997.

Sacramento Municipal Utility District Website: http://www.smud.org/energy/solar/become.html. 1998.

Siemens Solar Online. http://www.solarpv.com/. 1998.

Solarex. *1997-1998 Photovoltaic Product Catalog*. 630 Solarex Court. Fredrick, MD, 21703.

Strong, Steven J and William G. Scheller. *The Solar Electric House*. Still River, MA: Sustainability Press, 1993.

Strong, Steven J. Seminar Course: "Effective PV in Buildings." Engineering Professional Development, University of Wisconsin, Madison: November 1998.

Thermal Energy System Specialists. 2873 Cimarron Terrace. Madison, Wisconsin.

Townsend, Timothy U. *A Method for Estimating the Long-Term Performance of Direct-Coupled Photovoltaic Systems.* M. S. Thesis – Solar Energy Laboratory, University of Wisconsin, Madison: 1989.

Trace Engineering. 5916 195th Street, Northeast. Arlington, WA 98223.

Trzesniewski, Jason A. *Electric Utility Interest in Solar Energy Systems.* M. S. Thesis – Solar Energy Laboratory, University of Wisconsin, Madison: 1995.

Wan, Yih-huei and H. James Green. "Current Experience with Net Metering Programs." National Renewable Energy Laboratory: January, 1998.

White, Scott W. and Gerald L. Kulcinski. "'Birth to Death' Analysis of the Energy Payback Ratio and CO_2 Gas Emission Rates from Coal, Fission, Wind, and DT Fusion Electrical Power Plants." University of Wisconsin, Madison: 1998.

Wisconsin Electric. "1998 Price Information for Electric Customers."

Wisconsin Electric. "Wisconsin Electric 1990 Hourly Demand Application."

Wisconsin Public Service Corporation Website.
http://www.wpsr.com/found at/swschool.html. 1998.

APPENDIX A

Wisconsin Electric Generation Mix (1991)

PLANT	Capacity [MW]	Out1 start (m/d)	Out1 end (m/d)	Out1 start (m/d)	Out2 end (m/d)	Sched Out. [%]	Full Out. [%]	Partial Out. [%]	Partial Capacity [MW]	Operating Cost [$/kWh]
'PNT BEACH2'	497	3 1	5 1	9 20	11 20	6	1.9	0	0	0.0048
'PNT BEACH1'	497	3 1	5 1	9 20	11 20	6	1.9	0	0	0.0048
'PLEASNTPR2'	580	3 1	5 1	9 20	11 20	6	1	1.3	220	0.009
'PLEASNTPR1'	580	3 1	5 1	9 20	11 20	6	1	1.3	220	0.009
'EDGEWATER5'	97	3 1	5 1	9 20	11 20	4	2	5	38	0.0136
'OAK CREEK8'	305	3 1	5 1	9 20	11 20	5	1	1.6	85	0.0143
'OAK CREEK7'	280	3 1	5 1	9 20	11 20	5	1	1.6	85	0.0143
'OAK CREEK5'	258	3 1	5 1	9 20	11 20	5	2	2.9	82	0.0148
'OAK CREEK6'	260	3 1	5 1	9 20	11 20	5	2	3	82	0.0149
'PRESQUEIS4'	57	3 1	5 1	9 20	11 20	1	1	2.4	12	0.0162
'PRESQUEIS6'	85	3 1	5 1	9 20	11 20	1	1	2.2	20	0.0163
'PRESQUEIS5'	84	3 1	5 1	9 20	11 20	1	1	2.2	19	0.0163
'PRESQUEIS1'	25	3 1	5 1	9 20	11 20	0	0	0	0	0.0165
'PRESQUEIS2'	37	3 1	5 1	9 20	11 20	0	0	0	0	0.0167
'PRESQUEIS3'	58	3 1	5 1	9 20	11 20	1	1	2.4	12	0.017
'PORT WASH2'	80	3 1	5 1	9 20	11 20	0	4	1.3	29	0.0199
'PORT WASH1'	80	3 1	5 1	9 20	11 20	0	4	1.3	29	0.0203
'VALLEY2 '	62	3 1	5 1	9 20	11 20	8	2.5	3.9	30	0.0214
'VALLEY4 '	70	3 1	5 1	9 20	11 20	0	2.5	4	34	0.0216
'VALLEY1 '	64	3 1	5 1	9 20	11 20	8	1	13	7	0.0224
'PRESQUEIS9'	84	3 1	5 1	9 20	11 20	1	1	3	14	0.0227
'PRESQUEIS8'	83	3 1	5 1	9 20	11 20	1	1	3	14	0.0227
'PRESQUEIS7'	81	3 1	5 1	9 20	11 20	1	1	3.2	13	0.0227
'VALLEY3 '	70	3 1	5 1	9 20	11 20	0	1	15	14	0.023
'PORT WASH3'	82	3 1	5 1	9 20	11 20	0	4	1.4	29	0.0237
'PORT WASH4'	80	3 1	5 1	9 20	11 20	0	4	1.5	29	0.0267
'CONCORD4 '	83	3 1	5 1	9 20	11 20	0	1	0	0	0.047
'CONCORD3 '	83	3 1	5 1	9 20	11 20	0	1	0	0	0.047
'CONCORD2 '	83	3 1	5 1	9 20	11 20	0	1	0	0	0.047
'CONCORD1 '	83	3 1	5 1	9 20	11 20	0	1	0	0	0.047
'OAK CREEK9'	20	3 1	5 1	9 20	11 20	0	1	0	0	0.0557
'GERMNTOWN4'	53	3 1	5 1	9 20	11 20	0	1	0	0	0.06
'GERMNTOWN3'	53	3 1	5 1	9 20	11 20	0	1	0	0	0.06
'GERMNTOWN2'	53	3 1	5 1	9 20	11 20	0	1	0	0	0.06
'GERMNTOWN1'	53	3 1	5 1	9 20	11 20	0	1	0	0	0.06
'PNT BEACH5'	20	3 1	5 1	9 20	11 20	0	1	0	0	0.0637
'PORT WASH6'	18	3 1	5 1	9 20	11 20	0	1	0	0	0.0651